This document was prepared for the ETI by third parties under contract to the ETI. The ETI is making these documents and data available to the public to inform the debate on low carbon energy innovation and deployment.

Programme Area: Marine

Project: PerAWAT

Title: Weakly-Nonlinear Hydrodynamics of Freely Floating WECS

Abstract:

This deliverable describes the results associated with a linear and weakly nonlinear potential flow, hydrodynamic formulation, applied to an isolated truncated cylinder (point absorber device type) free to move in all degrees of freedom (DOFs). Plus to four cylinders arranged in a square (2x2) array. The review presented in this document is mostly focused on the methods available in WAMIT, which was used in this study to compute the first and second-order hydrodynamic forces and the unrestrained motions associated with a single cylinder and an array with four cylinders in regular and irregular waves.

Context:

The Performance Assessment of Wave and Tidal Array Systems (PerAWaT) project, launched in October 2009 with £8m of ETI investment. The project delivered validated, commercial software tools capable of significantly reducing the levels of uncertainty associated with predicting the energy yield of major wave and tidal stream energy arrays. It also produced information that will help reduce commercial risk of future large scale wave and tidal array developments.

GL Garrad Hassan

ETI MARINE PROGRAMME PROJECT
PerAWaT MA1003
WG1 WP1 D8: WEAKLY-NONLINEAR HYDRODYNAMICS OF FREELY FLOATING WECS

Client	Energy Technologies Institute
Contact	Geraldine Newton-Cross
Document No	104327/BR/04
Issue	1.0
Classification	Not to be disclosed other than in line with the terms of the Technology Contract
Date	28 April 2011

Author: J. Lucas

Checked by: J. Cruz

Approved by: R I Rawlinson-Smith

IMPORTANT NOTICE AND DISCLAIMER

1. This report ("Report") is prepared and issued by Garrad Hassan & Partners Ltd ("GH" or "Garrad Hassan") for the sole use of the client named on its title page (the "Client") on whose instructions it has been prepared, and who has entered into a written agreement directly with Garrad Hassan. Garrad Hassan's liability to the Client is set out in that agreement. Garrad Hassan shall have no liability to third parties (being persons other than the Client) in connection with this Report or for any use whatsoever by third parties of this Report unless the subject of a written agreement between Garrad Hassan and such third party. The Report may only be reproduced and circulated in accordance with the Document Classification and associated conditions stipulated or referred to in this Report and/or in Garrad Hassan's written agreement with the Client. No part of this Report may be disclosed in any public offering memorandum, prospectus or stock exchange listing, circular or announcement without the express written consent of Garrad Hassan. A Document Classification permitting the Client to redistribute this Report shall not thereby imply that Garrad Hassan has any liability to any recipient other than the Client.

2. This report has been produced from information relating to dates and periods referred to in this report. The report does not imply that any information is not subject to change.

KEY TO DOCUMENT CLASSIFICATION

Strictly Confidential	:	For disclosure only to named individuals within the Client's organisation.
Private and Confidential	:	For disclosure only to individuals directly concerned with the subject matter of the Report within the Client's organisation.
Commercial in Confidence	:	Not to be disclosed outside the Client's organisation
GH only	:	Not to be disclosed to non GH staff
Client's Discretion	:	Distribution for information only at the discretion of the Client (subject to the above Important Notice and Disclaimer).
Published	:	Available for information only to the general public (subject to the above Important Notice and Disclaimer and Disclaimer).

REVISION HISTORY

Issue	Issue date	Summary
A	28/04/11	Original issue (electronic version only)

CONTENTS

EXECUTIVE SUMMARY

The present report (WG1 WP1 D8) describes the results associated with a linear and weakly nonlinear potential flow hydrodynamic formulation applied to an isolated truncated cylinder free to move in all degrees of freedom (DOFs) and to four cylinders arranged in a square (2x2) array.

The main aim of this study is to quantify the relative importance of weakly nonlinear hydrodynamic effects associated with these floating structures which might occur for steeper incident waves and/or when the cylinders undergo large motions, for which the linear hydrodynamic formulation might provide an insufficient description.

The report is organised in eight sections which give a detailed overview of:

- The scope of the documents and its key objectives – Section 1;
- A brief introduction to potential flow theory and the difficulties associated with a fully non-linear implementation – Section 2;
- A brief description of first order hydrodynamic formulations – Section 3;
- A detailed description of the second-order (weakly) nonlinear hydrodynamic formulation – Section 4;
- The stochastic approach used to obtain irregular wave results - Section 5.
- The linear and weakly non-linear hydrodynamic results associated with a single truncated cylinder WEC free to move in all DOFs - Section 6;
- An extension of the linear and weakly nonlinear results to an array with four cylinders WEC free to move in all DOFs - Section 7;
- The next steps in terms of the implementation – Section 8.

The report starts by providing an overview of potential flow theory by describing the assumptions and difficulties associated with a mathematical fully non-linear formulation (Section 2).

All potential flow theories consider the fluid to be incompressible, inviscid and with no surface tension. The condition of irrotational flow allows the use of the Laplace equation, that should be satisfied in all fluid domain and a set of boundary conditions must also be satisfied at the fluid-air (i.e. free-surface) and fluid-solid (i.e. seabed and wet surface of the body) interfaces. The major difficulty associated with the complete (fully nonlinear) solution of the problem is associated with the nonlinear free-surface boundary condition which is mathematically difficult to solve and the instantaneous continuous change of the wetted profile due to the large motions requiring the generation and solution of a new system of equations at each time step, since the free-surface changes and the body surface moves to a new position.

The fully nonlinear approach is thus difficult and computationally intensive and as such a more common approach is to solve the hydrodynamic problem using approximations to the fully nonlinear equations i.e. first-order (or linear) and second-order (or weakly nonlinear) by assuming small amplitudes for the incident waves and small motions for the floating structure.

The linear approximation of the potential flow problem is described in Section 3, whereas the second-order approximation is described in detail in Section 4. The linear hydrodynamic problem is widely

known and well understood in the context applied to WECs (see Sections 3.2 and 3.3 of WG1 WP1 D1b) (Falnes 2002, Evans and Linton 1993, Evans 1981). However, this is not the case for the second-order formulation for which very few studies are applied to WECs.

The general solution of the second-order hydrodynamic problem takes into account weakly non-linear interactions between the fluid and the floating structure. The magnitude of these interactions is normally of second-order and occurs at frequencies away from that of the ambient waves and which result from dual combinations of all components in the incident wave group. The second order excitation forces are thus expressed as a function at the sum and difference frequency of the components of the incident wave group through the quadratic force transfer functions known as QTFs. As in the linear case, these QTFs depend on the wetted profile of the floating structure and are investigated in detail for the single truncated cylinder and for the square array.

The review presented in this document is mostly focused on the methods available in WAMIT, which was used in this study to compute the first and second-order hydrodynamic forces and the unrestrained motions associated with a single cylinder and an array with four cylinders in regular and irregular waves. These are no foreseeable differences between the use of this particular software package and other equivalents packages, i.e. the methodology and key findings in this report should be considered representative of a generic second-order solution.

The results found show that for the single truncated cylinder the second-order excitation force components associated with most regular waves are much smaller than the first-order excitation force component in surge and pitch. In heave and for wave periods close to resonance a peak in the second-order components is found. Away from resonance, the unrestrained motions are small and dominated by the first-order component for all modes of motion.

The excitation forces and unrestrained motions were computed for a Pierson-Moskowitz spectrum with significant wave height of 2.5m (and Tp=7.9s) and it was found that the first-order component of the excitation force is dominant for both surge and pitch modes. In heave, the second-order component has higher values with a significant contribution made to the total excitation force. The unrestrained motions were small with the first-order component being dominant for heave and pitch. In surge, the slowly varying drift motion was observed.

For the array with four cylinders an increase of the peak values associated with the sum-frequency force quadratic transfer functions (QTF) component was found mostly due to the array interactions. A sharp increase in the value of the absolute value of the sum-frequency force QTF was obtained for wave periods close to 7.5s for all modes of motion except heave. An increase in the second-order excitation force component in surge and heave for the front cylinder (1) in the array was found in comparison with isolated cylinder. The unrestrained motions of the cylinders in the array are dominated by the 1st order component, except for surge and sway where the slowly varying drift motion associated with the difference frequency component is observed.

1 INTRODUCTION

1.1 Scope of this document

This document describes the implementation of a weakly, second-order nonlinear model of floating wave energy converters (WECs) of the point-absorber type that allows a first assessment of the influence of nonlinear wave loads on the WEC response.

The document is divided in seven main sections. An overview of potential flow hydrodynamic theory is given in Section 2. The methodologies associated with the first and second-order formulations are given in Sections 3 and 4, and the stochastic approach used to obtain irregular wave results is detailed in Section 5. The report is concluded with the comparisons between the first and second-order simulations for a single WEC (Section 6), and an array of four WECs (Section 7).

Section 2 provides a brief introduction to potential flow theory and describes the assumptions and difficulties associated with the mathematical formulation. The fluid is considered as incompressible, inviscid and with no surface tension. The condition of irrotational flow allows the use of the Laplace equation, that should be satisfied in all fluid domain. A set of boundary conditions must also be satisfied at the fluid-air (i.e. free-surface) and fluid-solid (i.e. seabed and wet surface of the body) interfaces. A major difficulty associated with the complete (fully nonlinear) solution of the problem is associated with the nonlinear free-surface boundary condition which is mathematically difficult to solve. The hydrodynamic forces and moments are obtained through the integration of the pressure exerted by the fluid on the wetted profile of the floating structure, which is in turn derived from the velocity potential of the fluid via the Bernoulli equation. The dynamic equations of motion of the floating structure are obtained by equating the inertial forces to the applied forces which include the hydrodynamic forces, PTO force and mooring forces. However in the fully nonlinear case the hydrodynamic forces are accounted over the instantaneous wetted profile which is coupled to the motion of the floating structure. Most of methods developed to solve this complete set of nonlinear equations use a Mixed Eulerian-Lagrangian (MEL) time stepping technique for which the fully nonlinear boundary conditions are satisfied over the instantaneous free-surface and body surfaces. The unknowns of the linear equations which result from the discretisation of the geometry are distributed on the boundary of the whole computational domain and a new system of equations is generated and solved at each time step, since the free-surface changes and the body surface moves to a new position.

The fully nonlinear approach is thus difficult and computationally intensive and as such a more common approach is to solve the hydrodynamic problem taking into account approximations of the nonlinear equations to a first-order (or linear) and second-order (or weakly nonlinear) assuming small amplitudes for the incident waves and small motions for the floating structure.

The linear approximation of the potential flow problem is described in Section 3, whereas the second-order approximation is described in detail in Section 4. The linear hydrodynamic problem is widely known and well understood in the context applied to WECs (see Sections 3.2 and 3.3 of WG1 WP1 D1b) (Falnes 2002, Evans and Linton 1993, Evans 1981). However, this is not the case for the second-order formulation which is mostly applied to other offshore structures. The second-order problem requires a solution for the hydrodynamic interactions between the fluid and the floating structure at the sum and difference of the frequency of the incident waves. The magnitude of these interactions is normally of second-order and occurs at frequencies away from that of the ambient wave. However, as in the linear case, these depend on the wet surface of the floating structure and should be investigated in detail. Typical examples of second-order problems are sub-harmonic resonance of moored structures and the super-harmonic resonance of tension-leg-platforms.

The review presented in this document is mostly focused on the methods available in WAMIT, which was used in this study to compute the first and second-order hydrodynamic forces and the unrestrained motions associated with a single cylinder and an array with four cylinders in regular and irregular waves. There are no foreseeable differences between the use of this particular software package and other equivalents packages, i.e. the methodology and key findings in this report should be considered representative of generic second-order solutions.

1.2 Purpose of weakly nonlinear hydrodynamic simulations

The key objectives of this exercise are:

- to provide a potentially more accurate solution of the hydrodynamic problem, at the expense of computational effort;
- to compare such solution with other formulations, namely the first-order (linear) and fully nonlinear methodologies;
- to, if proven necessary, create the baseline procedure to use nonlinear excitation forces as input into the software tool(s) developed under PerAWaT.

1.3 Specific tasks associated with WG1 WP1 D8

The computation of the first and second-order hydrodynamic quantities was performed using WAMIT (V61s). GH in-house software was then used, using the nondimensional WAMIT data, to couple the obtained values with six different wave inputs (three regular, three irregular).

Further comparisons were made between the first and second-order solutions. These are directly relevant for WG1 WP1 D9.

1.4 WG1 WP1 D8 acceptance criteria

The acceptance criteria as listed in the Technology Contract and the sections of this report that demonstrate that they have been met are:

1. Results will be calculated and presented for a second-order hydrodynamic response of single uncontrolled axisymmetric device in regular waves, responding in multiple degrees of freedom. In so far as it is possible prior to validation, findings will be discussed and applications and limitations of this approach will be described, including any lesson learned on methodology. – Section 6.

2. Note that in preparation of the WG1 WP1 D9 activities, which follow a fully nonlinear hydrodynamics formulation, second-order results for an array of WECs are also presented in this report (exceeding the acceptance criteria).

2 BRIEF INTRODUCTION TO POTENTIAL FLOW HYDRODYNAMICS

In potential flow theory the fluid is considered to be incompressible, inviscid and surface tension effects are neglected. The flow is irrotational and so the velocity of the fluid ($\vec{v}$) at a certain point $\vec{r} = (x_1, x_2, x_3)$ in a Cartesian coordinate system (fixed in space) and time instant (t) is given by:

$$\vec{v}(\vec{r}, t) = \vec{\nabla}\Phi. \tag{1}$$

The total velocity potential (ϕ) satisfies the Laplace equation in all of the fluid domain:

$$\nabla^2\Phi = 0, \tag{2}$$

and also the boundary conditions at the air-fluid and solid-fluid interfaces that define the problem, i.e. the free-surface, the seabed and the floating structure, respectively. The complete formulation of these boundary conditions is in general difficult to solve and first or second-order approximations are typically used to define the respective hydrodynamic formulation. These are also referred to in the literature as the linear and weakly nonlinear formulations. The first and second-order approximations are detailed in Sections 3 and 4, respectively.

2.1 Boundary conditions

The complete boundary conditions are in general difficult to solve due to the strong nonlinearities involved. At the free-surface interface two boundary conditions can be defined. One known as *dynamic* is required to ensure that the pressure is the same at the air-fluid interface. This condition is derived from the Bernoulli equation and is expressed mathematically as:

$$\frac{\partial\Phi}{\partial t} + \frac{1}{2}\vec{\nabla}\Phi \cdot \vec{\nabla}\Phi + g\, x_3 = 0, \tag{3}$$

where g is the modulus of the acceleration of gravity.

The other boundary condition, known as the *kinematic* condition expresses that the particles at the water-air interface stay within this boundary. Representing the wave elevation by η, this boundary condition can be expressed mathematically as:

$$\frac{d}{dt}(x_3 - \eta) = \frac{\partial\Phi}{\partial x_3} - \frac{\partial\eta}{\partial t} - \frac{\partial\eta}{\partial x_1}\frac{\partial x_1}{\partial t} - \frac{\partial\eta}{\partial x_2}\frac{\partial x_2}{\partial t} - \frac{\partial\eta}{\partial x_3}\frac{\partial x_3}{\partial t} = 0 \quad (\text{on } x_3{=}0). \tag{4}$$

The above Equations (3) and (4) can be combined into a single expression for the *free-surface boundary condition* which is given by:

$$\frac{\partial^2\Phi}{\partial t^2} + g\,\frac{\partial\Phi}{\partial x_3} + 2\,\nabla\Phi\cdot\nabla\frac{\partial\Phi}{\partial t} + \frac{1}{2}\,\nabla\Phi\cdot\nabla\left(\nabla\Phi\cdot\nabla\Phi\right) = 0 \quad (\text{on } x_3{=}0). \tag{5}$$

At all solid boundaries, the normal velocities of the fluid and solid are required to be the same. For bodies in motion this condition is given by:

$$v_n = \vec{\nabla}\Phi\cdot\vec{n} = \frac{\partial\Phi}{\partial n} = u_n = \vec{n}\cdot\vec{u}, \tag{6}$$

where $\vec{n}$ is the normal to the body surface.

On fixed structures, at the seabed or walls, the velocity is zero ($u_n = 0$) and an *impermeability condition* applies:

$$v_n = \frac{\partial \Phi}{\partial n} = 0 \tag{7}$$

To ensure that at distances far away from the fluid domain (i.e. at infinity) the waves are outgoing with a proper amplitude behaviour, a *far-field radiation condition* (Sommerfeld) is imposed such that:

$$\lim_{\varrho \to \infty} \sqrt{\varrho} \left(\frac{\partial}{\partial \varrho} - i\, k \right) \Phi = 0 \tag{8}$$

in which $\varrho = \sqrt{x_1^2 + x_2^2}$ and k the wavenumber.

A time-domain simulation would also require the definition of initial conditions. These normally assume that that the body is at rest and velocity potential is null prior to the simulation time (t<0).

2.2 Hydrodynamic forces

The hydrodynamic forces and moments which result from the interaction of the fluid with a floating structure are obtained through the integration of the fluid pressure (*p)* over the instantaneous wetted profile of the structure as:

$$\vec{f}_h = \iint_{S_B(t)} p(\vec{r})\, \vec{n}\, dS, \tag{9}$$

$$\vec{m}_h = \iint_{S_B(t)} p(\vec{r})\, (\vec{r} \times \vec{n})\, dS. \tag{10}$$

The fluid pressure in these integrals is obtained in terms of velocity potential through the Bernoulli equation:

$$p = -\rho \left(\frac{\partial \Phi}{\partial t} + \frac{1}{2} \vec{\nabla}\Phi \cdot \vec{\nabla}\Phi + g\, x_3 \right). \tag{11}$$

The integration in Equations (9) and (10) is over the instantaneous wetted profile which changes as the structure moves in the fluid. The coupling between the body motion and the instantaneous change of the wetted profile carry mathematical difficulties which are difficult to solve.

The first and second-order approaches overcome this difficulty by approximating the above integrals to an integral over the mean wetted profile of the floating structure at the respective order. The main differences between these approaches are described in Sections 3 and 4 respectively.

2.3 Equations of motion

To conclude this brief introduction to potential flow hydrodynamics, the kinematic equations associated with the motion of a rigid body immersed in a fluid are presented.

A global coordinate system (GCS) located in an inertial Cartesian frame of reference is defined and assumed to be right-handed with the third component pointing upwards and its origin located at the mean water free-surface.

A second coordinate system which moves with the body and has its axis coincident with the GCS when the body is in an undisturbed position is referred to as the Body Fixed Coordinate System (BCS).

To distinguish between the quantities represented in the inertial frame of reference from those in the body-fixed coordinate system (BCS) a tilde is associated with the latter (see Figure 1).

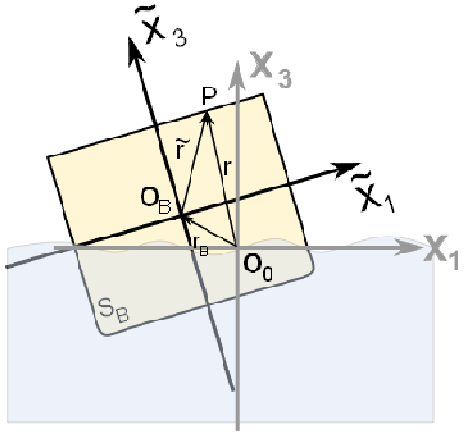

Figure 1: Global and body-fixed coordinate systems

The position vectors in the GCS and BCS are related by the linear transformation:

$$\vec{r} = \vec{r}_B + \vec{\xi} + \mathbf{T}^T \tilde{\vec{r}}, \tag{12}$$

with:

$$\mathbf{T} = \mathbf{T_3}\,\mathbf{T_2}\,\mathbf{T_1} = \begin{bmatrix} \cos\alpha_3 & \sin\alpha_3 & 0 \\ -\sin\alpha_3\ \cos\alpha_3 & 0 & \\ 0 & 0 & 1 \end{bmatrix} \begin{bmatrix} \cos\alpha_2 & 0 & -\sin\alpha_2 \\ 0 & 1 & 0 \\ \sin\alpha_2 & 0 & \cos\alpha_2 \end{bmatrix} \begin{bmatrix} 1 & 0 & 0 \\ 0 & \cos\alpha_1 & \sin\alpha_1 \\ 0 & -\sin\alpha_1 & \cos\alpha_1 \end{bmatrix}. \tag{13}$$

The vectors $\vec{\xi} = (\xi_1, \xi_2, \xi_3)$ and $\vec{\alpha} = (\alpha_1, \alpha_2, \alpha_3)$ in Equations (12) and (13) represent the translational and rotational displacements of the BCS relatively to the GCS. This is equivalent to say that these vectors represent the surge, sway, heave, roll, pitch and yaw motions, respectively.

The velocity associated with a generic point (*P*) in the inertial frame of reference is given by:

$$\vec{u} = \dot{\vec{r}} = \vec{U} + \vec{\Omega} \times \tilde{\vec{r}}, \tag{14}$$

where $\vec{U} = \dot{\vec{r}}_B$ is the velocity of the origin of the BCS, $\vec{\Omega}$ its angular velocity and $\tilde{\vec{r}}$ the position of the same point *P* described in the body fixed coordinate system. The acceleration is given by:

$$\dot{\vec{u}} = \ddot{\vec{r}} = \dot{\vec{U}} + \dot{\vec{\Omega}} \times \left(\vec{\Omega} \times \tilde{\vec{r}}\right) + 2\,\vec{\Omega} \times \vec{U} + \dot{\vec{\Omega}} \times \tilde{\vec{r}}. \tag{15}$$

For a single rigid body the equations of motion can be conveniently expressed in a Newton-Euler formulation as a system of six equations in which three describe the translations and three describe the rotations. This approach retains the physical meaning of each term in the equations, which in an inertial frame of reference can be related to:

$$\left(\frac{d\vec{p}}{dt}\right)_{GCS} = m\,\dot{\vec{u}} = \vec{f}; \tag{16}$$

$$\left(\frac{d\vec{L}}{dt}\right)_{GCS} = \left(\frac{d\vec{L}}{dt}\right)_{BCS} + \vec{\Omega} \times \vec{L} = \vec{m}. \tag{17}$$

In an inertial frame of reference, the variation of linear momentum ($\vec{p}$) is proportional to the acceleration of the centre of mass ($\dot{\vec{u}}$) and equal to the external forces applied to the system ($\vec{f}$). The variation of the angular momentum ($\vec{L}$) relative to any pivot point is equal to the external applied torque ($\vec{m}$) about the same point. In this approach, the constraint forces must be included in the equations of motion and are obtained as part of the solution.

The angular momentum in the body coordinate system can be written as: $\vec{L} = \mathbf{I}\,\vec{\Omega}$ and Equation (17) can be rewritten as:

$$\mathbf{I}\,\dot{\vec{\Omega}} + \vec{\Omega} \times \mathbf{I}\,\vec{\Omega} = \vec{m}. \tag{18}$$

In the present study the only applied forces and moment considered are hydrodynamic and so $\vec{f} = \vec{f}_h$ and $\vec{m} = \vec{m}_h$. Also only unrestrained motions are considered and so there are applied force to such as the power take-off (PTO) or mooring force to take into account.

The major difficulty associated with a fully nonlinear potential flow formulation is related to the solution of the nonlinear free-surface boundary conditions which has to be satisfied over the instantaneous free-surface which is unknown a priori. Most of methods developed use a Mixed Eulerian-Lagrangian (MEL) time stepping technique for which the fully nonlinear boundary conditions are satisfied over the instantaneous free-surface and body surfaces. The unknowns of the linear equations which result from the discretisation of the geometry are distributed on the boundary of the entire computational domain and a new system of equations is generated and solved at each time step, since the free-surface change and the body surface move to new positions. An advantage of second-order method described in Section 4 when compared with the fully nonlinear formulation is that through the approximations involved (and at the potential expense of accuracy) the linear system of equations to solve remains the same throughout the simulations (reducing the computational burden).

3 FIRST-ORDER APPROXIMATION

Linear potential flow theory is used in a variety of offshore engineering problems. This section gives a very brief overview of its fundamental aspects. For more detailed descriptions, see e.g. Newman (1977), Sarpkaya and Isacson (1989), Faltisen (1990) and Falnes (2002).

This theory considers, in addition to the potential flow assumptions described in Section 2, that the amplitudes of both the incident waves and of the motions of the floating structure are small when compared with the incident wavelength.

The total velocity potential is assumed to have an harmonic time dependency ($\Phi = \mathrm{Re}\{\phi\, e^{i\omega t}\}$) and to satisfy the Laplace equation throughout the fluid domain (as per Equation (2)). The boundary conditions are linearised and simplified accordingly.

3.1 Boundary conditions

In the first-order approach the inherent mathematical and numerical difficulties associated with the evaluation of the square of the velocities in Equations (3), (5) and (11) are avoided.

The dynamic and kinematic boundary conditions at the free-surface interface – see Equations (3) and (4) – are simplified in the first-order formulation to:

$$\eta = -\frac{1}{g}\frac{\partial \phi}{\partial t}, \quad \text{on } x_3 = 0; \tag{19}$$

$$\frac{\partial \eta}{\partial t} = \frac{\partial \phi}{\partial x_3}, \quad \text{on } x_3 = 0, \tag{20}$$

where □ is the complex amplitude of the harmonic velocity potential.

These two equations can be combined to express the free-surface boundary condition associated with Equation (5) which is simplified in the first-order formulation to:

$$\frac{\partial^2 \phi}{\partial t^2} + g\,\frac{\partial \phi}{\partial x_3} = 0, \quad \text{on } x_3 = 0. \tag{21}$$

The kinematic boundary condition is given by Equation (6) takes into account the first-order approximation of the body motions and is given by:

$$\frac{\partial \phi}{\partial n} = u_n = \vec{n}\cdot\vec{u} = \vec{n}\cdot\left(\vec{U} + \vec{\Omega}\times\tilde{\vec{r}}\right) = \vec{U}\cdot\vec{n} + \vec{\Omega}\cdot\tilde{\vec{r}}\times\vec{n} = i\omega\,\xi_j\,n_j. \tag{22}$$

Note that u_n is the normal component of the velocity at a surface element of the body which by assuming harmonic displacements is conveniently defined as a six dimensional generalised vector with components given by:

$$(\vec{n})_k = \begin{cases} n_k & \text{for } k = 1,2,3 \\ \left(\tilde{\vec{r}}\times\vec{n}\right)_{k-3} & \text{for } k = 4,5,6 \end{cases}$$

3.2 Hydrodynamic forces

The hydrodynamic forces and moments are obtained through the integration of the pressure over the wetted profile of the body as given by Equations (9) and (10), with the pressure being given by the first-order approximation of the Bernoulli equation:

$$p = -\rho \left(\frac{\partial \phi}{\partial t} + g\, x_3 \right). \tag{23}$$

The second term in Equation (23) is associated with the hydrostatic forces and moments. The hydrostatic force is given by:

$$\begin{pmatrix} \vec{f}_C \\ \vec{m}_C \end{pmatrix} = -\rho\, g \iint_{S_B} x_3 \begin{pmatrix} \vec{n} \\ \tilde{\vec{r}} \times \vec{n} \end{pmatrix} dS. \tag{24}$$

Under the first-order approximation, the integral over the instantaneous wetted profile in Equation (24) is approximated to a static integral over the mean wetted profile. By assuming small motions the integral in Equation (24) is evaluated in terms of the body-fixed coordinates and by using Stokes theorem converted to a volume integral.

The instantaneous volume is then decomposed into a static volume beneath the still water plane and a thin layer bounded by the planes between the body-fixed and inertial coordinate systems.

The linear hydrostatic force and moment are proportional to the displacements, represented in matrix form as:

$$[\vec{f}_C; \vec{m}_C] = -\mathbf{C}\, \vec{\xi}, \tag{25}$$

where **C** is a matrix with the hydrostatic coefficients which are a function of water plane areas, moments and centres of buoyancy of the structure.

To compute ϕ in Equation (23), and under the previously described assumptions, it is possible to decouple the problem and consider two distinct contributions associated with the interactions between the floating structure and the incoming wave field, respectively.

These separate contributions are commonly referred to as the solutions of the diffraction and of the radiation problems, and correspond respectively to: 1) the study of the interactions of the incident waves with the body held fixed and 2) the study of the interactions due to forced motions of the body in calm water.

Under the above assumption, ϕ can be given by:

$$\phi = \phi_I + \phi_D + \phi_R, \tag{26}$$

where the indices *I*, *D* and *R* refer to the incident, diffracted and radiated velocity potentials, respectively. Note that the sum of the *I* and *D* components is often referred to as the excitation potential.

The velocity potential (ϕ_I) due to a regular incident wave of frequency ω is computed by solving the Laplace equation in the absence of the structure, resulting in:

$$\phi_I = \frac{i\,g\,a}{\omega}\,\frac{\cosh k\ (x_3 + z_0)}{\cosh k\,z_0}\,e^{-i\,\vec{k}\cdot\vec{r}}, \tag{27}$$

with k being the wavenumber ($k = 2\,\pi/\lambda$), which satisfies the dispersion relation:

$$\omega^2 = g\,k\,\tanh\,(k\,z_0). \tag{28}$$

The first-order approximation assumes that the motions of the floating structure are sufficiently small so that the radiated potential (ϕ_R) is proportionally small (Newman, 1970) and given by:

$$\phi_R = Re\Big\{\sum_j^6 \xi_j(t)\,\phi_j(\vec{x})\Big\} \tag{29}$$

The force and moment due to the radiated waves are obtained by substituting Equation (29) into the linearised Bernoulli equation (Equations (23)) and into the hydrodynamic pressure integral (Equations (9) and (10)). The radiation force is given by:

$$\begin{aligned}\begin{pmatrix}\vec{f}_R(t)\\ \vec{m}_R(t)\end{pmatrix} &= -\,\rho\iint_{S_B}\frac{\partial\phi_R}{\partial t}\begin{pmatrix}\vec{n}\\ \vec{\tilde{r}}\times\vec{n}\end{pmatrix}dS = \\ &= -\,\rho\,Re\Big\{\sum_j^6 i\,\omega\xi_j(t)\iint_{S_B}\phi_j(\vec{x})\begin{pmatrix}\vec{n}\\ \vec{\tilde{r}}\times\vec{n}\end{pmatrix}dS\Big\} = \\ &= Re\Big\{\omega^2\,\mathbf{A}\,\vec{\xi} - i\,\omega\,\mathbf{B}\,\vec{\xi}\Big\}\end{aligned} \tag{30}$$

The matrices **A** and **B** represent the added-mass and radiation damping coefficients (respectively) and these depend on the wetted profile of the body, the period of the incident wave and the water depth.

The excitation (or scattered) potential is given by $\phi_S = \phi_I + \phi_D$. In a first-order approximation this is proportional to the amplitude of the incident wave (a):

$$\phi_S = Re\,\{a\,(\phi_I + \phi_D)\,e^{i\,\omega\,t}\}. \tag{31}$$

Substituting Equation (31) into Equations (23), (9) and (10), the excitation force (and moments) are given by:

$$\begin{pmatrix}\vec{f}_X\\ \vec{m}_X\end{pmatrix} = Re\,\Big\{a\,\vec{X}\,e^{i\,\omega\,t}\Big\} \tag{32}$$

where $\vec{X}$ is the complex amplitude vector of the excitation force or moment with their respective components:

$$X_j = -\rho\iint_{S_b}(\phi_I + \phi_D)\,\frac{\partial\phi_j}{\partial n}\,dS \tag{33}$$

The computation of the hydrodynamic forces and moments is thus reduced to the computation of the velocity potential and the surface integrals in Equations (33) and (30).

3.3 Velocity potential

The outline of the method used in the potential flow solver used in this study (WAMIT) to compute the velocity potential is detailed in e.g. Newman and Sclavounos (1988). It is based on the solution of integral equations computed on the wetted profile of the body by applying the Green theorem to source potentials defined by Green functions (G).

These integral equations are solved for the velocity potentials of the radiation and diffraction problems associated with Equation (26). The velocity potential due to the radiation problem is computed by solving:

$$2\,\pi\,\phi_k(\vec{x}) + \iint_{S_b} \phi_k(\vec{\sigma})\,\frac{\partial G(\vec{\sigma};\vec{x})}{\partial n_\sigma}\,dS_\sigma = \iint_{S_b} n_k\,G(\vec{\sigma};\vec{x})\,dS_\sigma, \tag{34}$$

and the diffraction potential is obtained by solving:

$$2\,\pi\,\phi_D(\vec{x}) + \iint_{S_b} \phi_D(\vec{\sigma})\,\frac{\partial G(\vec{\sigma};\vec{x})}{\partial n_\sigma}\,dS_\sigma = 4\,\pi\,\phi_0(\vec{x}), \tag{35}$$

in which the source potential or Green function for infinite water depth[1] in the surface of the floating body is given by:

$$G(\vec{x};\vec{\sigma}) = \frac{1}{r} + \frac{1}{r'} + \frac{2\,\omega^2}{g\,\pi}\int_0^\infty \frac{\exp\left(k(x_3+\sigma_3)\right)}{k-\omega^2/g}\,J_0(kR)\,dk, \tag{36}$$

with:

$$r^2 = (x_1-\sigma_1)^2 + (x_2-\sigma_2)^2 + (x_3-\sigma_3)^2;$$

$$r'^2 = (x_1-\sigma_1)^2 + (x_2-\sigma_2)^2 + (x_3+\sigma_3)^2,$$

where $\vec{\sigma} = (\sigma_1, \sigma_2, \sigma_3)$ is the position of the source of constant strength 4π and $J_0(x)$ the Bessel function of zero order. The irregular frequencies are removed from the velocity potential by extending the boundary integral equations (WAMIT2006).

The numerical solutions of the above integral equations require the wetted profile of the floating structure to be discretised. A low-order method was originally developed to describe the wetted profile using flat panels assuming in each a constant velocity potential and velocity normal at its centre. Higher-order methods have since been devised that allow a continuous representation of the velocity potential through functions which normally are polynomials of order higher than two. WAMIT uses B-spline functions to represent the velocity potential as a continuous function over the wetted profile

[1] For finite water depth the source potential assumes a different expression as given for example by Wehausen and Laiton (1960).

of the body. These are parameterised, smooth and continuous functions defined piecewise through a set of control points and base polynomials which are defined recursively and represent complex curves in an efficient way. The higher-order method (when compared with the lower-order with a comparable discretisation) achieves in general a faster convergence and higher accuracy (Lee et. al. 1996, 1998). Previous applications of both methods to WEC modelling have been presented in Section 3.2 of WG1 WP1 D1b.

3.4 Equations of motion

The linearisation of Equation (17) implies that $\vec{m} \approx \mathbf{I}\,\dot{\vec{\Omega}}$ and the inertia matrix is included into a mass matrix as explained in Newman (1977). Assuming that the only forces and moments in the system are the hydrodynamic components and substituting these into the equations of motion, a linear system of six equations is obtained, leading to:

$$\left[-\omega^2\left(\mathbf{M}+\mathbf{A}\right)+i\omega\,\mathbf{B}+\mathbf{C}\right]\vec{\xi}=a\vec{X} \qquad (37)$$

where **M** is the (6x6) mass matrix, **A**, **B** and **C** are the added mass, radiation damping and hydrostatic stiffness (6x6) matrices respectively; $\vec{\xi}$ the complex amplitude vector (6 component) of the body displacements; $\vec{X}$ the complex amplitude of the hydrodynamic excitation forces and moments; and *a* the amplitude of the incident waves.

The ratio $\vec{\xi}/a$ is the complex amplitude of motion in response to an incident wave. This quantity is a transfer function of the linear system and commonly known as the response amplitude operator or RAO.

4 SECOND-ORDER APPROXIMATION

Second-order, weakly nonlinear hydrodynamic theory assumes, as in the first-order case (Section 3), small amplitudes for the incident waves and motions in comparison with the wavelength of the incident wave. However, this theory takes into account a more detailed representation of the velocity potential (ϕ) and all derived variables by considering a second-order approximation through a Taylor expansion series about the mean positions.

The total velocity potential ϕ is given by a perturbation series in the parameter ε as:

$$\phi = \varepsilon\,\phi^{(1)} + \varepsilon^2\,\phi^{(2)} + \ldots \tag{38}$$

in which ε is a small quantity related to the wave-slope. For a regular wave this parameter is given by $\varepsilon = k\,a = 2\,\pi\,a/\lambda \ll 1$ with *k* satisfying the dispersion relation given by $\omega^2 = g\,k\,\tanh(k\,z_0)$.[2]

To generalise the second-order theory to wave-body interactions with irregular incident waves, it is sufficient to consider the general problem of the interaction of the structure with an arbitrary bi-chromatic pair of incident wave components (Kim, 1990).

In the presence of two plane incident waves with frequencies ω_1 and ω_2, the first-order velocity potential (bi-chromatic) is given by:

$$\phi^{(1)}(\vec{x},t) = Re\left\{\sum_{j=1}^{2}\phi_j^{(1)}(\vec{x})\,e^{i\,\omega_j\,t}\right\} \tag{39}$$

whereas the second-order potential is written in terms of the superposition of the sum and difference frequency terms:

$$\phi^{(2)}(\vec{x},t) = Re\left\{\sum_{j=1}^{2}\sum_{k=1}^{2}\phi_{jk}^{+}(\vec{x})\,e^{i\,\omega_{jk}^{+}\,t} + \phi_{jk}^{-}(\vec{x})\,e^{i\,\omega_{jk}^{-}\,t}\right\} \tag{40}$$

where $\phi_{jk}^{\pm}$ are the sum (+) and difference (-) frequency potentials at the sum and difference frequencies: $\omega_{jk}^{+} = \omega_j + \omega_k$ and $\omega_{jk}^{-} = \omega_j - \omega_k$, respectively. The functions $\phi^{\pm}$ satisfy the symmetry relations: $\phi_{jk}^{+} = \phi_{kj}^{+}$ and $\phi_{jk}^{-} = \phi_{kj}^{-\,*}$ (where the (*) refers to the complex conjugate).

To simplify the description of the problem, Equation (40) assumes that the waves are directly incident upon the floating structure. If a directional spreading of the incident waves is to be considered, the

[2] In deep-water the maximum wave steepness achieved by a non-breaking wave is approximately equal to $(2\,a)/\lambda < 0.142$. Thus at the wave breaking limit, $\varepsilon_{break} = 0.142\,\pi = 0.446$ which is at least one order of magnitude higher than the hypothesis used in Equation (38). To have $\varepsilon < 0.1$ it is required that the wave steepness to be at least $(2\,a)/\lambda < 0.032$.

sum and difference velocity potential ($\phi_{jl}^{\pm}(\vec{x})$) should be represented instead by a double summation over the wave headings (β_j, β_l).

Note that ϕ (composed of the first and second-order approximations) should satisfy the Laplace equation given by Equation (2) and the boundary conditions set out by Equations (5), (6), (7) and (8) under the second-order approximation (see Section 4.1).

4.1 Boundary conditions

The expansion in terms of Taylor series of the free-surface elevation and body motions as in Equation (38) allows the boundary value problem at each order to be considered independently and the velocity potential to be decomposed in terms of the incident (ϕ_I), diffracted (ϕ_D) and radiation (ϕ_R) potentials:

$$\phi = \varepsilon \left(\phi_I^{(1)} + \phi_D^{(1)} + \phi_R^{(1)}\right) + \varepsilon^2 \left(\phi_I^{(2)} + \phi_D^{(2)} + \phi_R^{(2)}\right) + \ldots \tag{41}$$

The first-order problem and the methods to compute the first-order potentials were described in Section 3. At second-order a similar decomposition of the velocity potential is performed. The second-order excitation potential $\phi_S^{(2)} = \phi_I^{(2)} + \phi_D^{(2)}$ collects all the terms associated with the second-order influence of the incident and diffracted waves and the forcing of all quadratic contributions of the first-order quantities. The second-order radiation potential ($\phi_R^{(2)}$) collects all the contributions of outgoing waves due to second-order motions in the absence of ambient waves or first-order disturbances.

It should be noted that the described decomposition is not unique. It is however advantageous as all the 'difficult' second-order effects are confined to the diffraction problem whereas the second-order radiation problem is identical to the first-order but at the respective sum and difference frequencies.

The knowledge of the first-order potentials is necessary to specify the forcing terms of the inhomogeneous free-surface (Q_F) and body boundary conditions (Q_B) associated with the second-order problem.

The *inhomogeneous free-surface condition* for the total second-order potential is given by:

$$\left(\frac{\partial^2}{\partial t^2} + g\frac{\partial}{\partial x_3}\right)\phi^{(2)} = Q_F, \tag{42}$$

with the quadratic forcing function (Q_F) evaluated at the mean free-surface $x_3 = 0$ and given by:

$$Q_F = \frac{1}{g}\frac{\partial\phi^{(1)}}{\partial t}\frac{\partial}{\partial x_3}\left(\frac{\partial^2\phi^{(1)}}{\partial t^2} + g\frac{\partial\phi^{(1)}}{\partial x_3}\right) - \frac{\partial}{\partial t}\left(\nabla\phi^{(1)}\right)^2. \tag{43}$$

The *body boundary condition* is evaluated at the mean body boundary and is expressed by:

$$\frac{\partial\phi^{(2)}}{\partial n} = Q_B(\vec{x}, t), \tag{44}$$

with the forcing function on the body boundary given by:

$$Q_B = -\frac{\partial \phi_I^{(2)}}{\partial n} + \vec{n}\cdot\dot{\mathbf{H}}\tilde{\vec{r}} + \left(\alpha^{(1)}\times\vec{n}\right)\cdot\left(\dot{\vec{\xi}}^{(1)} + \dot{\vec{\alpha}}^{(1)}\times\tilde{\vec{r}} - \vec{\nabla}\phi^{(1)}\right) - \vec{n}\cdot\left(\left(\vec{\xi}^{(1)} + \vec{\alpha}^{(1)}\times\tilde{\vec{r}}\right)\cdot\vec{\nabla}\right)\vec{\nabla}\phi^{(1)} + \sum_{k=1}^{6}\dot{\xi}_k\, n_k \quad (45)$$

The matrix **H** in Equation (45) results from the second-order approximation of the transformation between the body fixed coordinate system and corresponds to:

$$\mathbf{H} = \begin{bmatrix} -\frac{1}{2}\left[(\alpha_2)^2 + (\alpha_3)^2\right] & 0 & 0 \\ \alpha_1\alpha_2 & -\frac{1}{2}\left[(\alpha_1)^2 + (\alpha_3)^2\right] & 0 \\ \alpha_1\alpha_3 & \alpha_2\alpha_3 & -\frac{1}{2}\left[(\alpha_1)^2 + (\alpha_2)^2\right] \end{bmatrix}, \quad (46)$$

where in the above equations $\vec{\xi}$ and $\vec{\alpha}$ are associated with the translational and angular displacements between the body fixed coordinate system and the inertial coordinate system.

4.2 Velocity potential

To simplify the description the incident wave is assumed to be unidirectional and the water depth (z_0) uniform. The *first-order incident potential* ($\phi_I^{(1)}$) satisfies the Laplace equation and the boundary conditions as described in Section 3, but is given here for a bi-chromatic wave[3] at frequencies ω_1 and ω_2 while satisfying the dispersion relation:

$$\phi_I^{(1)} = \sum_{j=1}^{2} \frac{i\,g\,a_j}{\omega_j}\,\frac{\cosh k_j\,(x_3 + z_0)}{\cosh k_j\, z_0}\, e^{i\,k_j\,x_1}. \quad (47)$$

The second-order incident potential ($\phi_I^{(2)}$) satisfies the Laplace equation ($\nabla^2\phi_I^{(2)} = 0$), the non-porous bottom condition at the seabed ($\left(\frac{\partial\phi_I^{(2)}}{\partial n}\right)_{x_3=-z_0} = 0$) and the nonlinear free-surface condition given by Equation (42).

The sum and difference frequency second-order incident wave potentials ϕ_I^+ and ϕ_I^- are obtained by taking into account Equation (40) and substituting Equations (39) and (47) into Equation (42), resulting in:

$$\phi_I^+ = \frac{1}{2}\left(\gamma_{jl}^+ + \gamma_{lj}^+\right)\frac{\cosh(k^+(x_3 + z_0))}{\cosh(k^+\, z_0)}\, e^{i\,k^+\,x_1}, \quad (48)$$

[3] Note that in the limit of a single regular wave $\omega_j \to \omega_l$, and the bi-chromatic wave reduces to the second-order uniform stokes wave.

$$\phi_I^- = \frac{1}{2}\left(\gamma_{jl}^- + \gamma_{lj}^{-^*}\right)\frac{\cosh(k^-(x_3+z_0))}{\cosh(k^- z_0)}\, e^{i\,k^-\,x_1}, \tag{49}$$

with $k^\pm = k_j \pm k_l$ satisfying the dispersion relation $(\omega^\pm)^2 = g\,k^\pm\,\tanh\left(k^\pm\,z_0\right)$ and the $\gamma^\pm$ functions given by:

$$\gamma_{jl}^+ = \frac{i\,g\,a_j\,a_l}{2\,\omega_j}\,\frac{k_j^2\left(1-\tanh^2(k_j\,z_0)\right)+2\,k_j\,k_l\left(1-\tanh(k_j\,z_0)\,\tanh(k_l\,z_0)\right)}{\left(\omega_j+\omega_l\right)^2/g - k^+\,\tanh(k^+\,z_0)}; \tag{50}$$

$$\gamma_{jl}^- = \frac{i\,g\,a_j\,a_l^*}{2\,\omega_j}\,\frac{k_j^2\left(1-\tanh^2(k_j\,z_0)\right)+2\,k_j\,k_l\left(1+\tanh(k_j\,z_0)\,\tanh(k_l\,z_0)\right)}{\left(\omega_j-\omega_l\right)^2/g - k^-\,\tanh(k^-\,z_0)}. \tag{51}$$

The forcing functions Q_F and Q_B given by Equations (43) and (45) are then described in terms of the sum and difference frequencies by (see Lee, 1995):

$$Q_F^+ = \frac{i}{4\,g}\,\omega_k\,\phi_k\left(-\omega_l^2\frac{\partial\phi_l}{\partial x_3}+g\,\frac{\partial^2\phi_l}{\partial x_3^2}\right)+\frac{i}{4\,g}\,\omega_l\,\phi_l\left(-\omega_k^2\frac{\partial\phi_k}{\partial x_3}+g\,\frac{\partial^2\phi_k}{\partial x_3^2}\right)-\frac{1}{2}\,i\,(\omega_k+\omega_l)\,\vec{\nabla}\phi_k\cdot\vec{\nabla}\phi_l; \tag{52}$$

$$Q_F^- = \frac{i}{4\,g}\,\omega_k\,\phi_k\left(-\omega_l^2\frac{\partial\phi_l^*}{\partial x_3}+g\,\frac{\partial^2\phi_l^*}{\partial x_3^2}\right)-\frac{i}{4\,g}\,\omega_l^*\,\phi_l\left(-\omega_k^2\frac{\partial\phi_k}{\partial x_3}+g\,\frac{\partial^2\phi_k}{\partial x_3^2}\right)-\frac{1}{2}\,i\,(\omega_k+\omega_l)\,\vec{\nabla}\phi_k\cdot\vec{\nabla}\phi_l^*; \tag{53}$$

and:

$$\begin{aligned} Q_B^+ = &-\frac{\partial\phi_I^+}{\partial n}+\frac{i\,(\omega_k+\omega_l)}{2}\vec{n}\cdot\dot{\mathbf{H}}^+\vec{\tilde{r}} \\ &+\frac{i}{4}\left[(\vec{\alpha}_k\times\vec{n})\cdot\left(\omega_l\,\left(\vec{\xi}_l+\vec{\alpha}_l\times\vec{\tilde{r}}\right)-\vec{\nabla}\phi_l\right)+(\vec{\alpha}_l\times\vec{n})\cdot\left(\omega_k\left(\vec{\xi}_k+\vec{\alpha}_k\times\vec{\tilde{r}}\right)-\vec{\nabla}\phi_k\right)\right]; \\ &-\frac{1}{4}\vec{n}\cdot\left[\left(\left(\vec{\xi}_k+\vec{\alpha}_k\times\vec{\tilde{r}}\right)\cdot\vec{\nabla}\right)\nabla\phi_l+\left(\left(\vec{\xi}_l+\vec{\alpha}_l\times\vec{\tilde{r}}\right)\cdot\vec{\nabla}\right)\nabla\phi_k\right] \end{aligned} \tag{54}$$

$$\begin{aligned} Q_B^- = &-\frac{\partial\phi_I^-}{\partial n}+\frac{i\,(\omega_k-\omega_l)}{2}\vec{n}\cdot\dot{\mathbf{H}}^-\vec{\tilde{r}} \\ &+\frac{i}{4}\left[(\vec{\alpha}_k\times\vec{n})\cdot\left(\omega_l\,\left(\vec{\xi}_l^*+\vec{\alpha}_l^*\times\vec{\tilde{r}}\right)-\vec{\nabla}\phi_l^*\right)+(\vec{\alpha}_l^*\times\vec{n})\cdot\left(\omega_k\left(\vec{\xi}_k+\vec{\alpha}_k\times\vec{\tilde{r}}\right)-\vec{\nabla}\phi_k\right)\right]; \\ &-\frac{1}{4}\vec{n}\cdot\left[\left(\left(\vec{\xi}_k+\vec{\alpha}_k\times\vec{\tilde{r}}\right)\cdot\vec{\nabla}\right)\nabla\phi_l^*+\left(\left(\vec{\xi}_l^*+\vec{\alpha}_l^*\times\vec{\tilde{r}}\right)\cdot\vec{\nabla}\right)\nabla\phi_k\right] \end{aligned} \tag{55}$$

with:

$$\mathbf{H}^+ = \frac{1}{2}\begin{bmatrix} -\alpha_{2_k}\,\alpha_{2_l}-\alpha_{3_k}\,\alpha_{3_l} & 0 & 0 \\ \alpha_{1_k}\alpha_{2_l}+\alpha_{1_l}\alpha_{2_k} & -\alpha_{1_k}\,\alpha_{1_l}+\alpha_{3_k}\,\alpha_{3_l} & 0 \\ \alpha_{1_k}\alpha_{3_l}+\alpha_{1_l}\alpha_{3_k} & \alpha_{2_k}\alpha_{3_l}+\alpha_{2_l}\alpha_{3_k} & -\alpha_{1_k}\,\alpha_{1_l}+\alpha_{2_k}\,\alpha_{2_l} \end{bmatrix}; \tag{56}$$

$$\mathbf{H}^- = \frac{1}{2}\begin{bmatrix} -\alpha_{2_k}\,\alpha_{2_l}^*-\alpha_{3_k}\,\alpha_{3_l}^* & 0 & 0 \\ \alpha_{1_k}\alpha_{2_l}^*+\alpha_{1_l}^*\alpha_{2_k} & -\alpha_{1_k}\,\alpha_{1_l}^*+\alpha_{3_k}\,\alpha_{3_l}^* & 0 \\ \alpha_{1_k}\alpha_{3_l}^*+\alpha_{1_l}^*\alpha_{3_k} & \alpha_{2_k}\alpha_{3_l}^*+\alpha_{2_l}^*\alpha_{3_k} & -\alpha_{1_k}\,\alpha_{1_l}^*+\alpha_{2_k}\,\alpha_{2_l}^* \end{bmatrix}. \tag{57}$$

Note that in the above expressions the symmetry relations $Q_{kl}^{+} = Q_{lk}^{+}$ and $Q_{kl}^{-} = Q_{lk}^{-*}$ apply.

In Equations (54) and (55) the sum and difference components of the last term of Equation (45) were omitted since they are not a quadratic function of the first-order solution. These are proportional to the second-order motions and can be treated separately from the rest of body forcing.

The second-order potential ($\phi^{(2)}$) in Equations (42) and (44) is decomposed into three components in the sum and difference frequencies associated with the incident, diffracted and radiation as:

$$\phi^{\pm} = \phi_I^{\pm} + \phi_D^{\pm} + \phi_R^{\pm}. \tag{58}$$

The radiation potential $\phi_R^{\pm}$ describes the disturbance associated with the second-order motions of the floating structure. Assuming an incident wave with small amplitude, at second-order the motions are proportionally small and the radiation potential in the sum and difference frequencies is given by:

$$\phi_R^{\pm}(t) = \sum_j \xi_j^{\pm}(t)\, \phi^{\pm}(\vec{x}). \tag{59}$$

4.3 Scattering potential: boundary-integral equation for the sum and difference frequency second-order potentials

Panel methods can be used to solve the second-order velocity potential. The integral equation method is extended to second-order and includes the forcing terms ($Q_F^{\pm}$ and $Q_B^{\pm}$) given as first-order quantities:

$$2\,\pi\,\phi_S^{\pm}(\vec{x}) + \iint_{S_B} \phi_S^{\pm}(\vec{\sigma})\,\frac{\partial G^{\pm}(\vec{x};\vec{\sigma})}{\partial\, n_\sigma}\,dS = \iint_{S_B} Q_B^{\pm}(\vec{\sigma})\, G^{\pm}(\vec{x};\vec{\sigma})\,dS + \frac{1}{g}\iint_{S_F} Q_F^{\pm}(\vec{\sigma})\, G^{\pm}(\vec{x};\vec{\sigma})\,dS \tag{60}$$

The excitation (or scattering) potential ($\phi_S^{\pm}$) is obtained as a solution of the Green integral equation and the same equation with 2π substituted by 4π gives the solution for ($\phi_S^{\pm}$) in the fluid domain.

The left-hand side of Equation (60) is identical to the integral equation for the first-order potential and is solved with the methods developed for the computation of the first-order velocity potential.

The forcing terms in Equation (60) which corresponds to the right-hand side integrals are calculated in a piecewise manner by using flat panels as in the low-order method.

The first integral of the right hand-side of Equation (60) is evaluated over the wetted profile of the body (S_B) by numerical methods described in detail in Lee (1991; 1993). The second integral of the right hand-side of Equation (60) is evaluated over the free-surface which is discretised into quadrilateral flat panels and evaluated separately into two separate domains. A partition circle (of radius ϱ_0) is defined such to enclose the body and its local disturbance and that the effect of the evanescent waves outside the circle can be neglected. To reduce the computational burden, the inner region is further subdivided into two or more parts separated with a circle of radius $\varrho_1 (< \varrho_2 < \ldots < \varrho_0)$ which is large enough to enclose the body surface. For the region close to the body ($\varrho < \varrho_1$), the integration is carried out by numerical quadratures at each panel centre whereas in the annular region between $\varrho_1 < \varrho < \varrho_0$ and away from the body a more efficient procedure integration is used (Gauss-Chebychev quadrature in the azimuthal direction and Gauss-Legendre quadrature in the radial direction).

4.4 Hydrodynamic forces

At second-order, the fluid pressure given by the Bernoulli Equation (11) is fully taken into account.

However, the hydrodynamic forces and moments - Equations (9) and (10) - which result from the integration of the pressure over the instantaneous wet surface are approximated to second-order and the integral is taken instead over the mean wetted profile S_B.

By collecting the first and second-order quantities at each order, the second-order forces or moments due to the second-order incident and diffracted wave potential are given respectively by:

$$\begin{pmatrix} \vec{f}_I^{(2)} \\ \vec{m}_I^{(2)} \end{pmatrix} = -\rho_0 \iint_{S_B} \frac{\partial \phi_I^{(2)}}{\partial t} \begin{pmatrix} \vec{n} \\ \vec{r} \times \vec{n} \end{pmatrix} dS \tag{61}$$

and:

$$\begin{pmatrix} \vec{f}_D^{(2)} \\ \vec{m}_D^{(2)} \end{pmatrix} = -\rho_0 \iint_{S_B} \frac{\partial \phi_D^{(2)}}{\partial t} \begin{pmatrix} \vec{n} \\ \vec{r} \times \vec{n} \end{pmatrix} dS \tag{62}$$

The sum of these two quantities is defined as the second-order potential force and moment:

$$\begin{pmatrix} \vec{f}_p^{(2)} \\ \vec{m}_p^{(2)} \end{pmatrix} = \begin{pmatrix} \vec{f}_I^{(2)} + \vec{f}_D^{(2)} \\ \vec{m}_I^{(2)} + \vec{m}_D^{(2)} \end{pmatrix} \tag{63}$$

The components of the hydrodynamic forces and moments associated to the quadractic products of first-order quantities are known as the quadratic second-order forces and moments. These are given by:

$$\begin{aligned} \vec{f}_q^{(2)} = & -\rho_0 \iint_{S_B} \left[\frac{1}{2} \vec{\nabla} \phi^{(1)} \cdot \vec{\nabla} \phi^{(1)} + \left(\vec{\xi}^{(1)} + \vec{\alpha}^{(1)} \times \vec{r} \right) \cdot \frac{\partial}{\partial t} \vec{\nabla} \phi^{(1)} \right] \vec{n} \, dS \\ & + \frac{1}{2} \rho_0 \, g \int_{WL} (\eta_r^{(1)})^2 \, \vec{N} \, dl + \vec{\alpha}^{(1)} \times \vec{f}_h^{(1)} \\ & - \rho_0 \, g \, A_w \left[\alpha_1^{(1)} \, \alpha_3^{(1)} \, x_{1_f} + \alpha_2^{(1)} \, \alpha_3^{(1)} \, x_{2_f} + \frac{1}{2} \left[\left(\alpha_1^{(1)} \right)^2 + \left(\alpha_2^{(1)} \right)^2 \right] Z_0 \right] \vec{k} \end{aligned} \tag{64}$$

and:

$$\begin{aligned} \vec{m}_q^{(2)} = & -\rho_0 \iint_{S_B} \left[\tfrac{1}{2} \vec{\nabla} \phi^{(1)} \cdot \vec{\nabla} \phi^{(1)} + \left(\vec{\xi}^{(1)} + \vec{\alpha}^{(1)} \times \vec{r} \right) \cdot \tfrac{\partial}{\partial t} \vec{\nabla} \phi^{(1)} \right] (\vec{r} \times \vec{n}) \, dS + \tfrac{1}{2} \rho_0 \, g \int_{WL} (\eta_r^{(1)})^2 \left(\vec{r} \times \vec{N} \right) dl \\ & + \vec{\xi}^{(1)} \times \vec{f}_h^{(1)} + \vec{\alpha}^{(1)} \times \vec{m}_h^{(1)} \\ & + \rho_0 \, g \left[-\forall \, \xi_1^{(1)} \, \alpha_3^{(1)} + \forall \, \alpha_1^{(1)} \, \alpha_2^{(1)} \, x_{1_b} - \forall \, \alpha_2^{(1)} \, \alpha_3^{(1)} \, x_{3_b} - \tfrac{1}{2} \left[\left(\alpha_1^{(1)} \right)^2 - \left(\alpha_3^{(1)} \right)^2 \right] x_{2_b} \right. \\ & \left. - \alpha_1^{(1)} \, \alpha_3^{(1)} \, L_{12} - \alpha_2^{(1)} \, \alpha_3^{(1)} \, L_{22} - \tfrac{1}{2} \left[\left(\alpha_1^{(1)} \right)^2 + \left(\alpha_2^{(1)} \right)^2 \right] Z_0 \, A_w \, x_{2_f} \right] \vec{i} \\ & + \rho_0 \, g \left[-\forall \, \xi_2^{(1)} \, \alpha_3^{(1)} + \forall \, \alpha_1^{(1)} \, \alpha_3^{(1)} \, x_{3_b} + \tfrac{1}{2} \left[\left(\alpha_2^{(1)} \right)^2 - \left(\alpha_3^{(1)} \right)^2 \right] x_{1_b} \right. \\ & \left. + \alpha_1^{(1)} \, \alpha_3^{(1)} \, L_{11} + \alpha_2^{(1)} \, \alpha_3^{(1)} \, L_{12} + \tfrac{1}{2} \left[\left(\alpha_1^{(1)} \right)^2 + \left(\alpha_2^{(1)} \right)^2 \right] Z_0 \, A_w \, x_{1_f} \right] \vec{j} \\ & + \rho_0 \forall \, g \left[\xi_1^{(1)} \, \alpha_1^{(1)} + \xi_2^{(1)} \, \alpha_2^{(1)} + \alpha_2^{(1)} \, \alpha_3^{(1)} \, x_{1_b} + \alpha_1^{(1)} \, \alpha_3^{(1)} \, x_{2_b} \right] \vec{k} \end{aligned} \tag{65}$$

In the above equations the first-order relative wave height is defined as $\eta_r^{(1)} = \eta^{(1)} - \xi_3^{(1)} + (\vec{r} \times \vec{\alpha})_3$ and vector $\vec{N} = \vec{n}/\sqrt{(1-n_3^2)}$. The water plane area is A_w and the water plane moments are given by: $L_{ij} = \iint_{A_w} x_i \, x_j \, dS$. The second-order wave excitation force and moments are defined as the sum of the second-order potential force and moments with the quadratic second-order force and moments:

$$\vec{f}_X^{(2)} = \vec{f}_p^{(2)} + \vec{f}_q^{(2)} = \vec{f}_I^{(2)} + \vec{f}_D^{(2)} + \vec{f}_q^{(2)} \tag{66}$$

In the presence of bi-chromatic waves the second-order wave excitation force can be expressed at the sum and difference frequencies by (Kim, 1990):

$$\vec{f}_X^{(2)}(t) = Re\{\sum_k^N \sum_l^N \left[a_k \, a_l \, \vec{f}_{kl}^{+} \, e^{i\,\omega_{kl}^{+}\,t} + a_k \, a_l^* \, f_{kl}^{-} \, e^{i\,\omega_{kl}^{-}\,t} \right], \tag{67}$$

where: $\vec{f}_{kl}^{\pm} = \vec{f}_{q_{kl}}^{\pm} + \vec{f}_{p_{kl}}^{\pm}$ are the complete sum- and difference-frequency excitation force also known as quadratic transfer function (or QTF's) at the sum- and difference-frequencies, $\omega_{jk}^{+} = \omega_j + \omega_k$ and $\omega_{jk}^{-} = \omega_j - \omega_k$ respectively.

The second-order force and moments related to the radiation potential are given by:

$$\begin{pmatrix} \vec{f}_R^{(2)} \\ \vec{m}_R^{(2)} \end{pmatrix} = -\rho_0 \iint_{S_B} \frac{\partial \phi_R^{(2)}}{\partial t} \begin{pmatrix} \vec{n} \\ \vec{r} \times \vec{n} \end{pmatrix} dS. \tag{68}$$

In addition, the second-order radiation potential can be expressed in terms of the sum and difference frequencies as:

$$\phi_R^{(2)}(\vec{x}, t) = Re\Big\{ \sum_{kl} \phi_R^{+}(\vec{x}) \, e^{i\,\omega^{+}\,t} + \phi_R^{-}(\vec{x}) \, e^{i\,\omega^{-}\,t} \Big\} \tag{69}$$

Assuming a small incident wave and proportionally small motions at second-order as in Equation (59), this is further reduced to $\phi_R^{\pm}(t) = \sum_j \xi_j^{\pm}(t) \, \phi^{\pm}(\vec{x})$. After substituting into Equation (69), the second-order radiation potential can be given by:

$$\phi_R^{(2)}(\vec{x}, t) = Re\Big\{ \sum_{kl} \sum_j \xi_j^{+} \, \phi_j^{+}(\vec{x}) \, e^{i\,\omega^{+}\,t} + \xi_j^{-} \, \phi_j^{-}(\vec{x}) \, e^{i\,\omega^{-}\,t} \Big\} \tag{70}$$

The second-order radiation force is thus obtained by substituting Equation (70) into (68):

$$\begin{aligned} \vec{f}_R^{(2)}(t) = -\,\rho\, Re\Big\{ & \sum_{kl} \sum_j i\,\omega^{+}\,\xi_j^{+}\,e^{i\,\omega^{+}\,t} \iint_{S_B} \phi_j^{+}(\vec{x})\,\vec{n}\,dS \\ & + \sum_{kl} \sum_j i\,\omega^{-}\,\xi_j^{-}\,e^{i\,\omega^{-}\,t} \iint_{S_B} \phi_j^{-}(\vec{x})\,\vec{n}\,dS \Big\} \end{aligned} \tag{71}$$

Equation (71) can be further expanded, resulting in:

$$(\vec{f}_R^{(2)})_i = Re\left\{\sum_{kl}\sum_{j} \xi_j^+ \, e^{i\omega^+ t} \, g_{ij}^+ + \xi_j^- \, e^{i\omega^- t} \, g_{ij}^-\right\} \tag{72}$$

with:

$$g_{ij}^{\pm} = -(\omega^{\pm})^2 \, A_{ij}^{\pm} + i\,\omega^{\pm} \, B_{ij}^{\pm} \tag{73}$$

which leads to:

$$\vec{f}_R^{(2)} = Re\left\{\sum_{kl}\left[-(\omega^+)^2 \, \mathbf{A}^+ + i\,\omega^+ \, \mathbf{B}^+\right]\vec{\xi}^+ + \left[-(\omega^-)^2 \, \mathbf{A}^- + i\,\omega^- \, \mathbf{B}^-\right]\vec{\xi}^-\right\} \tag{74}$$

Finally, the second-order hydrostatic force and moment can be given by:

$$\vec{f}_C^{(2)} = -\rho_0 \, g \, A_w \left(\xi_3^{(2)} + \left(\vec{\alpha}^{(2)} \times \vec{r}_f\right)_3\right) \vec{k} \tag{75}$$

$$\begin{aligned}\vec{m}_C^{(2)} = &-\rho_0 \, g \left[-\forall \, \xi_2^{(2)} + A_w \, x_{2_f} \, \xi_3^{(2)} + (\forall \, x_{3_b} + L_{22}) \;\alpha_1^{(2)} - L_{12} \, \alpha_2^{(2)} - \forall \, x_{1_b} \, \alpha_3^{(2)}\right] \vec{i} \\ &-\rho_0 \, g \left[\forall \, \xi_1^{(2)} - A_w \, x_{1_f} \, \xi_3^{(2)} - L_{12} \, \alpha_1^{(2)} + (\forall \, x_{3_b} + L_{11}) \;\alpha_2^{(2)} - \forall \, x_{2_b} \, \alpha_3^{(2)}\right] \vec{j}\end{aligned} \tag{76}$$

In the next section the approach towards the modelling of scenarios involving irregular waves as input is described, for both the linear and nonlinear approximations.

5 STOCHASTIC APPROACH: IRREGULAR WAVES

Having defined the first (Section 3) and second-order (Section 4) approximations, it is necessary to consider the case where the input wave filed is of an irregular nature to study the response of floating structures under more realistic input conditions. Following the superposition principle, the free-surface elevation can be represented in terms of a stochastic process as a sum of *N* regular wave components:

$$\eta(t) = Re\{\sum_{j=1}^{N} a_j \, e^{i\,\omega_j\,t}\} \tag{77}$$

with $a_j = |a_j|\, e^{i\,\epsilon_j}$, where $|a_j|$ is the amplitude of the j^{th} component wave, given by $a_j = \sqrt{2\,S(\omega_j)\,\Delta\omega}$, with $S(\omega)$ the one-side wave amplitude spectra, and its random phase ϵ_j is uniformly distributed in the interval $[0, 2\,\pi]$.

By representing the input wave spectrum with *N* components, the time-series of the first-order excitation force can be given by:

$$\vec{f}_X^{(1)} = Re\{\sum_{j}^{N} a_j \, \vec{X}_j \, e^{i\,\omega_j\,t}\} \tag{78}$$

where $\vec{X}_j$ is the complex amplitude of the first-order excitation force associated with the j^{th} wave component.

Comparisons between the linear and the nonlinear formulation can focus the excitation force under irregular waves as a benchmark (see Section 6). The time-series of the second-order excitation force are directly calculated from the input wave spectrum and the second-order sum and difference frequency force quadratic transfer function (QTF):

$$F_X^{(2)}(t) = Re\{\sum_{k}^{N}\sum_{l}^{N}\left[a_k\,a_l\,f_{kl}^{+}\,e^{i(\omega_k+\omega_l)\,t} + a_k\,a_l^{*}\,f_{kl}^{-}\,e^{i(\omega_k-\omega_l)\,t}\right]\} \tag{79}$$

where the sum and difference-frequency force QTF satisfy the symmetry relations: $f_{kl}^{+} = f_{lk}^{+}$ and $f_{kl}^{-} = f_{lk}^{-*}$.

The one-sided spectra of the sum and difference frequency forces are obtained as:

$$S_F(\omega^-) = 8\int_0^{\infty} S(\mu)S(\mu+\omega^-)\,|f^-(\mu,\mu+\omega^-|^2\,d\mu \tag{80}$$

$$S_F(\omega^+) = 8\int_0^{\frac{1}{2}\omega^+} S(\tfrac{1}{2}\omega^+ + \mu)S(\tfrac{1}{2}\omega^+ - \mu)\,|f^+(\tfrac{1}{2}\omega^+ + \mu, \tfrac{1}{2}\omega^+ - \mu)|^2\,d\mu \tag{81}$$

The influence of the first and the second-order excitation force in the overall response of the floating bodies is accessed in Section 6 for the geometries under study. Results are further extended to arrays in Section 7.

6 HYDRODYNAMIC FORCES AND UNCONSTRAINED MOTIONS ASSOCIATED WITH A SINGLE TRUNCATED CYLINDER

This section presents the results associated with the computation of first and second-order hydrodynamic quantities for a single, freely floating truncated cylinder with diameter and draft equal to 20m. The water depth considered in this exercise is equal to 80m. Table 1 lists other main properties associated with this cylinder.

The hydrodynamic quantities computed in this exercise are:

- The first and second-order excitation forces;
- The first and second-order response amplitude operators (RAOs) for unconstrained motions.

The responses associated with these quantities are computed for a total of 45 different regular waves with different periods and the steady state time series responses are evaluated for 4 different values of wave steepness in Section 6.2.1.

The steady state responses associated with a unidirectional Pierson-Moskowitz (PM) spectrum with significant wave height of 2.5m (and T_p=7.9s) described by 16 and 8 frequency components are presented in Section 6.2.2.

The absolute value associated with the sum and difference frequency force QTFs are shown in terms of contour plots to show the levels associated with the second-order interactions and for which wave periods are more important.

For an axi-symmetric device the problem is simplified and the only modes that are relevant for head on waves are, surge, heave and pitch.

Main properties of the cylinder.	
Diameter:	20 m
Draft:	20 m
Volume of displaced water	6.28×10^3 m^3
Mass	6.44×10^6 kg
Position of the centre of mass (in the global CS)	$(x_{CM})_1 = 0.0$ m $(x_{CM})_2 = 0.0$ m $(x_{CM})_3 = -14.59$ m
Inertia matrix	$I_{11} = 2.38 \times 10^8$ kg m^2 $I_{22} = 2.38 \times 10^8$ kg m^2 $I_{33} = 1.82 \times 10^8$ kg m^2
Water depth	80 m.

Table 1: Main geometric properties associated with the cylinder.

6.1 Convergence tests: general notes

Prior to the evaluation of any hydrodynamic quantity the degree of accuracy of the numerical solution should be assessed to ascertain the influence of the discretisation of the geometry.

A finer discretisation may represent more accurately the geometry and therefore evaluate more accurately the velocity potential. However the computational effort increases with finer discretisation and so this convergence exercise is required to define the right balance between the required accuracy and computational effort.

There are not many studies related to convergence studies of second-order quantities computed with WAMIT. Birknes (2001) used this software to evaluate the wave elevation around four bottom mounted cylinders and four truncated cylinders at a spacing equal to 2*D*, with *D* being the cylinder's diameter. The study showed that the convergence is rapidly achieved for the first-order and the difference-frequencies second-order wave elevation. The main problems in the convergence were found for the sum-frequency component. The study also showed that the convergence was easier to achieve for long waves and some rules of thumb were defined to give general recommendations on the discretisation of the geometry of the floating bodies such to achieve better convergence results:

1) There should be at least 11 panels per second-order wavelength due to sum-frequencies (44 panels per linear wavelength).

2) Near the cylinders the free-surface should be discretised with a structured and dense mesh.

3) The width of the panels on the free-surface must not be too small compared with the length of the panels (aspect ratio ~0.5). For the panels which border on the cylinders, the longest side of the panel should border on the cylinder.

4) The cylinders should be discretised with small panels near the free-surface.

It should be also noted that the quadratic component of the second-order excitation force and moment given by Equations (64) and (65), depends on the products of first-order quantities and thus the accuracy of the second-order solution is dependent on the first-order results.

To evaluate the convergence of the first-order solution, the methodology presented by Roache (1997) which applies standard convergence procedures based on Richardson extrapolation method to computations performed with WAMIT higher order method is followed.

The exact value of a certain quantity (ϕ_0) is estimated by evaluating its value at three different discretisations of the geometry (ϕ_i). The error associated with the finer discretisations is given by:

$$E_1 = \phi_1 - \phi_0 = \frac{\phi_2 - \phi_1}{\left(\frac{h_2}{h_1}\right)^p - 1} \tag{82}$$

where are the values of the quantity being evaluated and h_i is the grid cell size associated with the discretisation *i*. The subscript 1 refers to a finer discretisation than 2 and 3 to a coarser discretisation than 1.

The order of convergence (*p)* is a quantity which depends on the implementation of the code itself and in general is not known. The value for this quantity is straightforward to compute for a constant

refinement ratio, i.e. $h_3/h_2 = h_2/h_1 = r = const.$ Assuming also that the asymptotic range has been reached, p is given by:

$$p = \frac{\ln\left(\frac{\phi_3-\phi_2}{\phi_2-\phi_1}\right)}{\ln\left(h_2/h_1\right)}. \tag{83}$$

The results of the convergence in the present study are evaluated through the error norm defined by:

$$L_\infty = |\max(\phi_i - \phi_0)|. \tag{84}$$

The grid convergence ratio (R) is a useful quantity to identify the behaviour of the convergence. This quantity defined by:

$$R = \frac{\phi_2 - \phi_1}{\phi_3 - \phi_2}, \tag{85}$$

and the solution is classified in terms of the value of R as:

- Oscillatory divergence, if $R < -1$;
- Oscillatory convergence, if $-1 < R < 0$;
- Monotonic convergence, if $0 < R < 1$;
- Monotonic divergence, if $R > 1$.

Finally, the uncertainty (U_k) associated with the computations finer discretisation (ϕ_1) is given by:

$$U = (F_s - 1)|E_1| \tag{86}$$

where F_s is a safety factor which may vary between 1 and 3. In the present study a conservative approach was taken and $F_s = 3$.

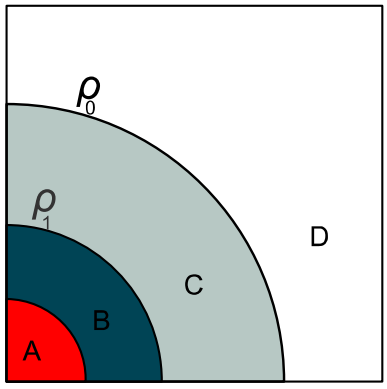

Figure 2: Representation of one quarter of the free-surface divided into the different integration regions. (A) Floating structure, (B) inner region, (C) annular region, (D) outer region.

The computation of the second-order hydrodynamic quantities also requires the discretisation of the free-surface. Therefore the spatial extension and the size of this additional mesh are additional parameters to consider.

Figure 2 presents a representation of the different regions that need to be considered. The free-surface is discretised into quadrilateral panels and the free-surface integral is evaluated separately in two domains separated by a partition circle with radius ϱ_0. This partition should be sufficiently large to enclose the body and its local disturbance and thus the effect of the evanescent waves outside the circle can be neglected. The outer region of the free-surface is defined by $\varrho = \sqrt{x_1^2 + x_2^2} \geq \varrho_0$ and both the Green function and the first-order potentials are expanded in Fourier-Bessel series.

The neglected evanescent terms are local and decay exponentially with radial direction in a fluid of finite depth. For this case, if ϱ_0/z_0 is large, the evanescent modes are proportional to $exp(-C\,\varrho_0/z_0)$ (with $\pi/2 < C < \pi$) and so resulting in a small error if $\varrho_0 \gg z_0$. In the infinite water depth limit the evanescent modes decay on the free-surface proportionally to $1/(k\,\varrho_0)^3$ and so the partition radius should ensure that $\varrho_0 > \lambda/2\pi$ so that there are no significant error contributions in the partitioned integral.

To achieve accurate results, the partition circle (ϱ_0) for shallow water depths should be of the same order as the water depth ($\varrho_0 \approx O\,(z_0)$) whereas for deep-water it is advised to be of the same order as the larger wavelength (($z_0 \gg \lambda$): $\varrho_0 \approx O\,(\lambda_{max})$).

In the inner region domain ($\varrho = \sqrt{x_1^2 + x_2^2} < \varrho_0$), the integration is carried out numerically. To further reduce the computational burden, the inner region is subdivided into two or more annular regions of radius, $\varrho_1 (< \varrho_2 < \ldots < \varrho_0)$. For regions close to the body ($\varrho < \varrho_1$), the integration is carried out by numerical quadratures whereas for the annular regions away from the body, between $\varrho_1 < \varrho < \varrho_0$, a more computationally efficient integration is performed by using Gauss-Chebychev quadrature in the azimuthal direction and Gauss-Legendre quadrature in the radial direction.

Finally, the inner partitions radius ($\varrho_1 < \varrho_0$) should be determined with care. If ϱ_1 is too close to the body the integration over the annular region may not be efficient as intended.

6.1.1 Convergence studies for the single cylinder: first and second-order

The geometry of the single truncated cylinder was discretised for three grid sizes as shown in Figure 3.

Following Roache (1997), the grid cell size (h_i) is related to the WAMIT higher order panel size parameter associated to an automatic discretisation of the geometry. Panel sizes equal to 8, 4 and 2[4] were considered and the hydrodynamic quantities were evaluated for ten wave periods randomly selected between 5 and 16s.

[4] The panel size parameter is only indicative of the discretisation in the physical space. For the present case the number of panels in one quarter of circle (angular direction) are equal to 8, 16 and 32 when the panel size parameter is equal to 8.0, 4.0 and 2.0.

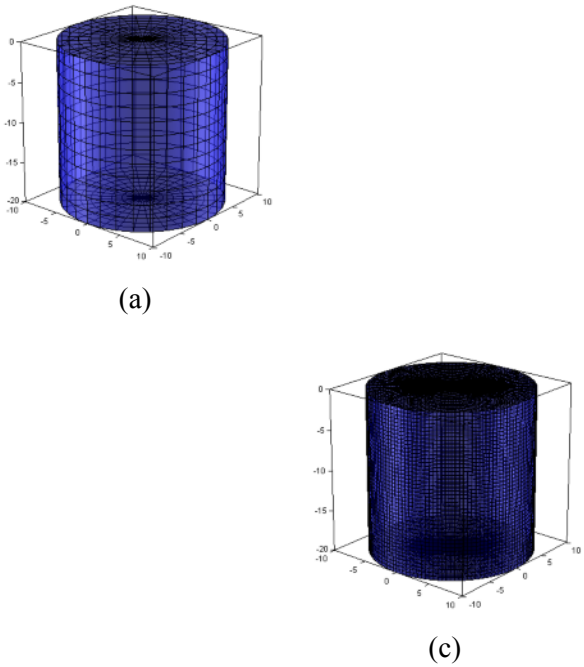

(a) (b)

(c)

Figure 3: Three discretisations of the geometry for the truncated cylinder used for the convergence tests. The panel size parameter equal to (a) 8.0, (b) 4.0 and (c) 2.0.

	Convergence Ratio (R)			Order of convergence (p)		
T (s)	$\lvert F_{X1} \rvert$	$\lvert F_{X3} \rvert$	$\lvert F_{X5} \rvert$	$\lvert F_{X1} \rvert$	$\lvert F_{X3} \rvert$	$\lvert F_{X5} \rvert$
5.32	0.740	0.601	0.467	0.435	0.735	1.100
6.85	0.684	0.525	0.469	0.548	0.929	1.094
7.01	0.630	0.532	0.475	0.666	0.912	1.074
7.64	0.549	0.528	0.493	0.866	0.922	1.019
10.39	0.490	0.555	0.494	1.029	0.849	1.018
11.34	0.475	0.578	0.499	1.074	0.790	1.004
12.84	0.475	0.581	0.496	1.073	0.783	1.012
13.86	0.480	0.592	0.492	1.060	0.756	1.024
14.75	0.476	0.570	0.494	1.072	0.810	1.018
15.77	0.477	0.586	0.489	1.067	0.772	1.032

Table 2: Convergence ratio (R) and order of convergence (p) associated with the absolute value of the linear excitation force for a discretisation triplet with panel sizes equal to 8.0, 4.0 and 2.0 for the truncated cylinder.

The convergence ratio (R) and the order of convergence (p) associated with the discretisation triplet used in this study are given in Table 2 for the linear excitation forces. The values of R depend on the hydrodynamic quantity being evaluated and on the frequency. Most of the values are between 0 and 1 and the solution for the evaluated cases can be classified as monotonic convergent.

An estimation of the exact solution for the linear excitation force associated with the incident wave periods and the uncertainty associated with the finer mesh (panel size equal to 2.0) for the linear excitation forces is present in Table 3.

The evolution of the convergence for four different discretisations is presented in terms of the error norm L_∞ defined by Equation (84) for the linear excitation forces (Figure 4). WAMIT does not provide the solution on each panel, and it also does not output the total number of panels. Throughout the study the number of equations (N) in the linear system (which corresponds to the number of unknowns) is used as a measure of the total number of panels. The relationship between N and the panel size is presented in Table 4. Overall the uncertainty estimates are relatively small when compared to the absolute value of the excitation force for all tested wave frequencies.

	Exact value estimation			**Uncertainty associated with the finer discretisation**		
T (s)	$\lvert F_{X1} \rvert$	$\lvert F_{X3} \rvert$	$\lvert F_{X5} \rvert$	$\lvert F_{X1} \rvert$	$\lvert F_{X3} \rvert$	$\lvert F_{X5} \rvert$
5.32	265.39	6.96	2389.48	0.135	0.077	0.695
6.85	398.5	29.94	3094.2	0.317	0.144	1.616
7.01	404.8	33.3	3105.44	0.266	0.157	1.714
7.64	412.98	47.06	3043.5	0.233	0.180	1.951
10.39	313.5	111.83	2078.03	0.192	0.256	1.627
11.34	274.83	132.04	1783.86	0.160	0.289	1.518
12.84	224.72	159.64	1423.8	0.134	0.271	1.272
13.86	197.25	175.73	1234.54	0.121	0.272	1.111
14.75	176.94	188.1	1097.85	0.106	0.226	1.021
15.77	157.27	200.53	967.83	0.096	0.229	0.892

Table 3: Estimations of the exact value and uncertainty of the finer discretisation associated with the linear excitation force for the incident wave periods considered in this study.

Panel Size (m)	1.0	2.0	4.0	8.0
Number of Unkowns	882	290	108	52
Simulation time per wave period (POT module) (s)	100	7	<1	<1

Table 4: Relation between panel size parameter and the number of unknowns in the equations in WAMIT for the OC3-Hydrowind discretisations of the geometry.

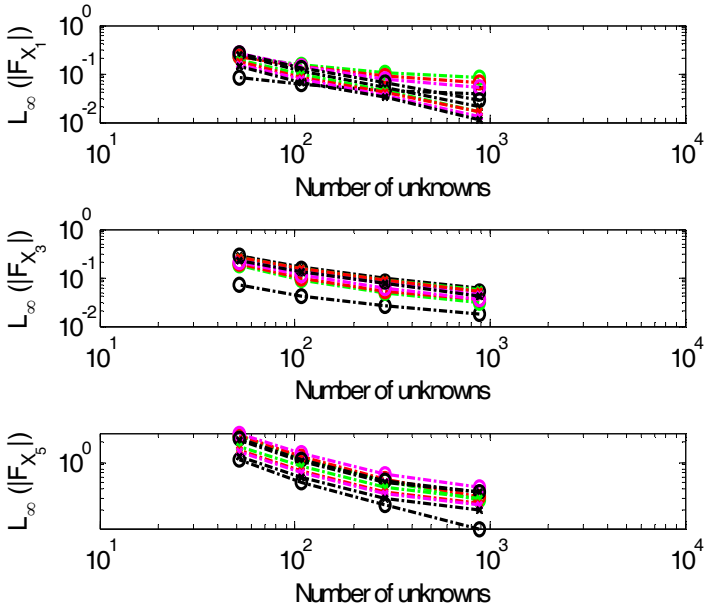

Figure 4: Evolution of the convergence in terms of the error norm L_∞ for the linear excitation force associated with the single truncated cylinder.

Run	1st order		Free-surface parameters								Comp. Time [min]	Sum-freq. force QTFs		
	Panel Size	Number of Unknowns	scale	Partition radius (ρ_0) [m]	Inner Circle (ρ_i) [m]	NAL	DELR	NCIRE	NGSP	Number of panels in the free-surface		|f+| (Surge)	|f+| Heave	|f+| Pitch
01	2.0	290	1.0	50	50	0	0	0	0	7299	21	23.49	3.69	153.38
02	2.0	290	1.0	50	25	1	25	4	8	1674	6	18.31	3.68	99.74
03	2.0	290	1.0	50	25	1	25	4	16	1674	8	23.59	3.69	154.59
04	2.0	290	1.0	150	25	5	25	4	16	1674	12	24.23	4.57	157.8
05	2.0	290	1.0	175	25	6	25	4	25	1674	12	24.06	4.61	155.5
06	2.0	290	1.0	175	25	3	50	4	50	1674	13	24.06	4.61	155.5
07	2.0	290	1.0	174.9	12.5	8	20.3	6	20	296	31	24.09	4.6	156.04
08	4.0	108	0.5	175	25	6	25	4	25	1583	2	23.35	4.51	146.64
09	4.0	108	0.25	175	25	6	25	4	25	6110	6	23.34	4.51	146.66

Table 5: Computed values of the sum frequency force QTF for a regular wave with T=5s associated different discretisations of the free-surface and cylinder geometry.[5]

[5] **(NAL – number of annular regions; DELR- length of the annular region; NCIRE – related with the number of nodes for the azimuthal integration (Gauss-Chebichev quadrature); NGSP – number of radial nodes (Gauss-Legendre Quadrature).**

The influences of the parameters associated with the discretisation of the free-surface were investigated initially for a regular wave with period equal to 5.0s. For this regular wave, the associated deep-water wavelength is equal to 37.5m and the second-order sum-frequency wavelength is equal to 9.4m. Following the recommendations by Birknes (2001) a suitable length for the free-surface panel is approximately 0.85m.

Table 5 show the values obtained for the sum-frequency QTF obtained for different discretisations of the free-surface. Run 01 took into account a definition with no annular region. The partition radius is coincident with the inner radius and equal to 50m (see Figure 2). Such a definition is computationally less efficient than if an annular region was defined but the integration over this region should give more accurate results. To decrease the computation time it is thus recommended to define an annular region. Runs 02 to 07 test the influence of several parameters in the definition of the free-surface. It was also observed that a coarser mesh with panel size equal to 4.0 (instead of 2.0) decreases substantially the computation time with small variation in the computed value of the sum-frequency force (roughly 5%).

To assess the influence of the spatial extension of the partition radius in the sum-frequency force QTF, a series of simulation runs which considered increasingly larger annular regions were performed. In these runs, the sum-frequency combination between three monochromatic waves with periods equal to 5.0, 10 and 16s were considered for a fixed radius of the inner region (equal to 25 m) and a panel size of 4.0. The scale factor for the discretisation of the free-surface was chosen to be equal to 0.5, giving a total number of panels associated with the inner region equal to 1583. Figure 6 shows the results associated with the sum-frequency force QTF for the three modes of motion (surge, heave and pitch). Overall the variation of the results with the partition radius is small. Oscillations in the solution were observed for the smaller wave periods of the sum-frequency force QTF for partition radius larger than 400m. The small dispersion observed for the larger sum-frequency wave periods gives an indication that there is no visible advantage to define a partition radius much larger than the largest of the wavelengths. Hereafter this parameter will be defined as being equal to 425m.

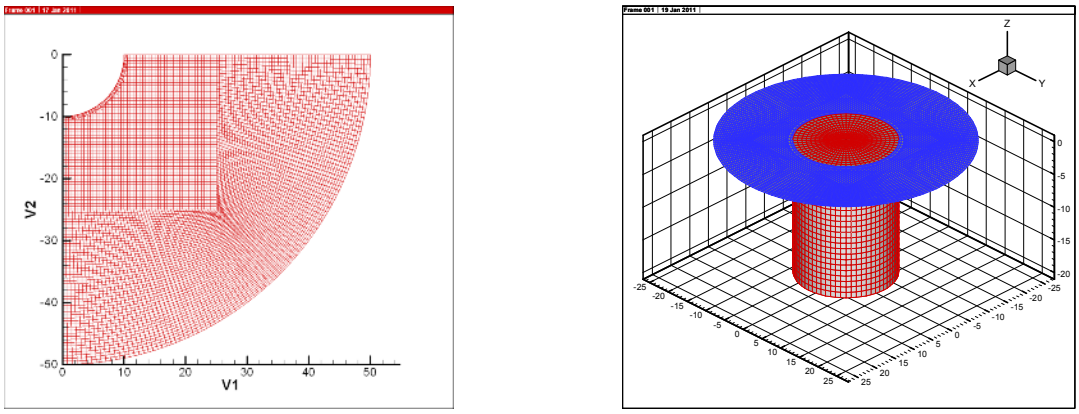

(a) **(b)**

Figure 5: (a) Top view of the discretisation of the free-surface used in run 01, (b) Isometric view of the discretisation used for run 08.

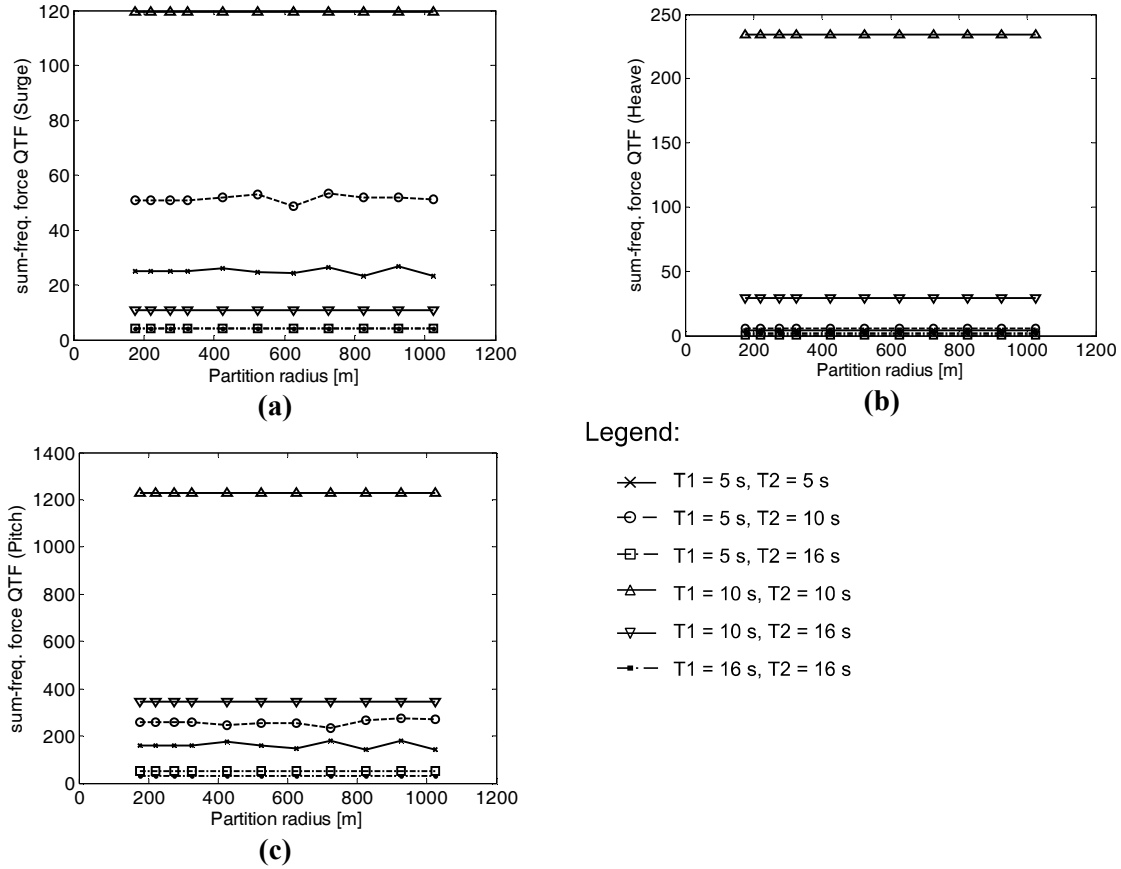

Figure 6: Variation of the sum-frequency force QTF with the length of the partition radius.

However it should be pointed out that the sum-frequency force QTFs in heave at the resonance frequency (T~10.25s) did not converge and so special attention should be considered for this mode for periods near resonance. This might be related with the large heave motions attained at resonance and the dependence of the quadratic second order force component (fq) on the first-order motions of the structure (see Section 4.4).

6.2 Results: single truncated cylinder

6.2.1 Regular waves

This section presents the first and second-order hydrodynamic quantities computed for the single truncated cylinder.

The frequency dependence of the added-mass and damping coefficients required to compute the radiation force (see Equation (30)) is shown in Figure 7 and Figure 8, respectively.. The symmetry of the added-mass matrix imply that all crossed terms are equal ($A_{kl} = A_{lk}$ for $k,l=1,\ldots,6$) and the axi-symmetry of the structure implies that the terms in surge and sway are equal ($A_{11}=A_{22}$), as are the roll

and pitch terms (A_{44}=A_{55}). The crossed terms are all null apart from A_{15} = -A_{24}. Note that the same relations apply to the hydrodynamic damping components.

The hydrodynamic coefficients are given as non-dimensional quantities. To convert to dimensional quantities, both coefficients should be multiplied by the value of density of the fluid (ρ) and the hydrodynamic damping should be also multiplied by the angular frequency of the incident wave (ω):

$$\widetilde{A_{kl}} = \rho\, A_{kl}, \text{ and } \widetilde{B_{kl}} = \omega\, \rho\, B_{kl} \tag{87}$$

Henceforth the modes of motion surge, sway, heave, roll, pitch and yaw are referred to by the subscript numbers 1,2,3,4,5,6 respectively.

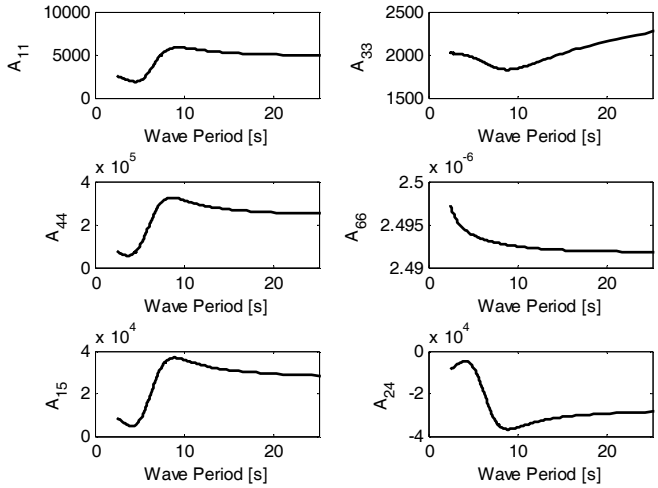

Figure 7: Added-mass coefficients for the truncated cylinder (head-on waves).

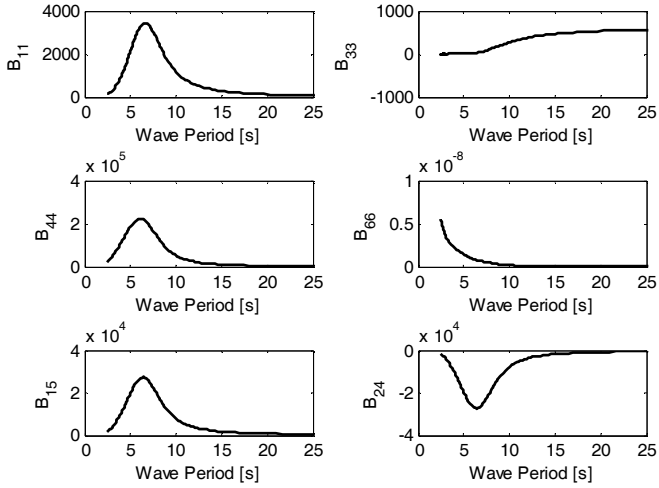

Figure 8: Hydrodynamic damping coefficients for the truncated cylinder (head-on waves).

As shown in Section 4.4 the computation of the second-order radiation force is identical to the first-order but at the respective sum and difference frequencies.

The linear hydrostatic force is proportional to the displacements of the structure and is given in terms of the hydrostatic coefficients by Equation (25). The non-dimensional hydrostatic coefficients for the truncated cylinder are shown in Table 6. These coefficients do not depend on the frequency of the incident wave and are computed relatively to the origin of the body coordinate system which is coincident with the centre of mass of the structure. The axi-symmetry of the structure implies that the hydrostatic coefficient in roll (C_{44}) is the same as in pitch (C_{55}). The dimensional values of these coefficients can be obtained by multiplying the non-dimensional values by ρ and g:

$$\widetilde{C_{kl}} = \rho\, g\, C_{kl} \tag{88}$$

$\mathbf{C_{33}}$	314.157
$\boldsymbol{C_{44}}$, $\boldsymbol{C_{55}}$	36693.9

Table 6: Non-dimensional hydrostatic coefficients associated with the truncated cylinder.

The first and second-order excitation forces and moments associated with monochromatic waves with periods between 5 and 16s are shown in Figure 9. These are computed at the centre of mass of the structure and are given as non-dimensional quantities.

The dimensional value of the first-order excitation forces is obtained by multiplying the non-dimensional value of the force or moment by the density of the water (ρ), the gravitational constant (g) and the wave amplitude (a):

$$\widetilde{F_X} = \rho\, g\, a\, F_X. \tag{89}$$

The dimensional value of the sum- and difference-frequency force QTF are obtained by:

$$\widetilde{F_X}^{+} = \rho\, g\, a\, a\, F_X^{+} \quad \text{and} \quad \widetilde{F_X}^{-} = \rho\, g\, a\, a^{*}\, F_X^{-},$$

where the a^* is the complex amplitude of the incident wave.

The importance of the second-order component of the excitation force increases with the amplitude of the incident wave. In Section 4 it was shown that in the weakly nonlinear hydrodynamic approximation perturbation theory is used to separate the problem into a first and second-order formulation and the final solution is obtained by the superposition of the two. The time-series of the *total excitation force* is thus obtained via $\vec{f}_X(t) = \vec{f}_X^{(1)}(t) + \vec{f}_X^{(2)}(t)$.

For a monochromatic wave, the second-order excitation force given by Equation (79) is reduced to the computation of the sum and difference frequency force QTFs ($f^{\pm}$) at the double ($\omega^{+} = \omega + \omega = 2\,\omega$) and zero frequency ($\omega^{-} = \omega - \omega = 0$). The second-order excitation force is thus given by:

$$F_X^{(2)}(t) = Re\{a^2\, f^{+}\, e^{-i\,2\,\omega\, t} + a^2\, f^{-}\} \tag{90}$$

where a is the complex amplitude of the incident (monochromatic) wave which has a phase component (ϵ) uniformly distributed between [*0, 2π*]:$a = |a|e^{i\epsilon}$.

A comparison between the non-dimensional absolute value of the first and the second order sum and difference frequency excitation forces is given in Figure 9 for surge, heave and pitch modes. The results show that for most of the wave periods the first order excitation force is much higher than both second order sum and difference frequency components. For most of the (monochromatic) wave periods it is also shown that the sum frequency component is dominant over the difference frequency. In heave mode, for the wave period equal to 10.25 s, the absolute value of the second order components has a peak value which is higher than the correspondent first order component. This particular wave period is close to the resonance in heave of the freely floating cylinder and as such some care should be taken in the interpretation of the results as poor convergence was observed for the sum-frequency component of the excitation force.

The force time series associated with regular waves with the steepness values given in Table 7 are presented in Figure 10 to Figure 16 for surge, heave and pitch modes. In surge, first-order effects are dominant except for the steepest wave (T=10.25s, H=6m) for which the sum-frequency component of the second-order force is maximum (see Figure 9). In heave, for the shorter waves, the second-order component of the excitation force is of the same order as the first-order. In pitch the first-order component is dominant for the less steep waves and the relative importance of the second-order component increases substantially for the two largest waves.

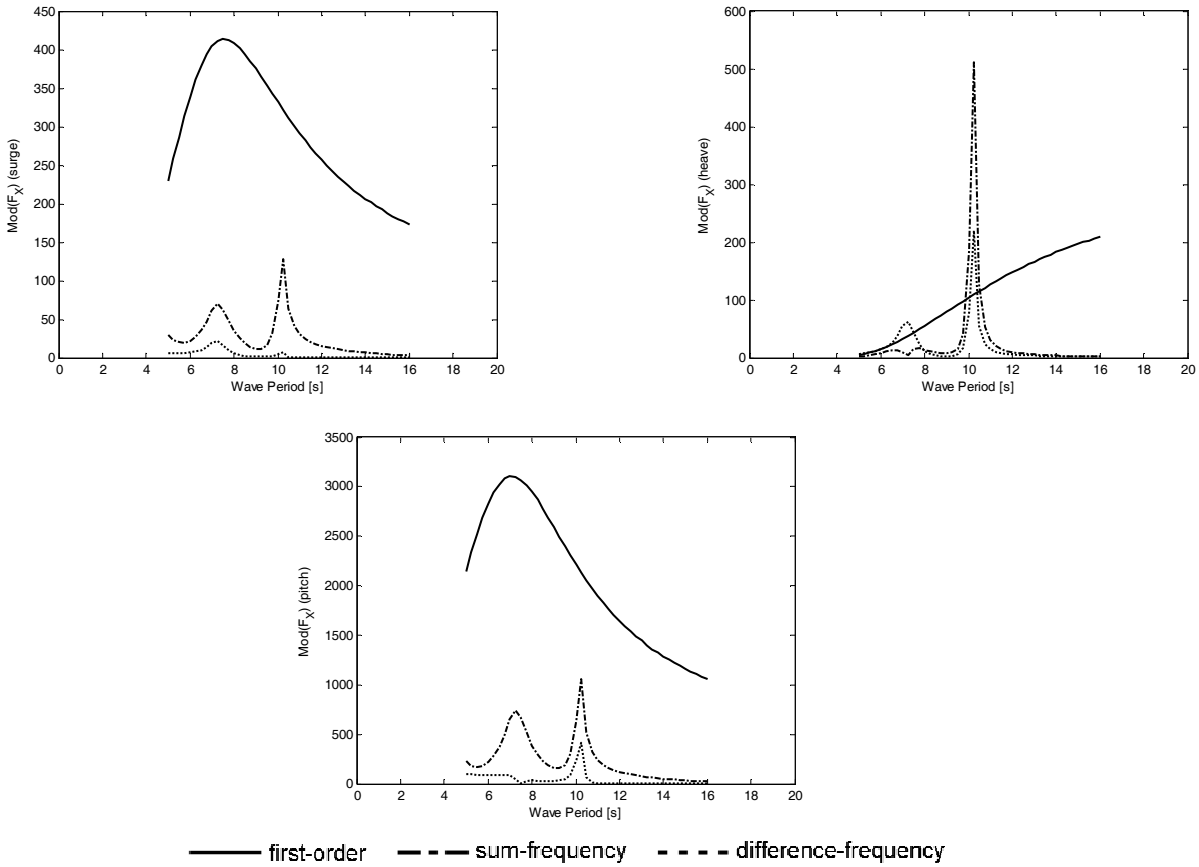

Figure 9: Absolute value of the first and second-order components of the excitation force in surge, heave and pitch for the truncated cylinder.

Period (T) [s]	Height (H) [m]	Wavelength (λ) [m]	Steepness (H/λ)
5.0	1.0	37.5	0.0267
7.0	2.0	73.5	0.0272
9.0	4.0	121.5	0.0329
10.25	6.0	157.6	0.0381

Table 7: Wave periods of the monochromatic waves considered for the comparisons between linear and second-order hydrodynamic quantities.

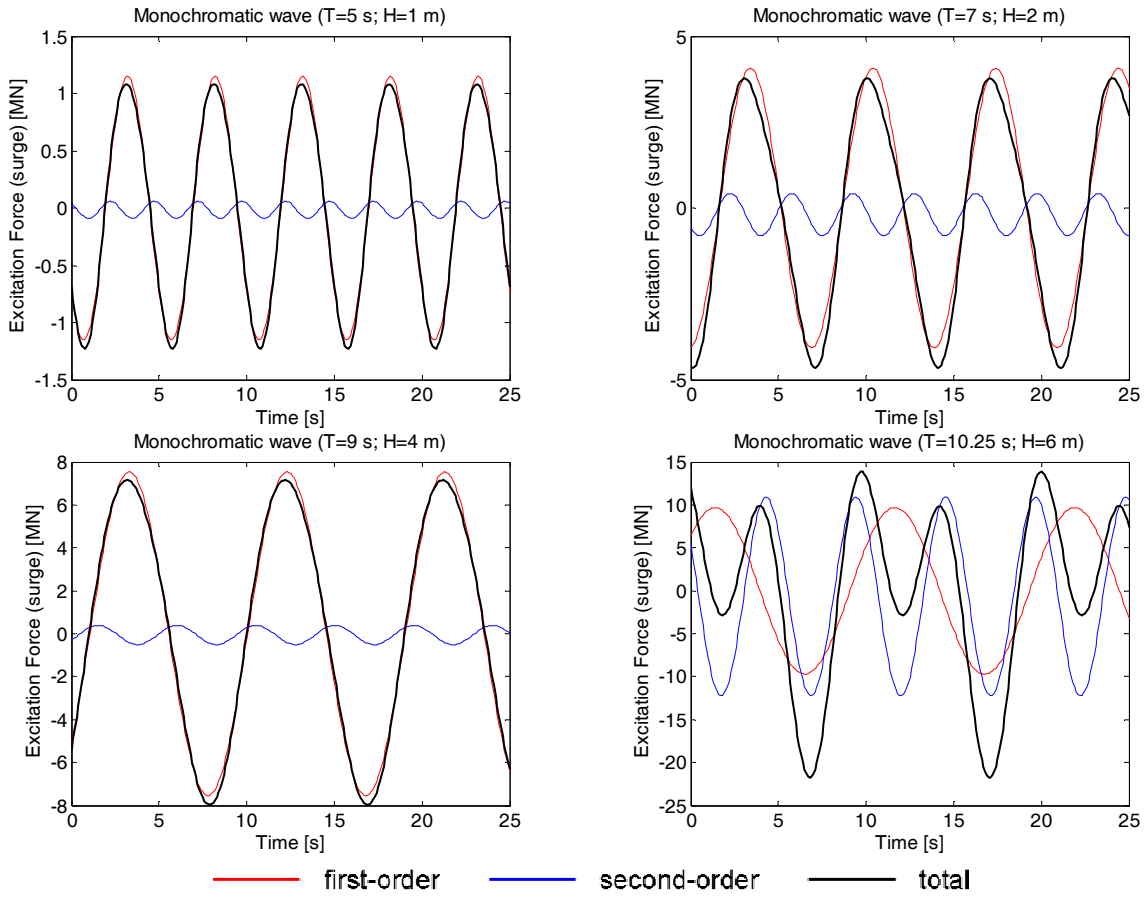

Figure 10: First, second-order and total excitation force in surge for four regular waves with parameters given in Table 7.

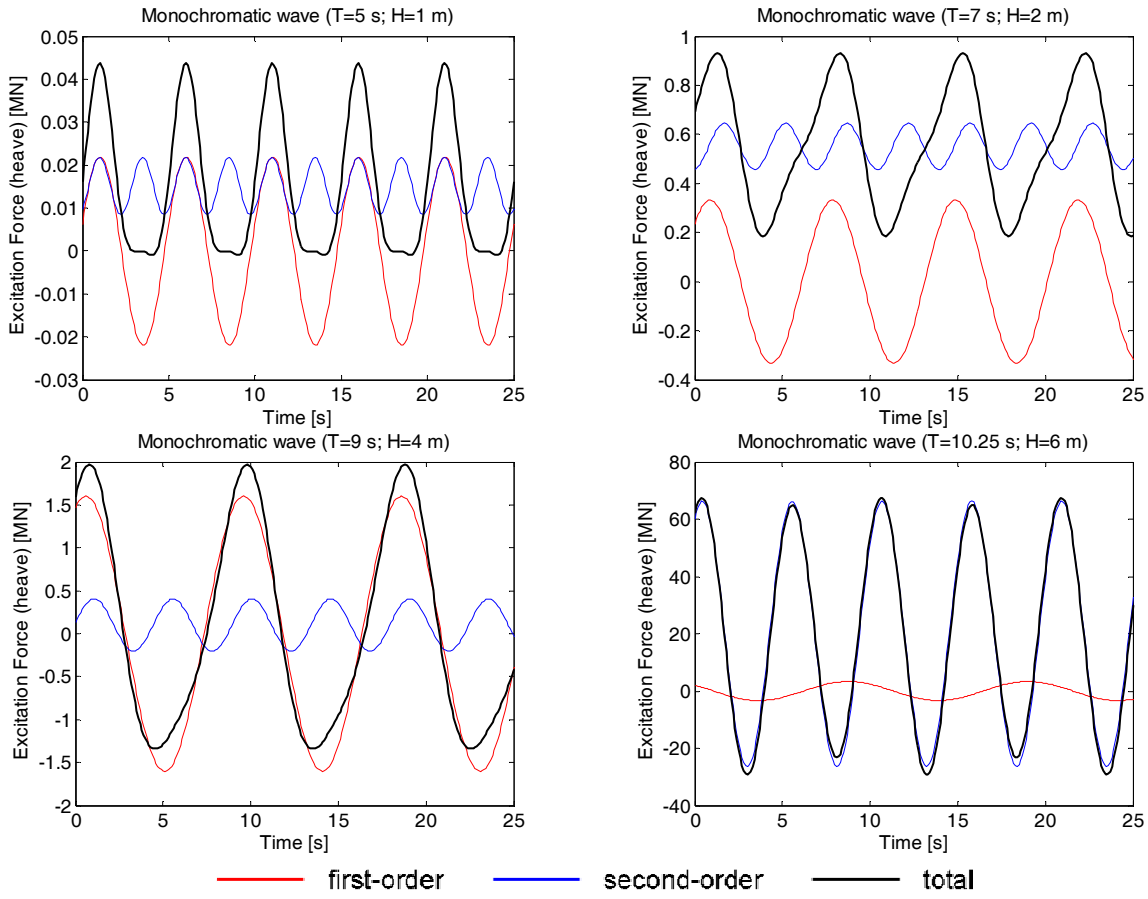

Figure 11: First, second-order and total excitation force in heave for four regular waves with parameters given in Table 7.

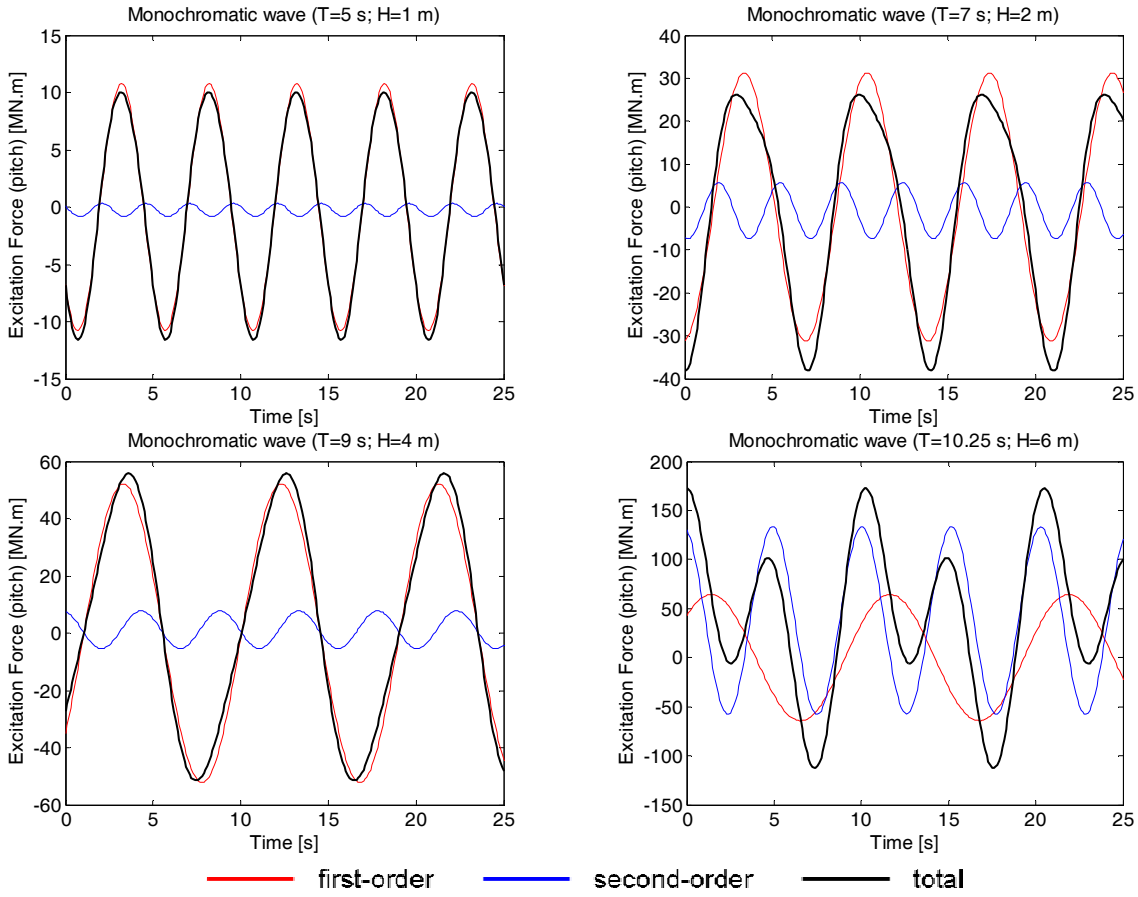

Figure 12: First, second-order and total excitation force in pitch for four regular waves with parameters given in Table 7.

The frequency dependence of the first and second-order components of the response amplitude operator (RAO) for the unconstrained motions of the truncated cylinder is shown in Figure 13. The freely floating truncated cylinder has a resonance period in surge and pitch at about 8.5s and in heave at about 10.3s. The absolute value of the second-order RAOs associated with the monochromatic waves are of an order of magnitude smaller than the first-order.

The time series of the first and second-order components of the unrestrained motions in surge, heave and pitch for the regular waves presented in Table 7 are shown in Figure 14 to Figure 16.

In surge and pitch the first-order unrestrained motions are dominant except for the steepest wave with period equal to 10.25s and height of 6m, for which the second-order component of the motions is of the same order of magnitude as the first-order. In heave the first-order motions are dominant for the regular waves considered in this study.

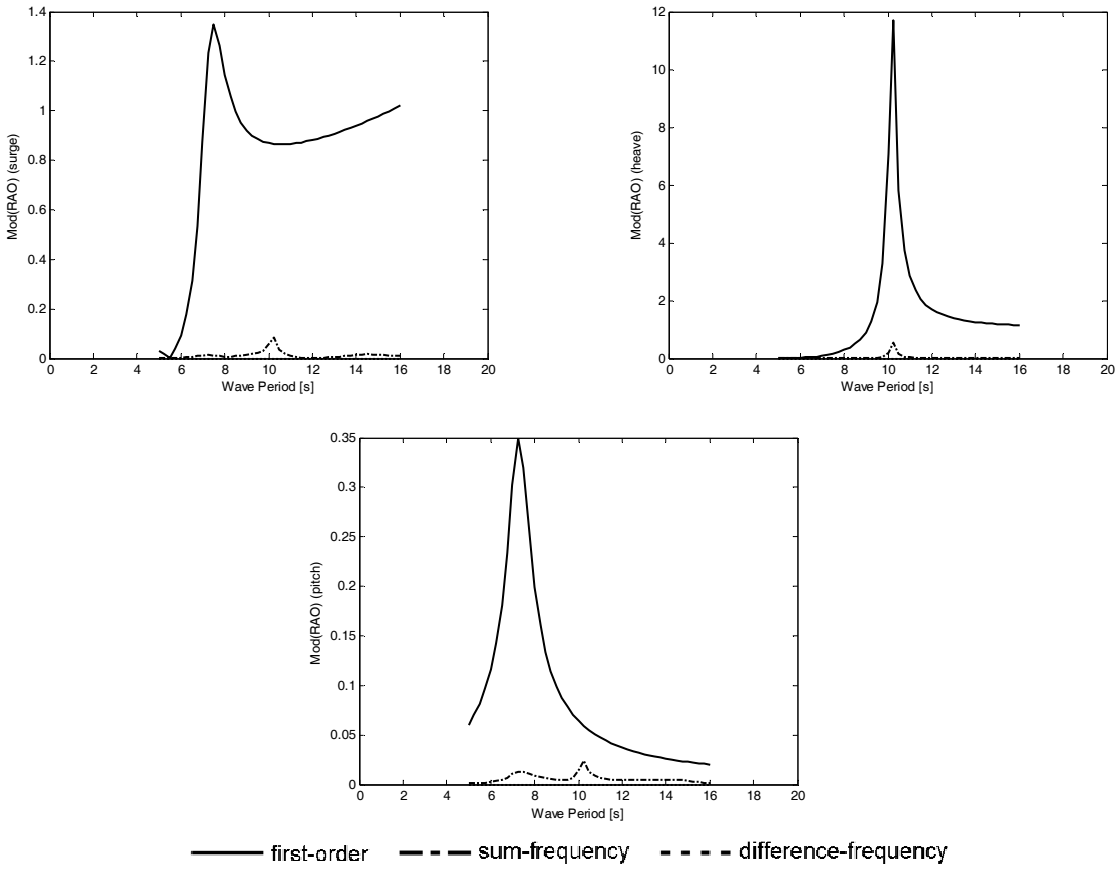

Figure 13: First and second-order components of response amplitude operator (RAO) for the unrestrained motions in surge, heave and pitch for the truncated cylinder.

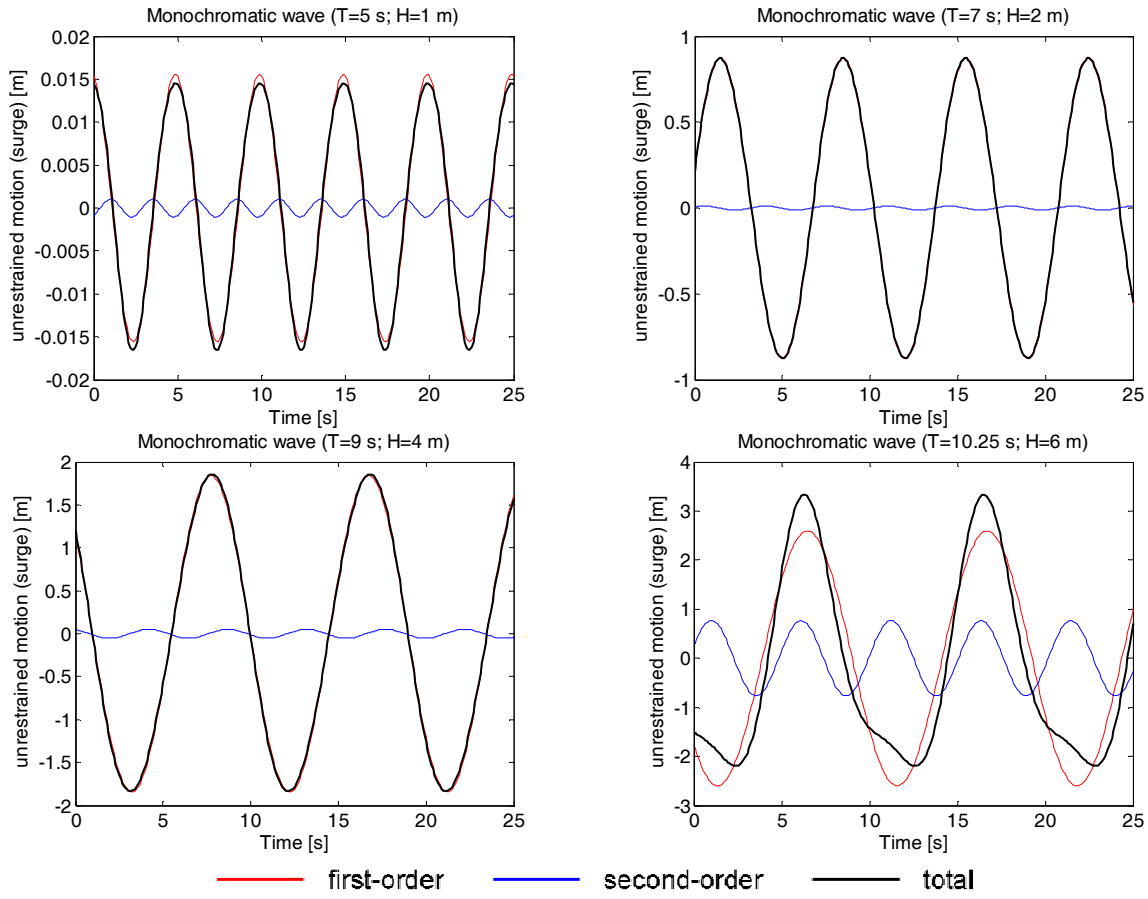

Figure 14: First, second-order and total unrestrained motion of the truncated cylinder in surge for four regular waves with parameters given in Table 7.

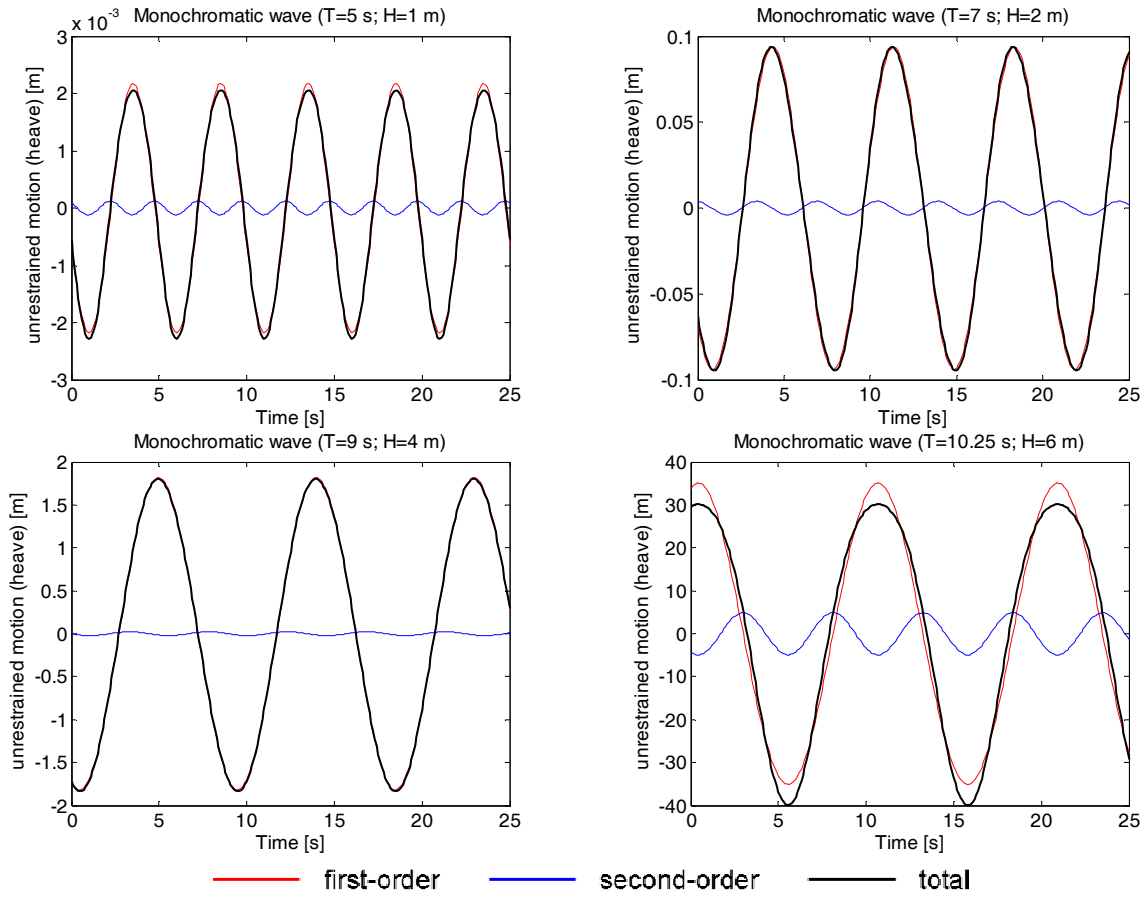

Figure 15: First, second-order and total unrestrained motion of the truncated cylinder in heave for four regular waves with parameters given in Table 7.

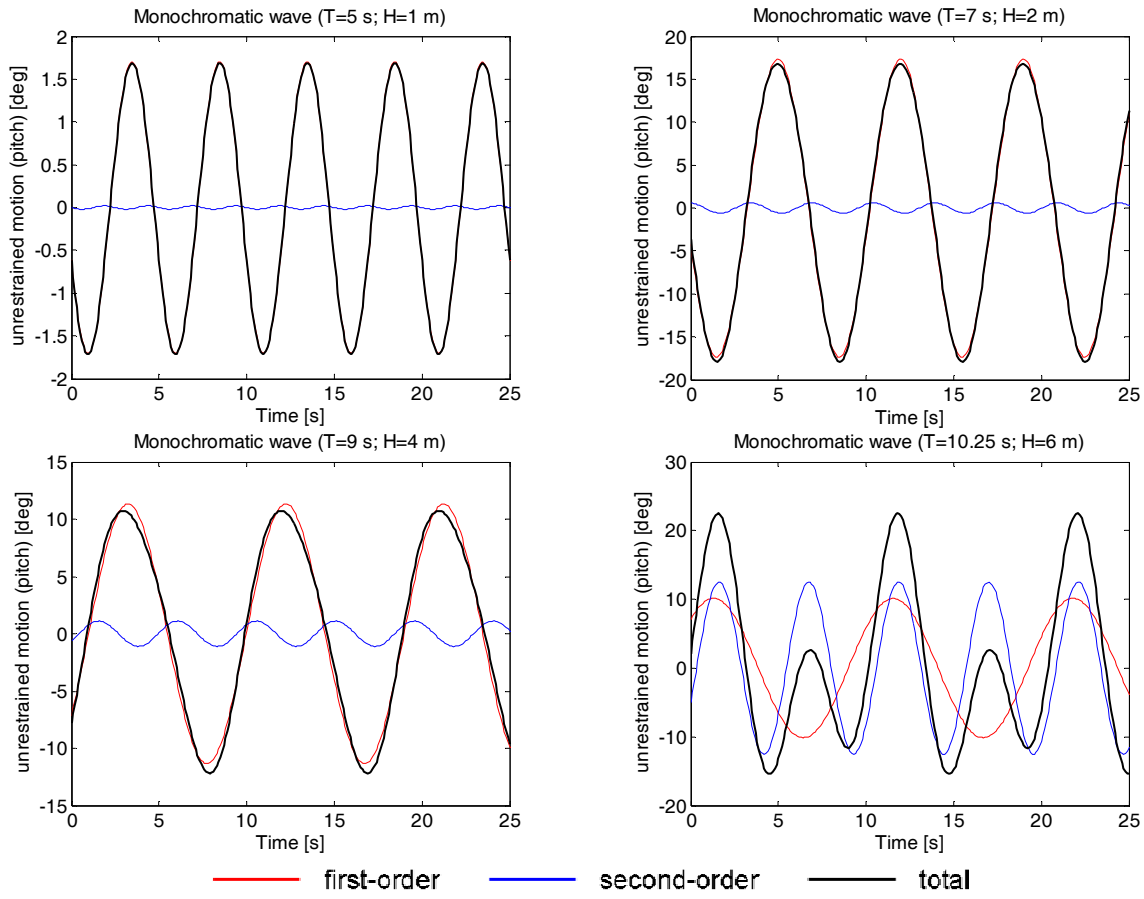

Figure 16: First, second-order and total unrestrained motion of the truncated cylinder in heave for four regular waves with parameters given in Table 7.

6.2.2 Irregular waves

This subsection describes the first and second-order simulations associated with a truncated cylinder for a sea state described by a Pierson-Moskowitz spectrum. As for regular waves (Section 6.2.1) the excitation forces and unrestrained body motions were calculated.

The Pierson-Moskowitz spectrum is used to describe fully developed seas. The variance density, *S*(*f*), that obeys the Pierson-Moskowitz formula can be defined (Tucker and Pitt, 2001):

$$S(f) = \frac{\alpha\, g^2}{(2\,\pi)^4\, f^5}\, \exp\left[-\beta\, \left(\frac{f_0}{f}\right)^4\right], \tag{91}$$

where $\alpha = 8.1 \times 10^{-3}$ and $\beta = 0.74$ are fixed dimensionless parameters of the distribution, f_0 is a parameter which is related to the wind speed. It can also be related to the significant wave height (H_s) and the peak frequency ($f_p = 0.877\, f_0$) of the spectrum:

$$H_s = 0.0520/f_0^2 = 0.0400/f_p^2 = 0.0400\, T_p^2 \tag{92}$$

The absolute value of the amplitude associated with each spectral component is given by $|a_j| = \sqrt{2\, S\,(f_j)\; df}$ and the free-surface elevation can be represented in terms of a stochastic process as a sum of *N* regular wave components with random phase as given by Equation (77).

Using the input wave spectrum and the second-order sum and difference frequency force QTFs (f^+, f^-), the time series of the second-order excitation force is directly calculated from:

$$F_X^{(2)}\,(t) = Re\{\sum_{k=1}^{N}\sum_{l=1}^{N}\left[a_k\, a_l\, f_{kl}^{+}\, e^{i(\omega_k+\omega_l)\,t} + a_k\, a_l^{*}\, f_{kl}^{-}\, e^{i(\omega_k-\omega_l)\,t}\right]\}, \tag{93}$$

where the sum and difference-frequency force QTF satisfy the symmetry relations: $f_{kl}^{+} = f_{lk}^{+}$ and $f_{kl}^{-} = f_{lk}^{-*}$.

This study considered a unidirectional Pierson-Moskowitz spectrum with H_s=2.5m (leading to T_p=7.9s). This was described by sixteen and eight components equally spaced by 0.01 and 0.02Hz (respectively), as shown by the histograms (Figure 17, top). The histograms at the bottom of the same figure show the wave amplitudes and periods associated with each spectrum.

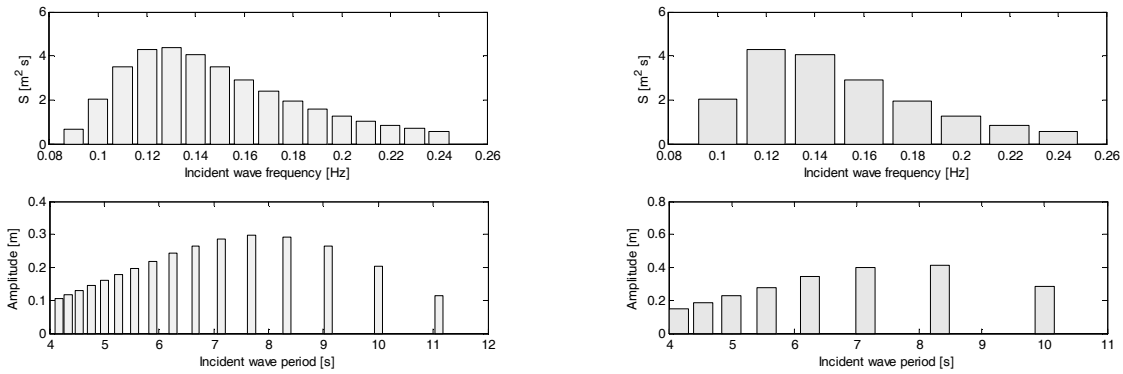

(a) (b)

Figure 17:(Top) Pierson-Moskowitz spectrum with H_s= 2.5m (T_p = 7.9s), (Bottom) Wave amplitude and period associated with the top spectrum. The left spectrum is discretised with sixteen components whereas the right spectrum by eight.

The sum- and difference- frequency force QTFs (f^+, f^-) computed for the truncated cylinder in surge, heave and pitch modes for the sixteen frequency components associated with this spectrum are shown in Table 9 to Table 15 of Appendix A.

Figure 18 shows the associated contour plots for the absolute value of the sum and difference frequency QTFs. Note that these plots are consistent with the results obtained for the monochromatic waves (Figure 9) with the main peaks located at the wave period interactions where the higher values were found.

The first and second-order excitation forces in surge, heave and pitch modes for the truncated cylinder associated with the Pierson-Moskowitz spectrum with H_s=2.5m (T_p=7.9s) are shown in Figure 19. The plots represent the response associated with the same spectrum discretised with sixteen (left) and only eight (right) components. The repeat periods are respectively equal to 100 and 50s. The plots show that for the truncated cylinder, the first order excitation forces are dominant for surge and pitch modes. For the heave mode the second order excitation force shows a more important contribution for the total force. It is also seen that the differences between the responses obtained with the spectrum discretised with sixteen and eight components is small except in heave.

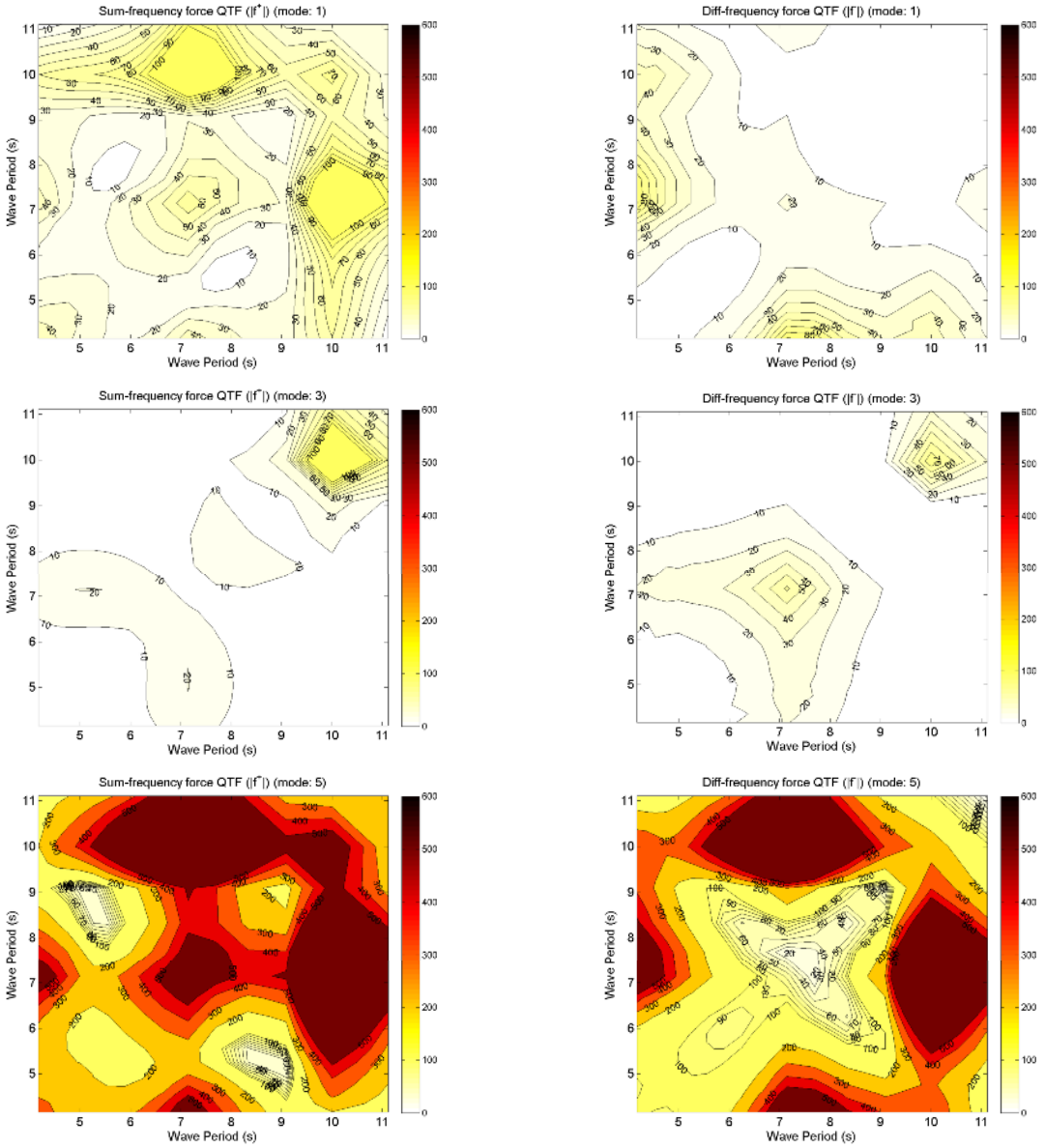

Figure 18: Contour plots for the sum and difference frequency force QTFs (16 components) associated with the truncated cylinder for the modes of motion: surge (1), heave (3) and pitch (5).

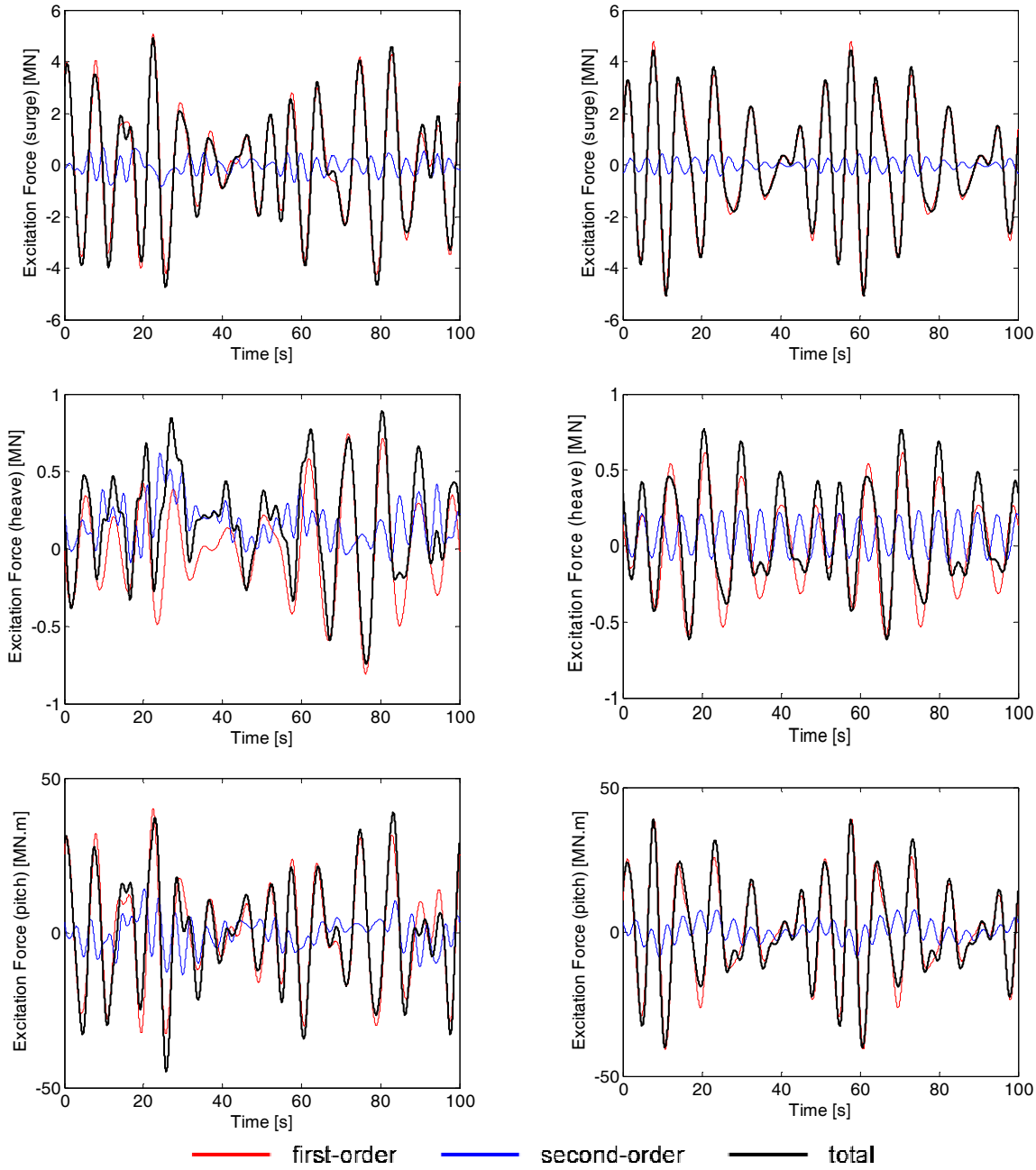

Figure 19: First, second and total excitation forces in surge, heave and pitch for the truncated cylinder for a Pierson-Moskowitz spectrum with Hs=2.5m (Tp=7.9s) described by sixteen (left) and eight components (right).

The comparisons of first and second-order unrestrained motions in surge, heave and pitch for the truncated cylinder associated with a Pierson Moskowitz spectrum with H_s=2.5 m (T_p=7.9 s) described by sixteen and eight components are shown in Figure 20.. The unrestrained motions for the truncated cylinder are small. The first order unrestrained motions are dominant for heave and pitch. In surge,

one can observe the slowly drift motion associated with the difference frequency component. The representation of this motion seems to be affected by the number of components chosen to represent the input spectrum and the long drift period is associated with the repeat period of the spectrum.

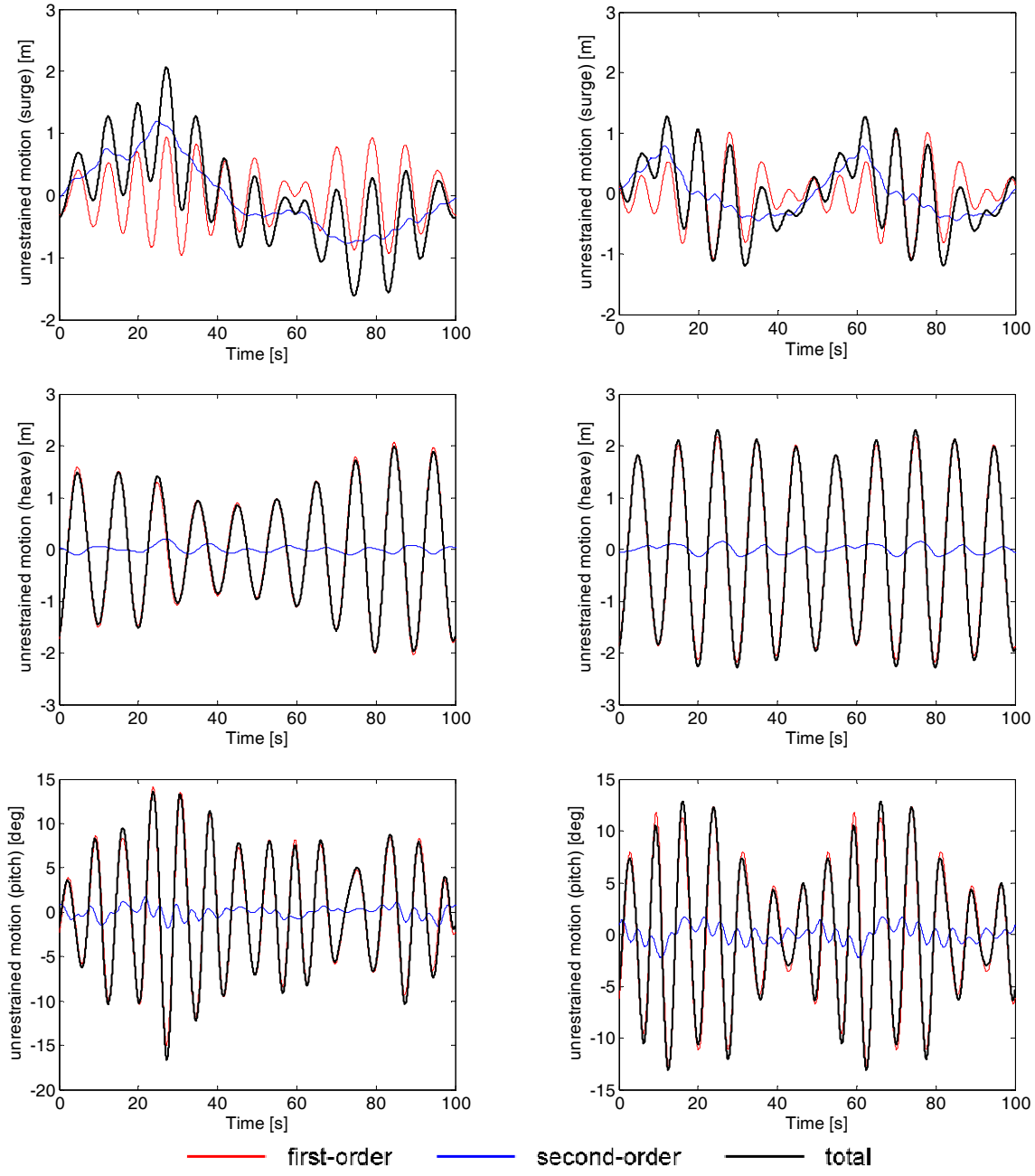

Figure 20: First, second and total unrestrained motions in surge, heave and pitch for the truncated cylinder for a Pierson-Moskowitz spectrum with Hs=2.5m (Tp=7.9s) described by sixteen (left) and eight components (right).

7 HYDRODYNAMIC FORCES AND UNCONSTRAINED MOTIONS ASSOCIATED WITH AN ARRAY WITH FOUR TRUNCATED CYLINDERS

This section presents the results associated with the computation of first and second-order hydrodynamic quantities associated with a square array with four truncated cylinders spaced three diameters (*D*) apart. Each cylinder in the array has a diameter (and draft) equal to 20m and is free to move in six degrees-of-freedom. The geometric and mass properties of the cylinders are presented in Table 1 and are the same as the cylinders presented in (Cruz, 2010). The present study extends some of the results presented in Cruz (2010) to the second-order hydrodynamic interactions obtained for head on waves for the array with the above spacing.

The cylinders in the array are numbered in the anti-clockwise direction. The DOF are numbered consecutively following the order of the cylinders in the array (up to a total of 24). For example, the heave mode of cylinder 3 is given by mode 15 (see Figure 21). This study only considers head-on waves which as shown in Figure 21 . For each cylinder all modes of motion are of interest except yaw. The water depth considered in this exercise is equal to 50m.

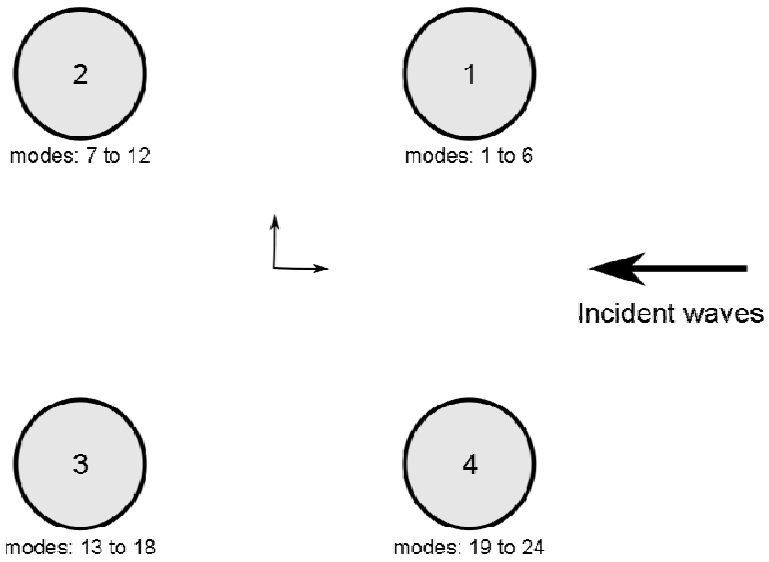

Figure 21: Top view for the layout of the array with four cylinders. Each cylinder in the array is numbered in the anti-clockwise direction and the modes of motion (surge, sway, heave, roll, pitch, yaw) are numbered continuously for each cylinder.

The hydrodynamic quantities are computed for forty nine regular waves, with frequencies between 4.0s to 16.0s equally spaced by 0.25s, and for a unidirectional Pierson-Moskowitz spectra with a significant wave height of 2.5m described by sixteen frequency components. The hydrodynamic quantities computed in this exercise are:

- The first and second-order exciting forces ;
- The first and second-order Response Amplitude Operator (RAO) for unconstrained motions.

7.1 Convergence tests

For the four cylinder array the computational time required to obtain the solutions for the first and second-order quantities increases very significantly when compared with the single truncated cylinder case (Section 6). This is mainly due to the impossibility to use planes of symmetry to describe the geometry of each cylinder, thus multiplying by 4 the number of panels for each cylinder and by 16 for the full array. Furthermore, the computation of second-order quantities requires the discretisation of the free-surface to be increased so as to include the entire array.

For the convergence of first order quantities, the same procedure described for the single truncated cylinder was followed (see Section 6.1), evaluating the hydrodynamic quantities for 10 random wave periods in the interval between 5 and 16s for three panel sizes equal to 8m, 4m and 2m, respectively. The convergence was found to be monotonic for most cases and the uncertainty estimates were relatively small when compared to the absolute value of the exciting force for the tested wave periods. The evolution of the convergence of the exciting forces for the four cylinders is presented in terms of the error norm L_∞ (given by Equation 84) in Figure 23. For this plots a total of six different discretisations was considered for which the relationship between the number of unknowns (N) of the first order solution and the panel size is given in Table 8. The panel size equal to 4.0m was selected and the discretised geometry of the array is shown in Figure 22.

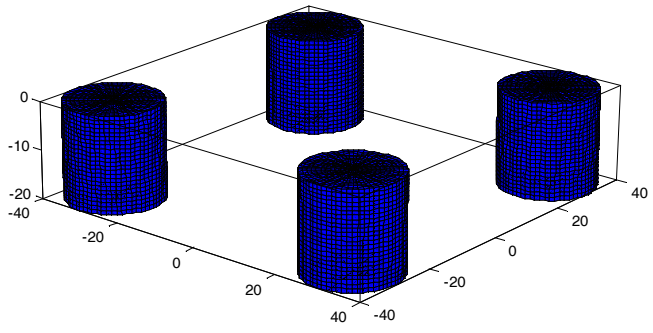

Figure 22:Discretisation of the geometry for the array with four cylinders (panel size 4.0)

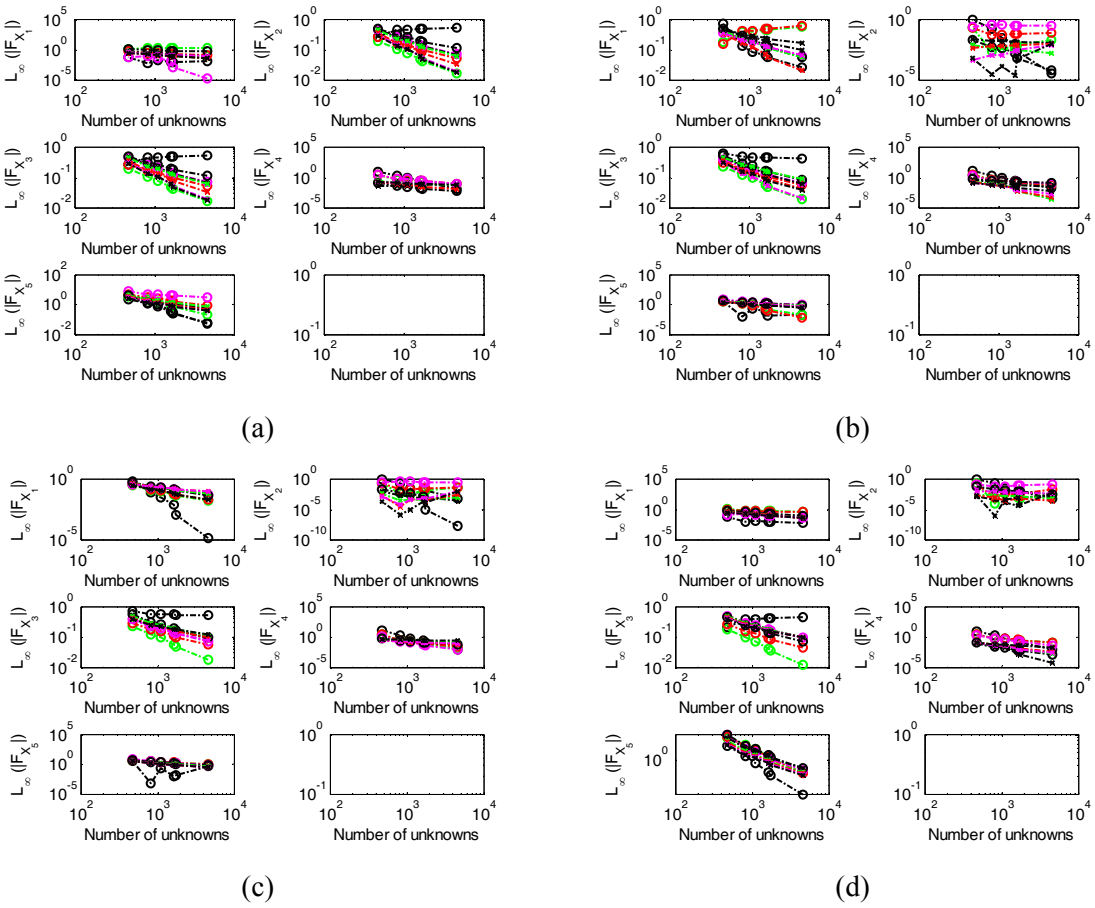

Figure 23:Evolution of the convergence in terms of the error norm L_∞ for the linear exciting force associated with the array with four cylinders.

Panel Size (m)	2.0	4.0	5.0	6.0	8.0	16.0
Number of Unkowns	4640	1728	1632	1120	832	480

Table 8: Relationship between the panel size and the number of unknowns used to test the evolution of the convergence.

The second-order computations were performed with the free-surface discretised for an inner circle equal to 65.5m and a partition circle equal to 120m. For the sum-frequency problem, the free-surface was discretised with a very fine mesh with the same spacing as used in the case of the single truncated cylinder. Because it is possible to achieve convergence for the difference-frequency problem with a coarser mesh, the computation of the difference-frequency quantities considered a mesh with larger

panels. The meshes used to compute the sum-frequency and the difference frequency problem are shown in Figure 24.

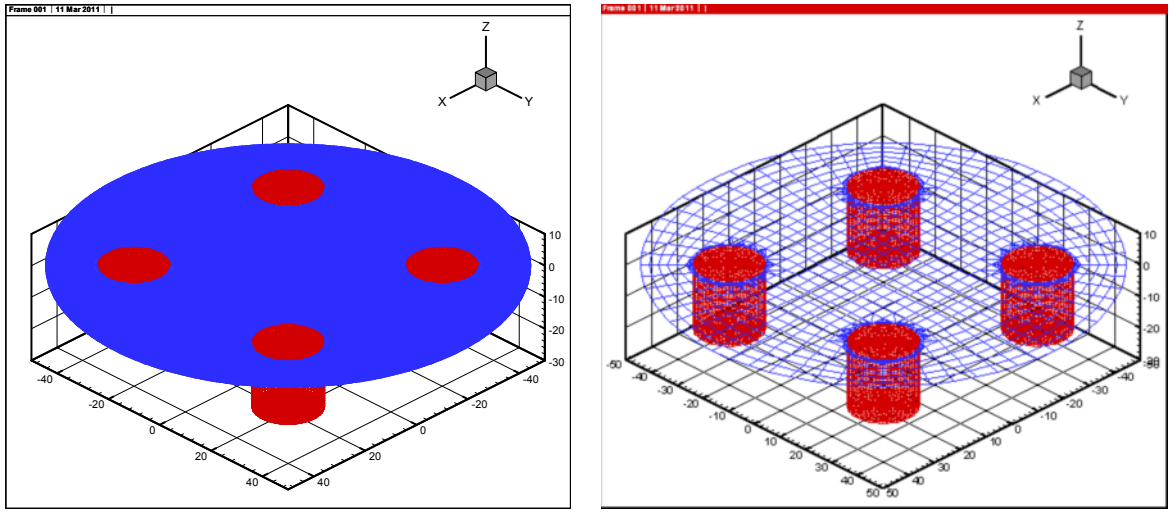

Figure 24:Discretisation used to compute the sum-frequency (left) and difference-frequency (right) problem.

7.2 Results for the array with four cylinders.

7.2.1 Regular Waves

This subsection is focused on the comparison between the non-dimensional absolute value of the first and the second-order sum and difference-frequency exciting forces for the cylinders 1 and 2 in the array for monochromatic waves (see Figure 21). The results are shown in Figure 25 and Figure 26 for all relevant modes of motion for these two cylinders. The curves associated with the first-order exciting forces show the expected variations due to the interactions between the cylinders of the array. When comparing with the plots computed for the single cylinder (Figure 9), an increase of the peak values associated with the sum-frequency component can be seen, whereas a decrease for the difference-frequency can also be observed. In surge, sway, roll and pitch and for both cylinders there is a sharp increase of the peak located around the wave period equal to 7.5s with values that are of the same order or higher than the first order component.

The plots for the components of the absolute value of the first and second-order sum-frequency RAOs are shown in Figure 27 and Figure 28 for the modes of motion of interest. The plots show that for all modes the second-order component of the RAOs is much smaller than the first-order component and so the first-order unrestrained motions are dominant.

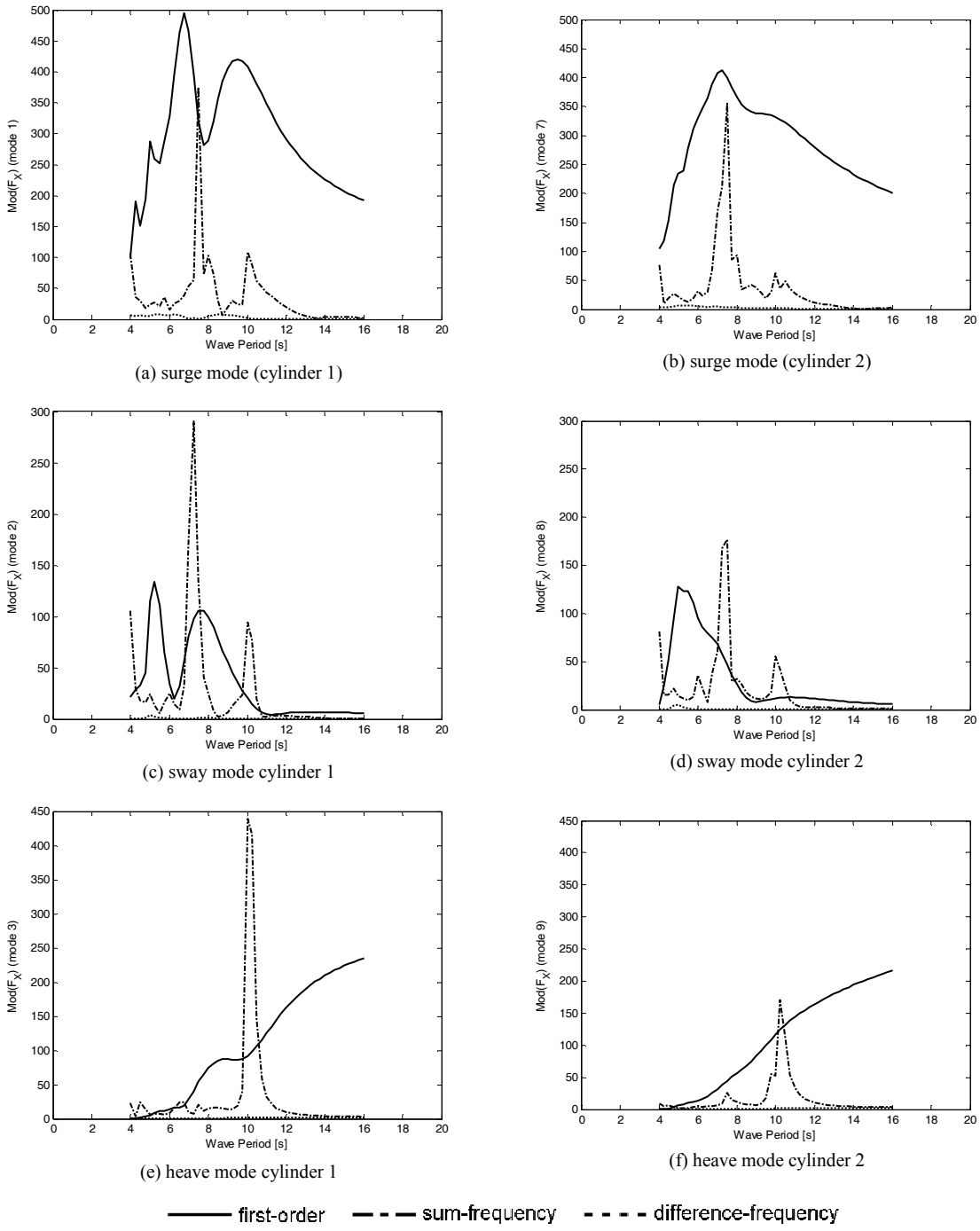

Figure 25: Absolute value of the first and second-order sum and difference frequency components of the exciting force in surge, sway and heave for cylinders 1 and 2 of the array.

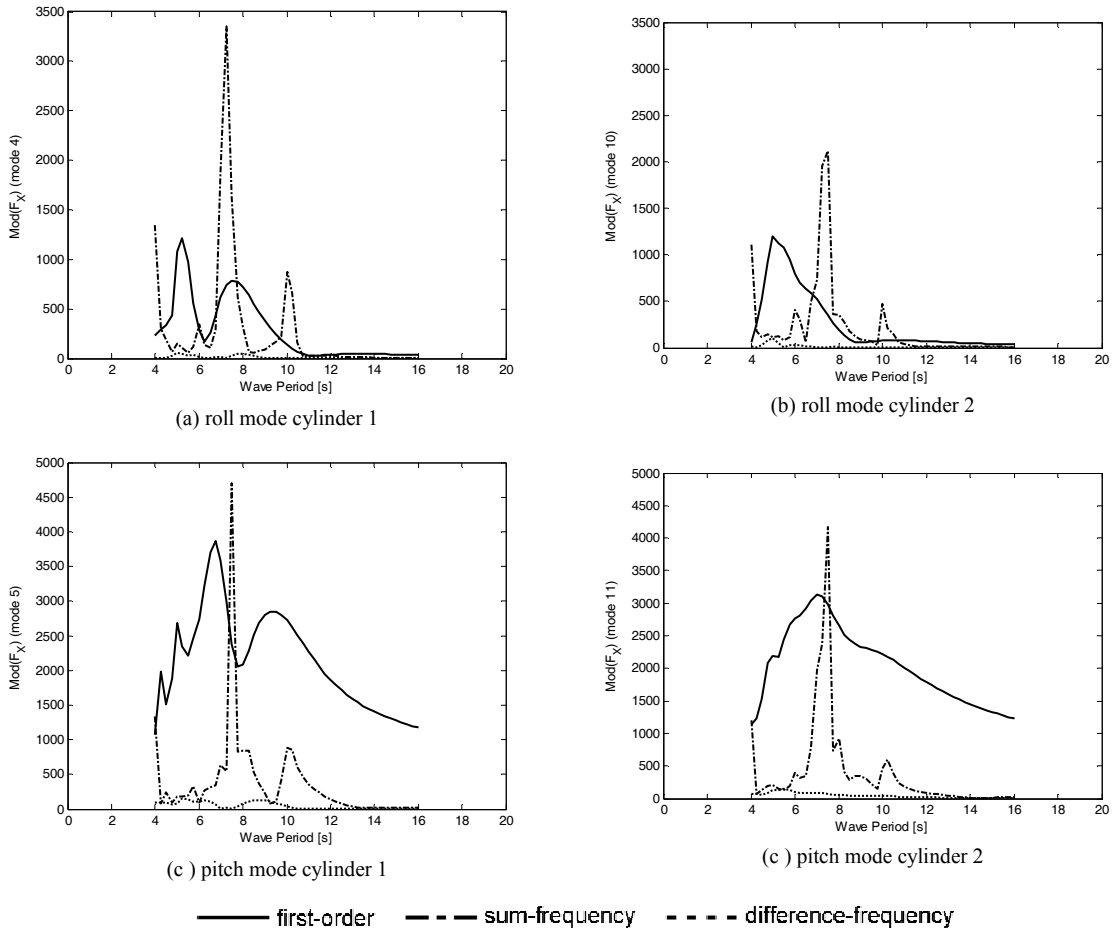

Figure 26: Absolute value of the first and second-order sum and difference frequency components of the exciting force in roll and pitch for cylinders 1 and 2 of the array.

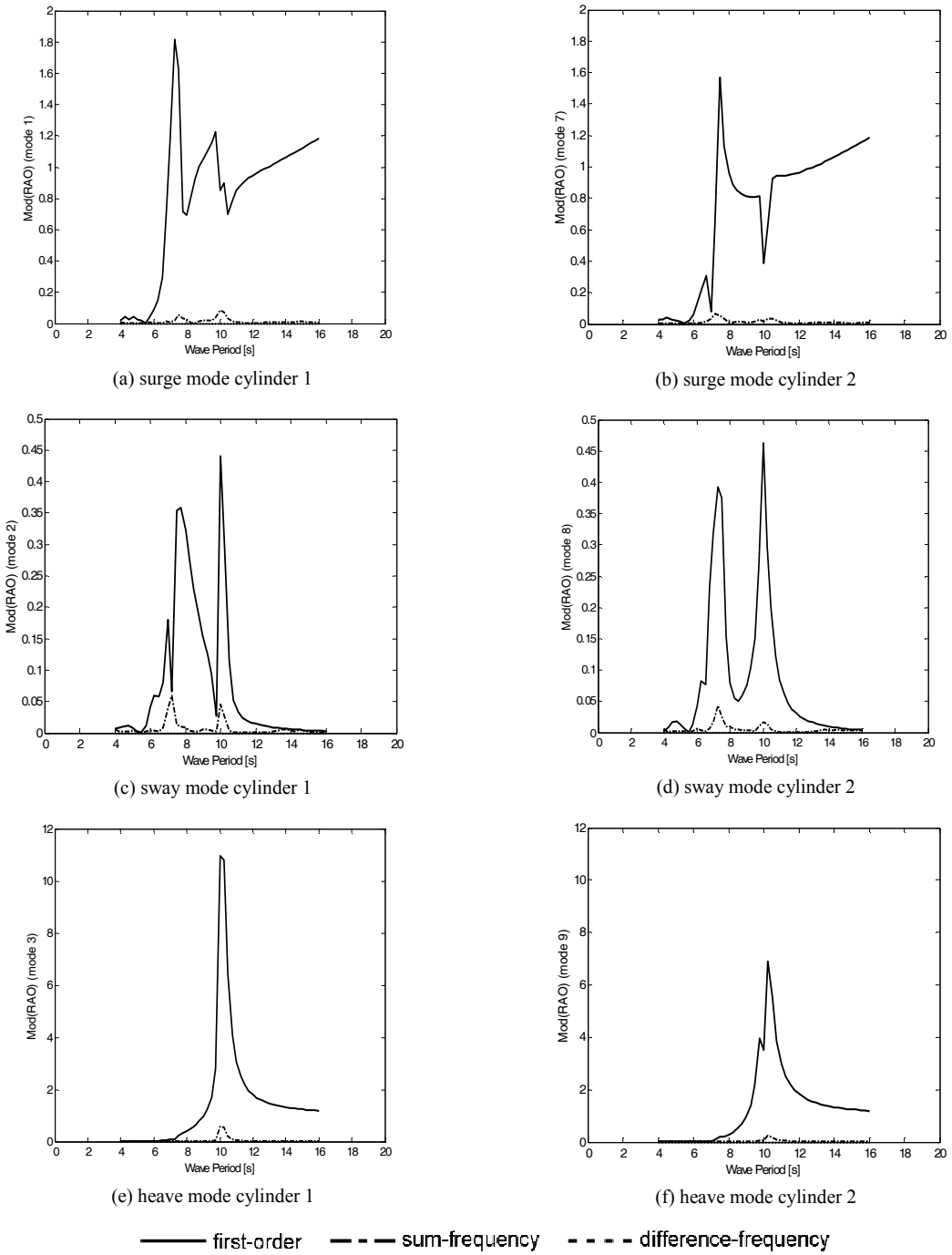

Figure 27:First and second order sum-frequency component RAOs in surge, sway and heave of the unrestrained cylinders 1 and 2 in the array.

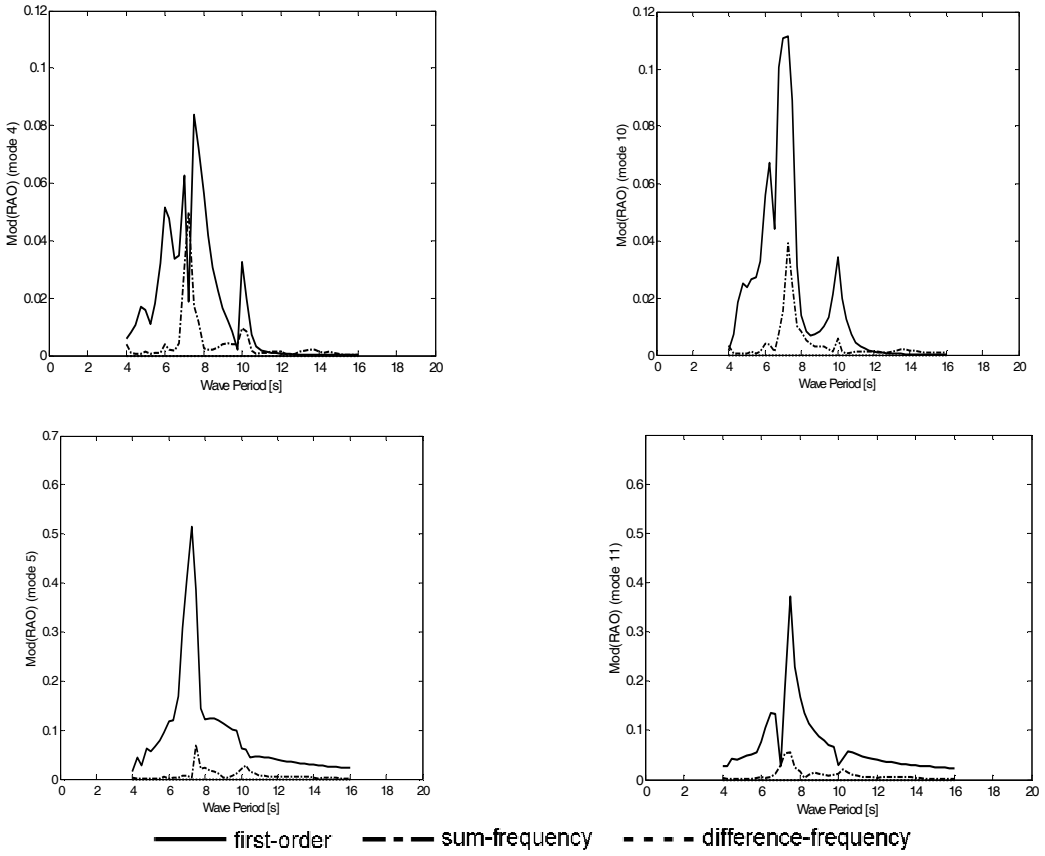

Figure 28:First and second order sum-frequency component RAOs in roll and pitch of the unrestrained cylinders 1 and 2 in the array.

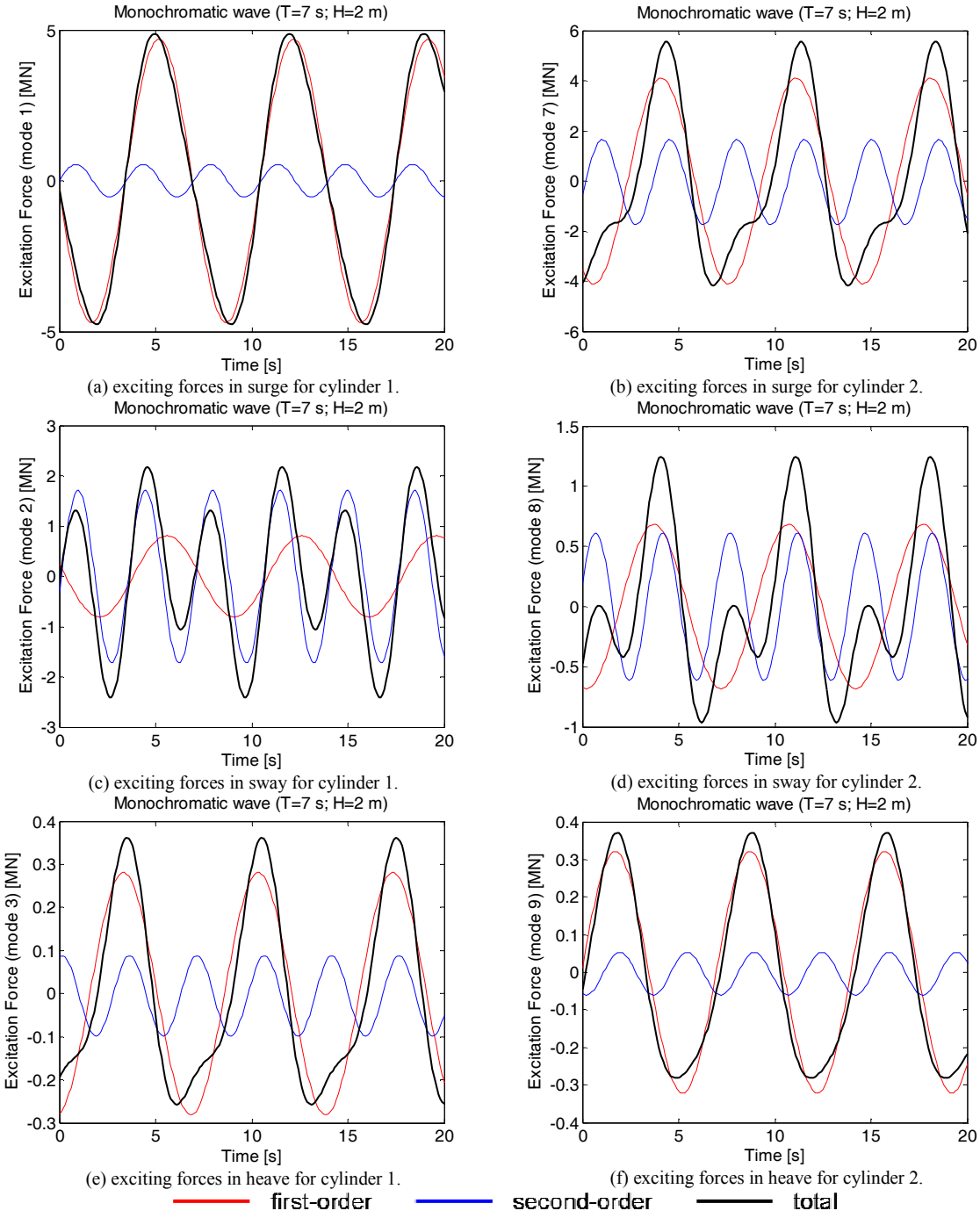

(a) exciting forces in surge for cylinder 1.

(b) exciting forces in surge for cylinder 2.

(c) exciting forces in sway for cylinder 1.

(d) exciting forces in sway for cylinder 2.

(e) exciting forces in heave for cylinder 1.

(f) exciting forces in heave for cylinder 2.

Figure 29: First, second-order and total exciting force in surge, sway and heave for cylinders 1 and 2 in the array for a wave with period T=7s and height H=2m.

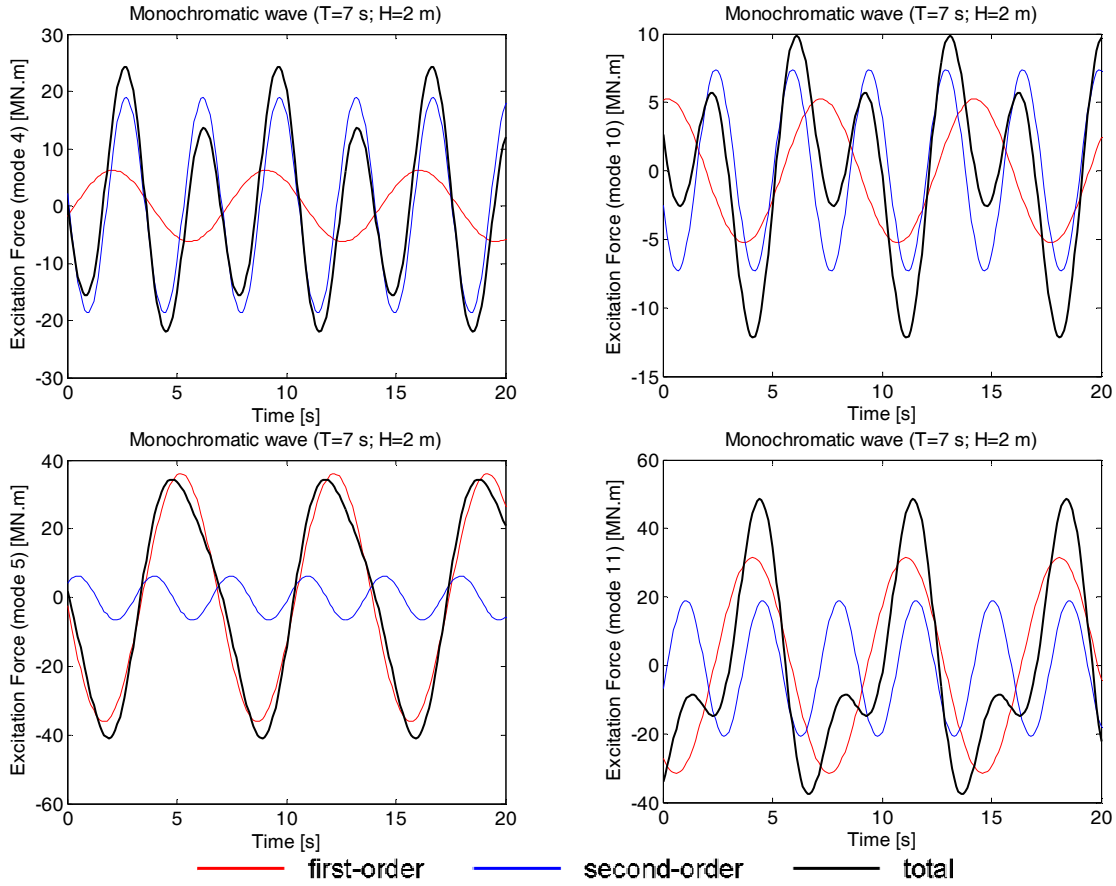

Figure 30: First, second-order and total exciting force in roll and pitch for cylinders 1 and 2 in the array for a wave with period T=7s and height H=2m.

7.2.2 Irregular waves.

In this subsection irregular wave results obtained for the array of four truncated cylinders are presented. The input sea state was selected as a unidirectional Pierson-Moskowitz spectrum for which the variance density is given by Equation (91). A H_s equal to 2.5m was selected (leading to T_p=7.9s). The direction of the incident waves is shown in Figure 21. The spectrum is discretised with 16 components equally spaced by 0.01 Hz.

The time series associated with the first, second and total exciting forces computed by Equations (78) and (79) and associated with this spectrum are shown for all relevant modes of motion for cylinders 1 and 2 in the array in Figure 31 and Figure 32. The plots show that the first order exciting force component is dominant for most modes of motion. Comparing with the case of the single truncated cylinder, it can be observed that due to the array interactions a higher second-order component in surge occurs for the front cylinder (1) in the array and also that the second-order exciting force component in heave for the front cylinder has an important contribution for the total exciting force, as was the case for the single truncated cylinder.

The contour plots obtained for the absolute value of the sum and difference-frequency QTFs for cylinders 1 and 2 in the array for all modes of motion are shown in Figure 33 to Figure 36. When comparing these with the single truncated cylinder case (Figure 18), the plots show in general higher values around the peaks for the front cylinder (1). The results are also consistent with what was observed for the regular waves case for which the peaks are found at the interacting wave periods around 7 and 10s which have higher values for the regular waves.

The first and second-order unrestrained motions for cylinders 1 and 2 in the array for all relevant modes of motion are shown in Figure 37 and Figure 38. As in the case of the single cylinder, the first-order unrestrained motions are dominant in most cases, except for surge and sway where the slowly drift motion associated with the difference-frequency component is observed.

The time series responses of the excitation forces associated with cylinders 1 and 2 in the array are shown in Figure Figure 29 and Figure 30. Due to the array interactions, the excitation forces in sway roll are of the same order of magnitude as the forces in surge and pitch respectively which did not occur for the case of the single truncated cylinder where these forces were negligible due to the axisymmetric propertied of the cylinder. For these modes of motion the second order components are dominant relatively to the first order. It is also observable that the relative importance of the second order component of the excitation forces increases for cylinder number 2 for surge and pitch modes of motion.

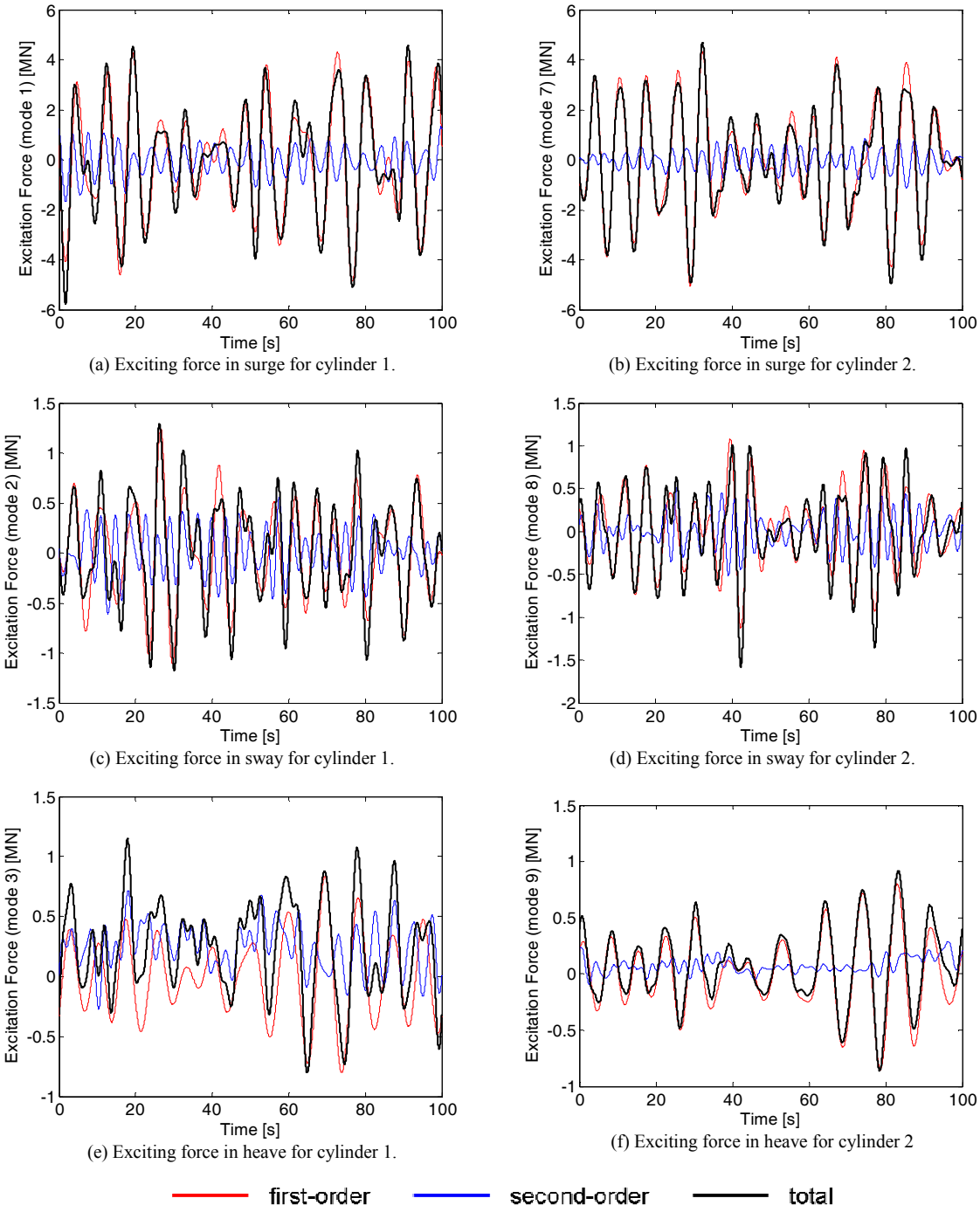

Figure 31: First, second and total exciting forces in surge, sway and heave for cylinders 1 and 2 in the array for Pierson-Moskowitz spectrum with Hs=2.5m (Tp=7.9s) described with sixteen components .

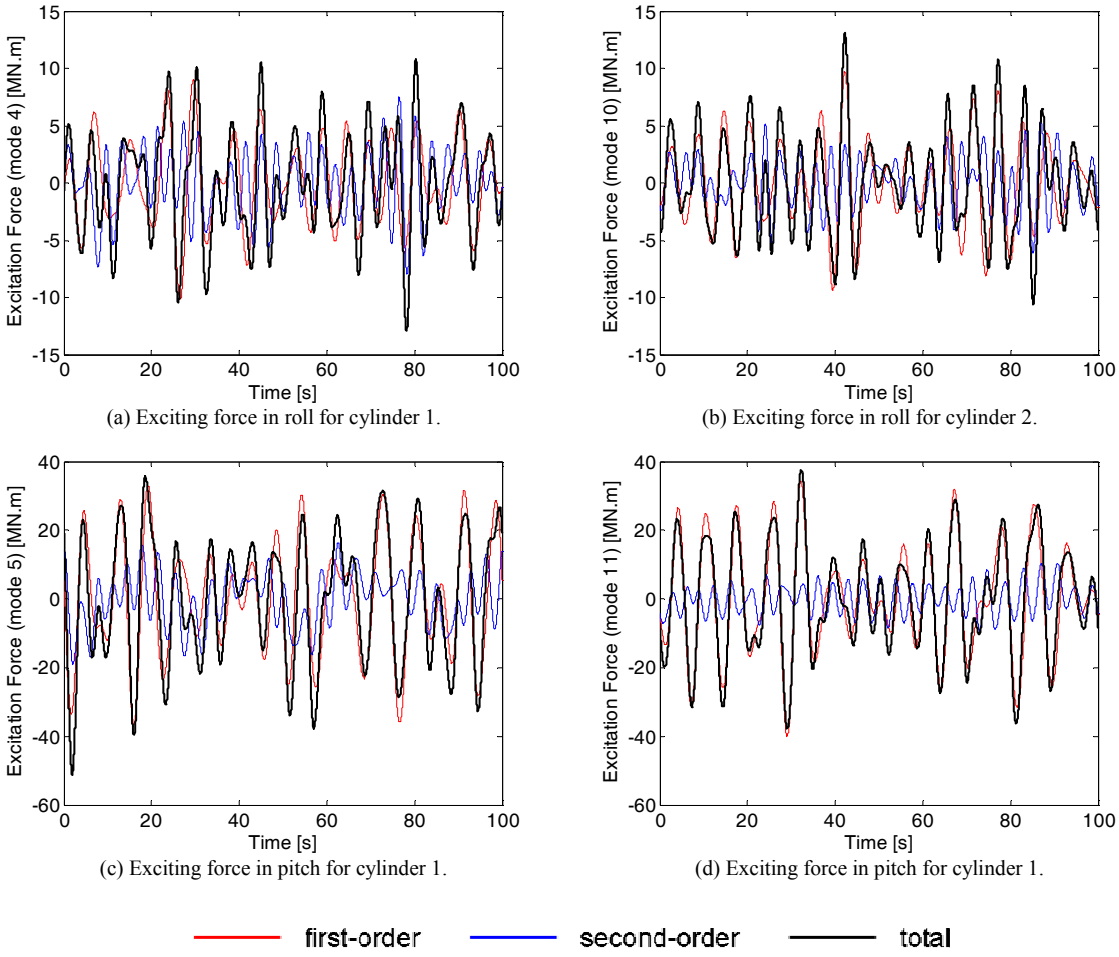

(a) Exciting force in roll for cylinder 1.

(b) Exciting force in roll for cylinder 2.

(c) Exciting force in pitch for cylinder 1.

(d) Exciting force in pitch for cylinder 1.

Figure 32: First, second and total exciting forces in roll and pitch for cylinders 1 and 2 in the array for Pierson-Moskowitz spectrum with Hs=2.5m (Tp=7.9s) described with sixteen components .

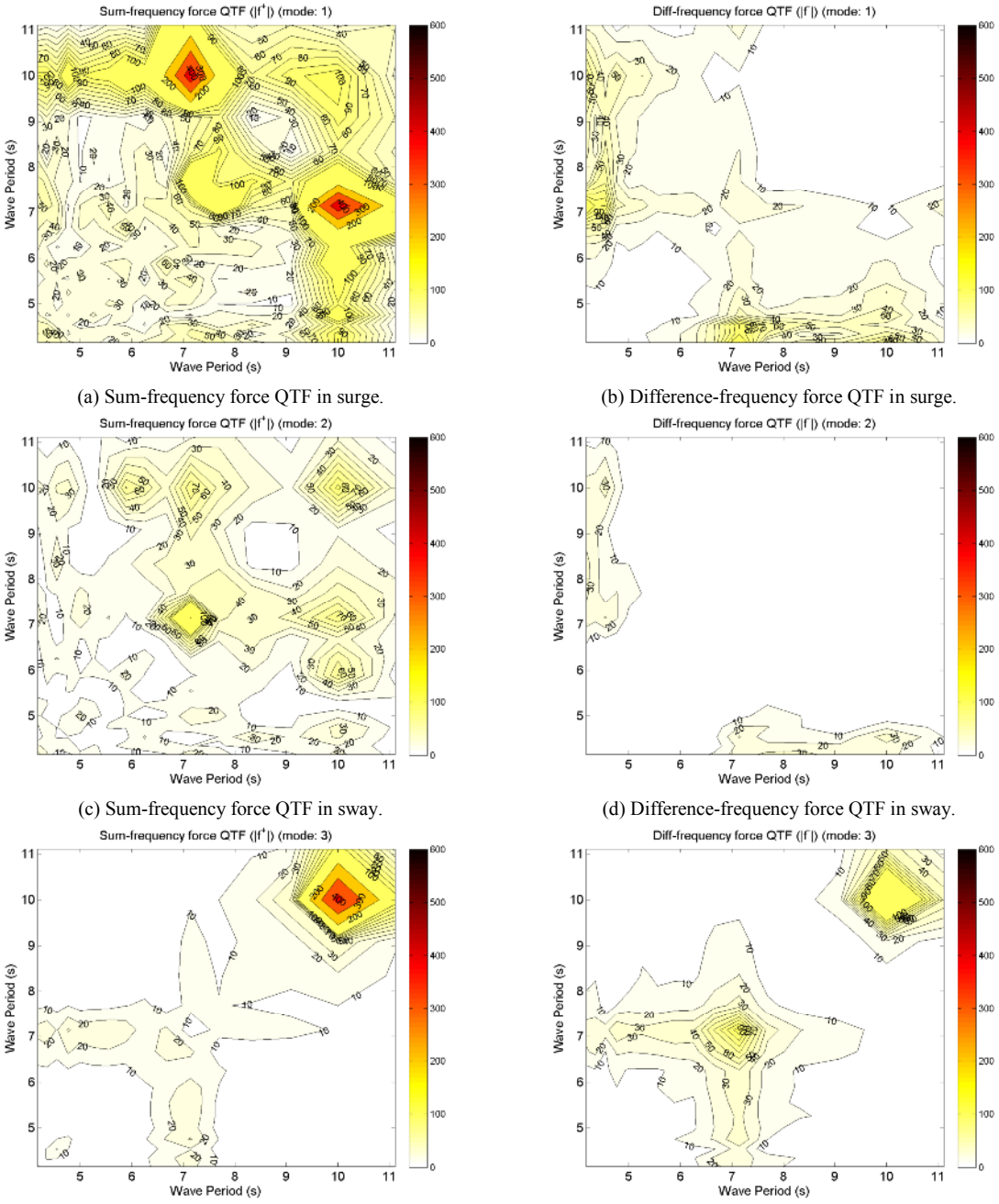

(a) Sum-frequency force QTF in surge.

(b) Difference-frequency force QTF in surge.

(c) Sum-frequency force QTF in sway.

(d) Difference-frequency force QTF in sway.

(e) Sum-frequency force QTF in heave.

(f) Difference-frequency force QTF in heave.

Figure 33: Contour plots of the absolute value of the sum and difference frequency force QTFs for cylinder 1 in the array.

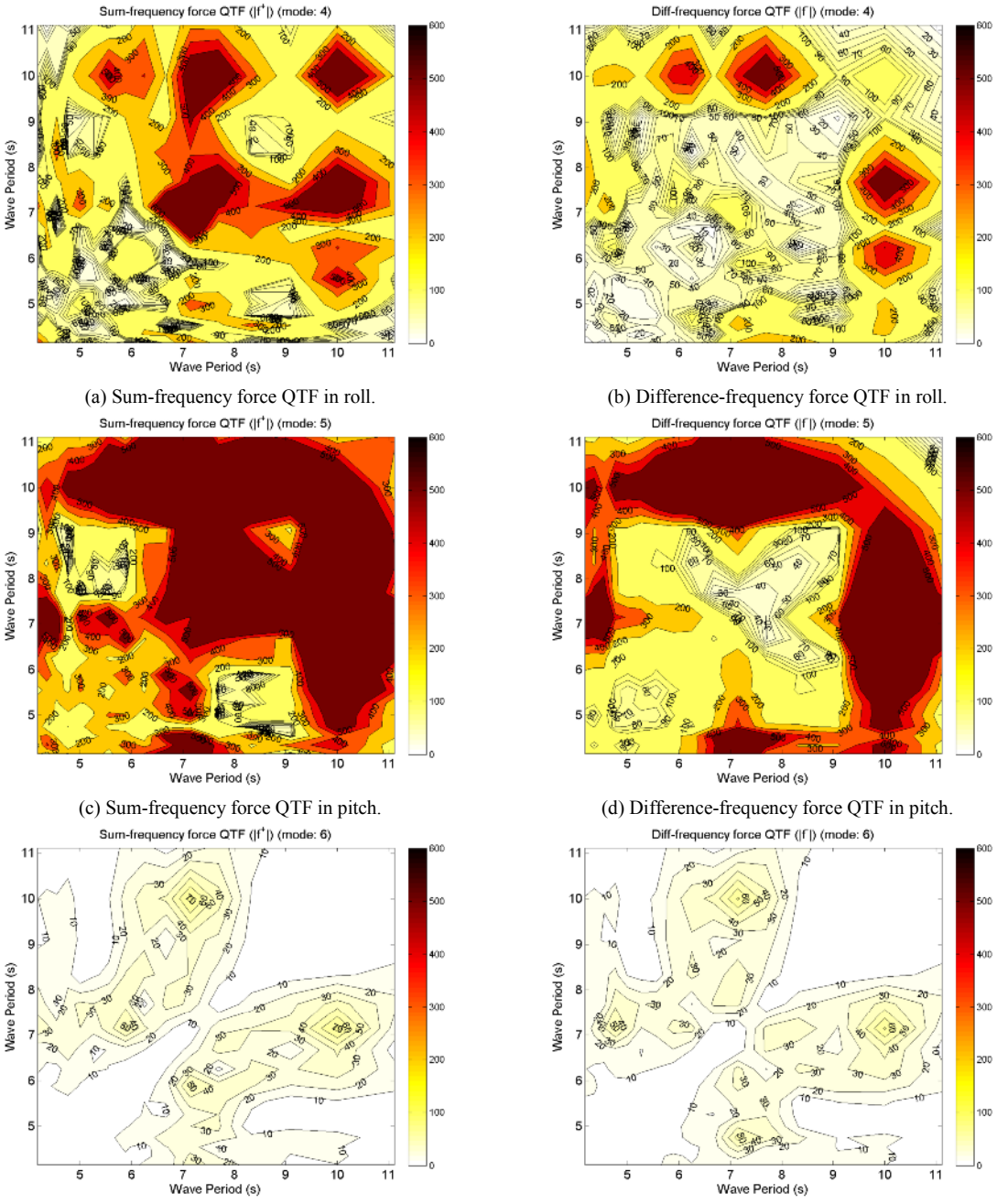

(a) Sum-frequency force QTF in roll.

(b) Difference-frequency force QTF in roll.

(c) Sum-frequency force QTF in pitch.

(d) Difference-frequency force QTF in pitch.

(e) Sum-frequency force QTF in yaw.

(f) Difference-frequency force QTF in yaw.

Figure 34: Contour plots of the absolute value of the sum and difference frequency force QTFs for cylinder 1 in the array.

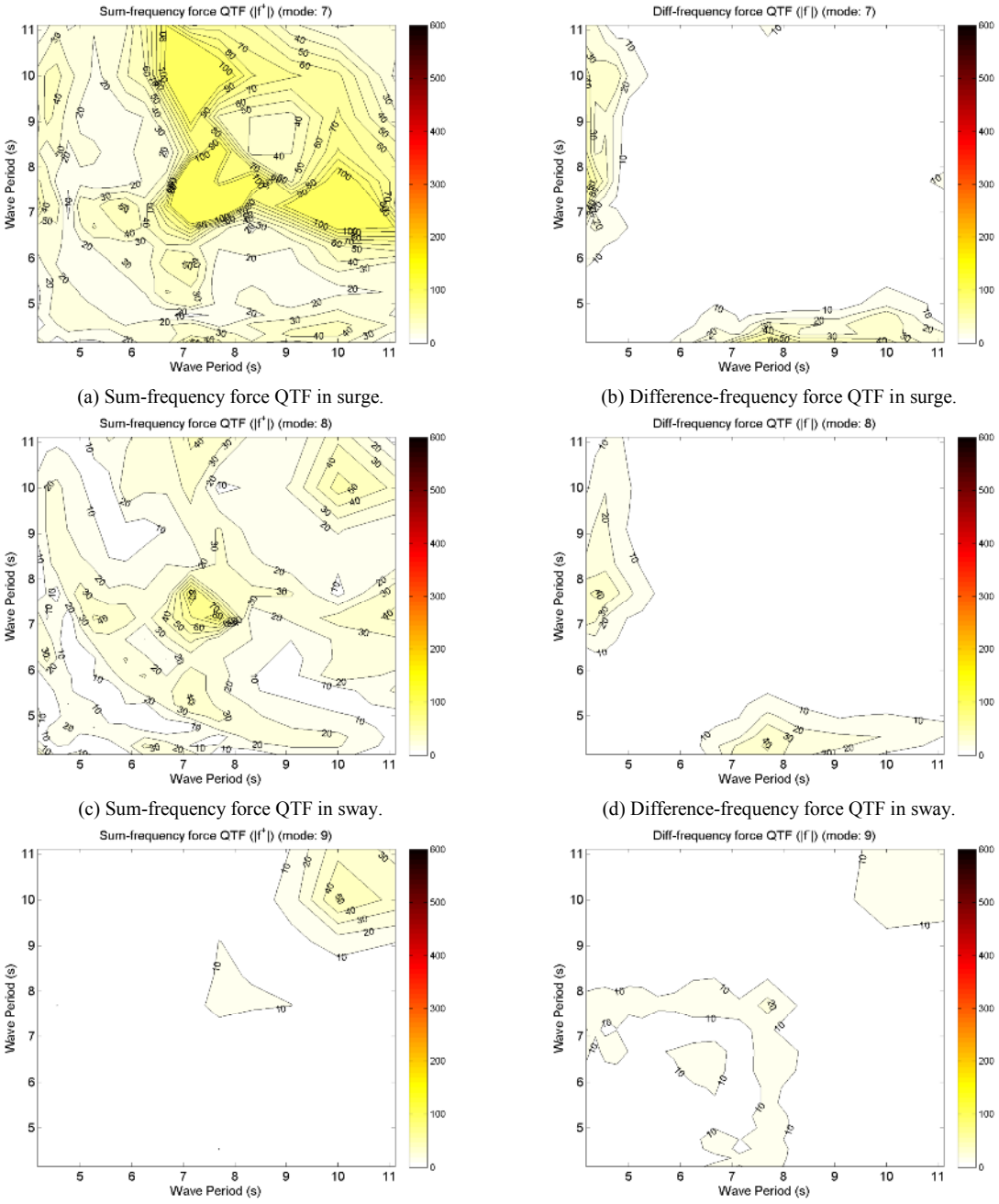

(a) Sum-frequency force QTF in surge.

(b) Difference-frequency force QTF in surge.

(c) Sum-frequency force QTF in sway.

(d) Difference-frequency force QTF in sway.

(e) Sum-frequency force QTF in heave.

(f) Difference-frequency force QTF in heave.

Figure 35: Contour plots of the absolute value of the sum and difference frequency force QTFs for cylinder 2 in the array.

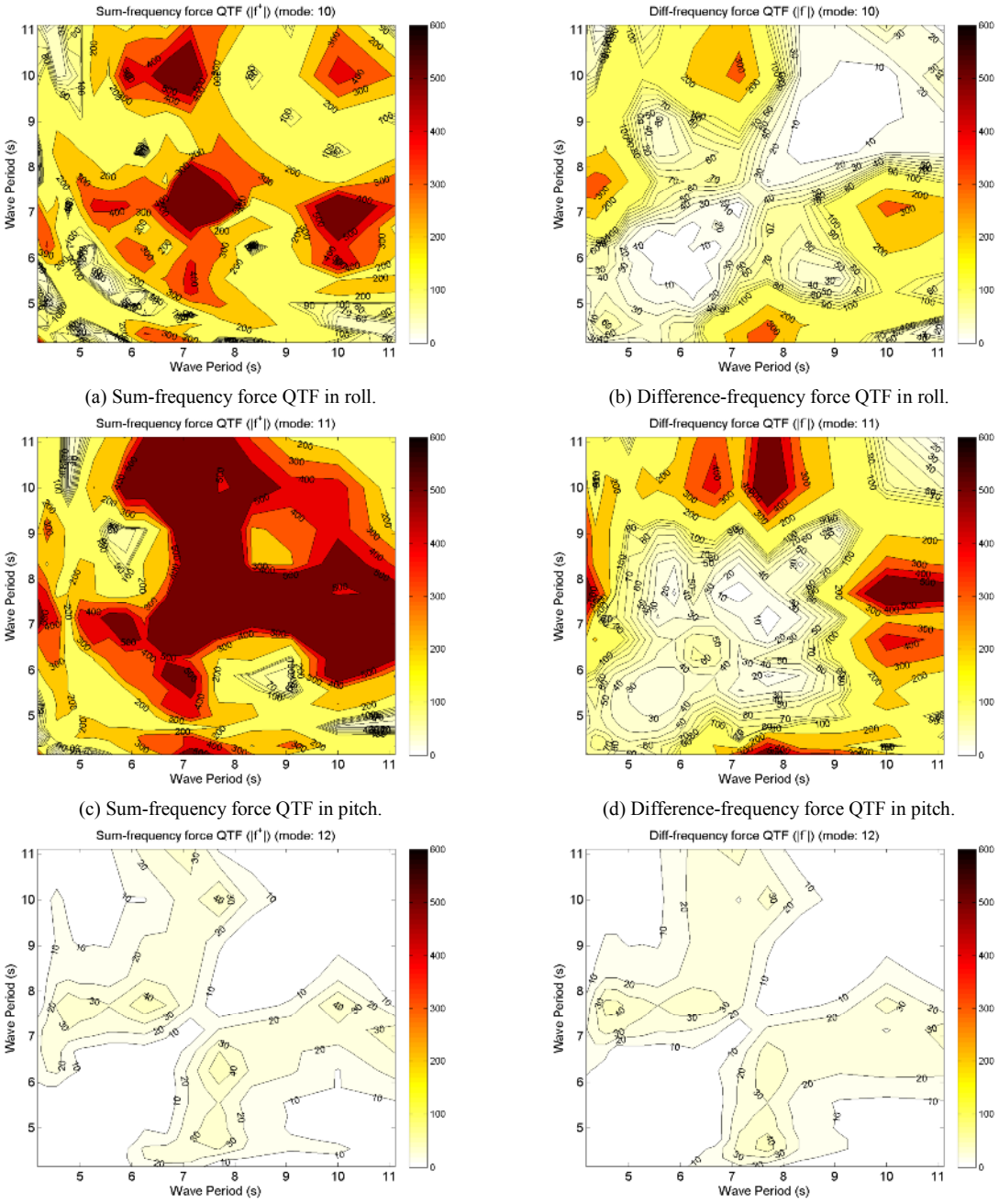

(a) Sum-frequency force QTF in roll.

(b) Difference-frequency force QTF in roll.

(c) Sum-frequency force QTF in pitch.

(d) Difference-frequency force QTF in pitch.

(e) Sum-frequency force QTF in yaw.

(f) Sum-frequency force QTF in yaw.

Figure 36: Contour plots of the absolute value of the sum and difference frequency force QTFs cylinder 2 in the array.

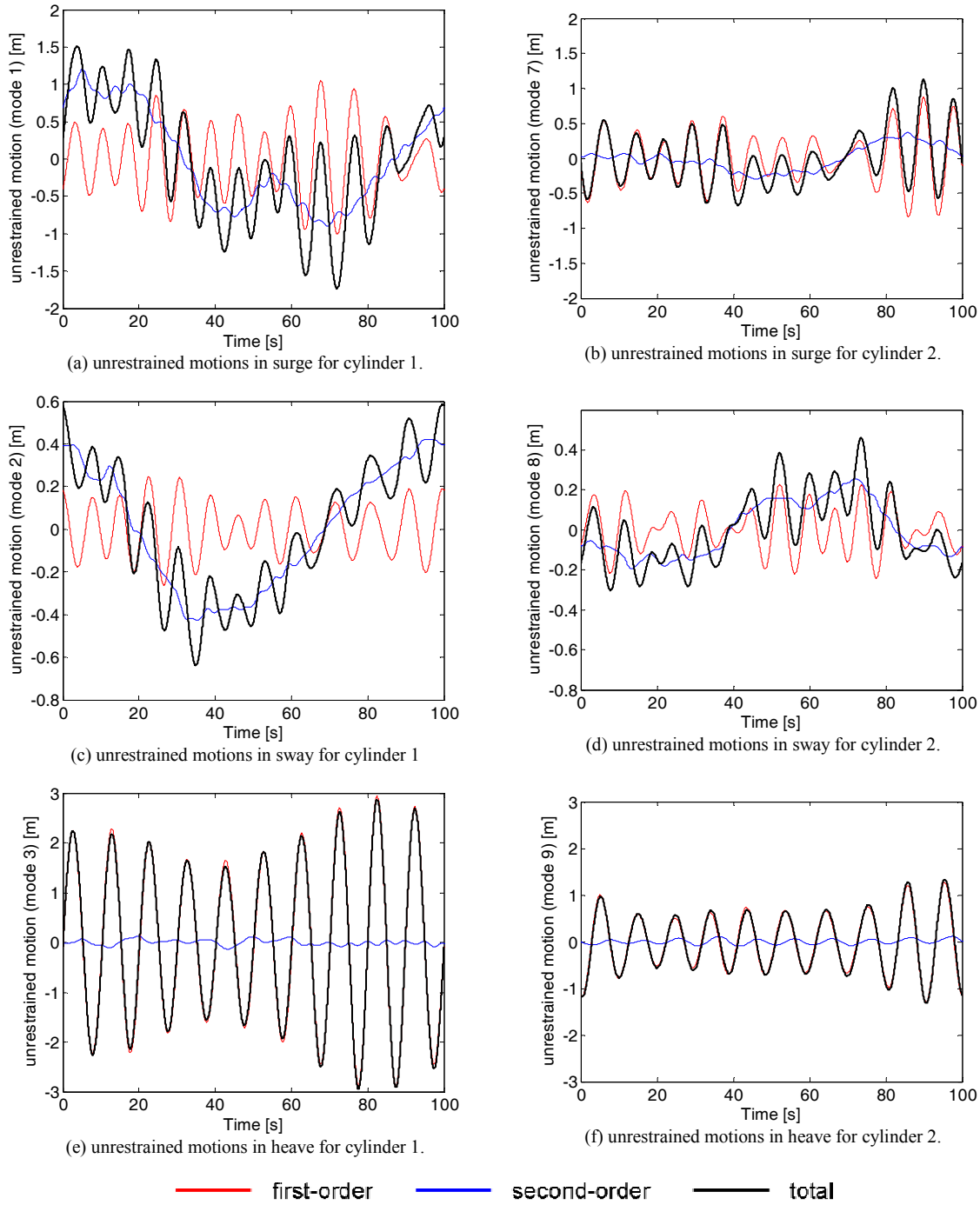

(a) unrestrained motions in surge for cylinder 1.

(b) unrestrained motions in surge for cylinder 2.

(c) unrestrained motions in sway for cylinder 1

(d) unrestrained motions in sway for cylinder 2.

(e) unrestrained motions in heave for cylinder 1.

(f) unrestrained motions in heave for cylinder 2.

Figure 37: First, second and total unrestrained motions in surge, sway and heave for cylinder 1 and 2 in the array for a Pierson-Moskowitz spectrum with Hs=2.5m (Tp=7.9s) described by sixteen components.

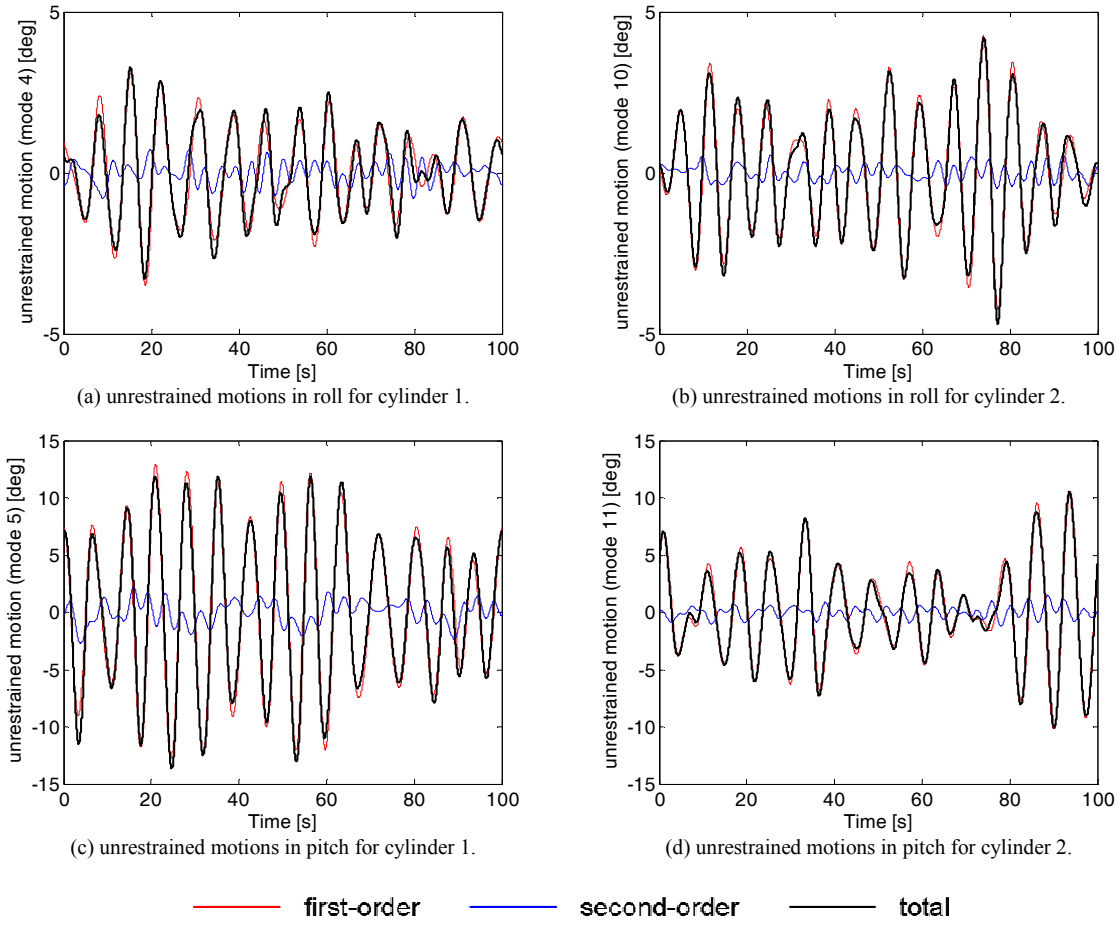

(a) unrestrained motions in roll for cylinder 1.

(b) unrestrained motions in roll for cylinder 2.

(c) unrestrained motions in pitch for cylinder 1.

(d) unrestrained motions in pitch for cylinder 2.

Figure 38: First, second and total unrestrained motions in roll and pitch for cylinder 1 and 2 in the array for a Pierson-Moskowitz spectrum with Hs=2.5m (Tp=7.9s) described by sixteen components.

8 FINAL REMARKS AND NEXT STEPS

The present report presents the results obtained for the linear and weakly nonlinear hydrodynamic forces and unrestrained motions associated with a single truncated cylinder and an array with four cylinders which can be used as point absorber WECs. The cylinders are free to move in all modes of motion and no PTO mechanism or mooring arrangement is considered in the present report.

The hydrodynamic forces are obtained through potential flow theory which assumes an incompressible and inviscid fluid under a irrotational flow condition. The fluid velocity is described by a potential function required to satisfy the Laplace equation in all fluid domain and boundary conditions at the interfaces. The full expression of these boundary conditions is mathematically difficult to solve and computationally intensive as the numerical methods developed require the redefinition of the problem conditions at each time step to fully cover the changes of the free-surface of the fluid and describe fully the floating structure motions.

It is usual, however, to approximate the hydrodynamic solution of the problem to first or second-order by assuming that the wave amplitude of the incoming waves is small in relation to the wavelength. These approximations are computationally more efficient as a time stepping solution can be avoided by computing the hydrodynamic forces and motions over the mean wet surface instead of the instantaneous wet surface of the floating structure.

It should be noted that the present report does not access any result associated with fully nonlinear potential flow hydrodynamic models.

The commercial software WAMIT (v6.1s) was used to compute both the linear and weakly nonlinear hydrodynamic loads and unrestrained motions for a single cylinder and an array with four cylinders. This software solves the hydrodynamic problem in the frequency domain and a description of the methods which are used is given in Sections 3 and 4 respectively.

The generalisation of the second-order theory to the case of wave-body interactions with irregular waves requires the definition of bi-chromatic wave components and the solution is obtained in terms of the sum and difference frequency components of the usual hydrodynamic quantities. The second-order excitations forces are obtained as the sum of the force quadratic transfer functions (QTF) in the sum- and difference-frequency as given by Equation (67).

For the single truncated cylinder the second-order excitation force components associated with most regular waves are much smaller than the first-order excitation force component in surge and pitch. In heave the second order components are high at the wave periods close to resonance. The unrestrained motions are small and dominated by the first-order component for all modes of motion. However, for the steepest wave (with period equal to 10.25s and wave height equal to 6m) the second-order component was found to be of the same importance as the first-order.

Similar results were found for the single truncated cylinder excited by irregular waves. The excitation forces and unrestrained motions were computed for a PM spectrum with significant wave height of 2.5m (and T_p=7.9s) and it was found that the first-order component of the excitation force are dominant for both surge and pitch modes. In heave, the second-order component has higher values with a non negligible contribution for the total excitation force. The unrestrained motions were small with the first-order component being dominant for heave and pitch. In surge, the slowly varying drift motion associated with the difference frequency component was observed.

For the array with four cylinders an increase of the peak values associated with the sum-frequency force QTF component was found whereas a decrease was found for the difference-frequency component. A sharp increase in the value of the absolute value of the sum-frequency force QTF is found for wave periods close to 7.5s for all modes of motion except heave. When comparing with the single truncated cylinder, there was found to be an increase in the second-order excitation force component in surge and heave for the front cylinder (1) in the array. The unrestrained motions of the cylinders in the array are dominated by the first-order component, except for surge and sway where the slowly drift motion associated with the difference frequency component is observed.

The weakly nonlinear results obtained in the present report for the isolated cylinder and the array with four cylinders are suitable for comparisons with the fully nonlinear hydrodynamic approach to be envisaged in WG1 WP1 D9 and WG1 WP1 D10. A further investigation to evaluate the importance of second-order components associated with more realistic setups for which the cylinders are restrained through a PTO system and mooring arrangement should be pursued. Such comparisons for the fully nonlinear case will be performed in WG1 WP1 D11 and WG1 WP1 D12 for a single and array of four cylinders respectively. Further comparisons with experimental results from WG2 WP1 and WG2 WP1 will require additional geometries to be modelled, thus it is recommended (as proposed in WG0 D1) that the linear, second-order and fully nonlinear simulations are firstly compared for the geometry described in this report to allow preliminary findings to taken (verification exercise) regarding the particular input settings to test experimentally.

REFERENCES

Birknes, J. (2001), A Convergence Study of Second-Order Wave Elevation on Four Cylinders, Proceedings of the Eleventh International Offshore and Polar Engineering Conference, Stavanger, Norway, June 17-22, 2001.

Cruz., J. (2009), "Numerical and Experimental Modelling of Offshore Wave Energy Converters.", PhD thesis, Instituto Superior Técnico.

Evans, D. V. (1981). "Power from water waves", Annual reviews of fluid mechanics, 13:157–187.

Evans, D. V. and Linton, C. M. (1993), "Hydrodynamics of wave-energy devices". Technical report, University of Bristol, Department of Mathematics.

Falnes, J. (2002),."Ocean waves and oscillating systems", Cambridge University Press.

Faltinsen, O. M. (1990) "Sea loads on ships and offshore structures". Cambridge University Press.

Kim, M.-H. and Yue, D. K. P. (1989), "The complete second-order diffraction solution for an axisymmetric body Part 1. Monochromatic incident waves", J. Fluid Mech., vol. 200. pp . 235-264.

Kim, M.-H. and Yue, D. K. P. (1990), "The complete second-order diffraction solution for an axisymmetric body Part 2. Bichromatic incident waves and body motions", J. Fluid Mech., vol. 211. pp . 557-593.

Lee, C.-H. (1991), "Second-order wave loads on a stationary body", 6th International workshop on water waves and floating bodies.

Lee, C.-H. (1993), "Second-order diffraction and radiation solutions on floating bodies", 8th International workshop on water waves and floating bodies.

Lee, C.-H.(1995), "WAMIT Theory Manual", MIT Department of Ocean Engineering, Report No. 95-2.

Lee, C.-H., Newman, J. N., Kim, M.-H (1991), "The computation of second-order wave loads", OMAE, Stavanger, Norway.

Lee, C.-H. and Newman, J. N.(2007), Computation of wave effects using the panel method, Numerical models in Fluid-Structure Interaction.

Lee, C.-H, Maniar, H. D., Newman, J. N., and Zhu, X.. (1996) Computations of wave loads using a B-spline panel method. In Proceedings of the 21st symposium on naval hydrodynamics, pp 75–92, Trondheim, Norway.

Lee , C.-H., Farina, L., and Newman, J. N. (1998). A geometry-independent higher-order panel method and its application to wave-body interactions. In Proceedings of the 3rd engineering mathematics and applications conference, pages 303–306, Adelaide, Australia.

Mei, C. C. (1989), "The applied dynamics of ocean surface waves",. Advanced Series on Ocean Engineering. World Scientific., Singapore, 2nd edition.

Newman, J. N. (1977), "Marine Hydrodynamics", The MIT Press.

Newman, J. N. and Sclavounos, P. D. (1988). "The computation of wave loads on large offshore structures". In "BOSS" Conference, Trondheim, Norway.

Roache, P. J. (1997), "Quantification of uncertainty in computational fluid dynamics.", Annual Review of Fluid Mechanics, 29(1):123–160.

Sarpkaya , T. and Isaacson, M. (1981). "Mechanics of wave forces on offshore structures". Van Nostrand Reinhold Company.

Tucker, M. J. and Pitt, E. G. (2001), Waves in ocean engineering, Elsevier Science Ltd., 2001.

WAMIT (2006), "User Manual (Versions 6.4, 6.4PC, 6.3S, 6.3S-PC)", WAMIT, Inc., 2006. URL www.wamit.com.

Wehausen, J. V., (1971). "The motion of floating bodies". *Annual reviews of fluid mechanics*, 3: 7–268.

Wehausen, J. V. and Laitone, E. V. (1960). "Surface Waves", *volume IX of Encyclopaedia of Physics*, pages 446–778. Springer Verlag,.

NOMENCLATURE

$\vec{\alpha}$	Angular displacement vector between the body fixed and the inertial coordinate systems.
β	Angle of incidence of the incident wave.
ϵ	Random phase uniformly distributed between [0, 2 π] associated with the incident wave.
η	Free-surface elevation.
λ	Wavelength of the incident wave.
$\vec{\xi}$	Linear displacement vector between the body and the inertial coordinate systems.
$\vec{\xi}^{\pm}$	Sum and difference frequency displacement vector.
ρ	Density of the fluid.
ϱ_0	Partition radius.
ϱ_1	Inner partition radius.
ϕ	Velocity potential.
$\phi^{(1)}$	First order velocity potential.
$\phi^{(2)}$	Second order velocity potential.
$\phi^{\pm}$	Sum(+) and difference(-) frequency velocity potential.
ϕ_D	Velocity potential of the diffracted wave.
ϕ_I	Velocity potential of the incident wave.
ϕ_R	Velocity potential of the radiated wave.
ϕ_S	Velocity potential of the scattered wave.
$\phi_I^{\pm}$ / $\phi_D^{\pm}$ / $\phi_R^{\pm}$	Sum and difference frequency potential velocity associated with the incident, diffracted and radiated wave.
$\vec{\Omega}$	Angular velocity of the floating structure
ω	Angular frequency of the incident wave.
$\omega_{jl}^{\pm} = \omega_j \pm \omega_l$	Sum and difference angular frequency associated with two components of an incident wave spectrum.
A	Added mass matrix.
a	Wave amplitude.
B	Hydrodynamic damping matrix.
C	Hydrostatic stiffness matrix.
$\vec{f}_h$ / $\vec{m}_h$	Total hydrodynamic force / moment.

$\vec{f}_X$ / $\vec{m}_X$	Total excitation force / moment.
$\vec{f}_X^{(1)}$ / $\vec{m}_X^{(1)}$	First-order excitation force / moment.
$\vec{f}_X^{(2)}$ / $\vec{m}_X^{(2)}$	Second-order excitation force / moment.
$\vec{f}_R^{(1)}$/ $\vec{m}_R^{(1)}$	First-order radiation force / moment.
$\vec{f}_R^{(2)}$ / $\vec{m}_R^{(2)}$	Second-order radiation force / moment.
$\vec{f}_C^{(1)}$ / $\vec{m}_C^{(1)}$	First-order hydrostatic force / moment.
$\vec{f}_C^{(2)}$ / $\vec{m}_C^{(2)}$	Second-order hydrostatic force / moment.
$\vec{f}_p^{(2)}$ / $\vec{m}_p^{(2)}$	Second-order potential force / moment.
$\vec{f}_q^{(2)}$	Second-order quadratic force / moment.
$\vec{f}_I^{(2)}$	Second-order force force / moment due to the incident wave.
$\vec{f}_D^{(2)}$	Second-order force force / moment due to the diffracted wave.
$\vec{f}^{\pm}$	Sum(+) and difference(-) frequency force quadratic transfer functions (QTFs).
g	Gravitational constant.
H	Second-order approximation of the rotation matrix between the body fixed and global coordinate systems.
I	Inertia matrix (at the principal axis). ??? Check.
k	Wave number of the incident wave.
M	Mass matrix.
$\vec{n}$	Normal to the wetted profile pointing out of the fluid volume (and hence into the body)
p	Fluid pressure.
(Q_F)	Forcing function associated with the second-order free-surface boundary condition.
(Q_B)	Forcing function associated with the second-order boundary condition at the solid boundaries of the floating structure.
$\vec{r} = (x_1, x_2, x_3)$	Position vector.
t	Time variable.
T	Wave period.
T	Rotation matrix between the body fixed and the global coordinate system.
$\vec{u}$	Velocity of the floating structure.
$\vec{U}$	Velocity of the origin of the body fixed CS

$\vec{v}$	Velocity of the fluid vector.
$\vec{X}$	Complex amplitude vector of the excitation forces.
(x_1, x_2, x_3)	Cartesian coordinate the global (inertial) reference frame.
$(\tilde{x}_1, \tilde{x}_2, \tilde{x}_3)$	Cartesian coordinates in the body fixed coordinate system.

APPENDIX A: SUM- AND DIFFERENCE- FORCE QTFS FOR THE SINGLE TRUNCATED CYLINDER

The tables in this appendix present the sum- and difference- frequency force QTFs (f^+, f^-) computed for the truncated cylinder in surge, heave and pitch modes associated with the sixteen frequency components of the Pierson-Moskowitz spectra with Hs=2.5m considered in Section 6.2.2.

Each table is divided by a shaded diagonal to which the top side represents the real part of the complex force QTF whereas the bottom part of the table represents the imaginary part.

Note that the sum-frequency component of the force QTF is symmetric satisfying the relation: $f_{kl}^{+}(\omega_k + \omega_l) = f_{lk}^{+}(\omega_l + \omega_k)$, whereas the difference-frequency force QTFs are complex conjugate symmetric satisfying the relation: $f_{kl}^{-}(\omega_k - \omega_l) = f_{lk}^{-*}(\omega_l - \omega_k)$.

The components of the diagonal correspond to the to the sum- and difference- force QTFs at double and zero frequency and are shown in a separate table.

	Real part:															
T [s]	**11.11**	**10.00**	**9.09**	**8.33**	**7.69**	**7.14**	**6.67**	**6.25**	**5.88**	**5.56**	**5.26**	**5.00**	**4.76**	**4.55**	**4.35**	**4.17**
11.11	*	11.20	27.58	46.09	77.66	42.74	-3.69	-7.03	-5.25	-3.62	-2.01	-0.82	0.35	1.64	2.59	3.03
10.00	-20.55	*	-14.54	-25.70	-85.50	-186.80	-119.40	-85.48	-73.57	-69.39	-68.32	-67.99	-66.48	-64.64	-62.58	-59.27
9.09	4.49	-53.56	*	10.14	9.06	-16.98	-19.03	-15.90	-15.30	-16.27	-17.94	-18.80	-19.15	-19.36	-19.73	-20.07
8.33	3.99	-78.58	-11.27	*	27.74	3.80	-7.45	-7.19	-7.82	-9.62	-11.48	-13.26	-15.74	-17.47	-18.90	-20.73
7.69	-20.15	-118.70	-22.84	-21.70	*	18.61	4.38	3.51	2.42	0.39	-1.61	-3.58	-3.20	-4.61	-7.24	-9.79
7.14	-87.22	-22.80	-23.53	-34.81	-48.53	*	-7.20	-4.16	0.02	4.59	9.57	14.04	19.06	24.99	30.67	33.42
6.67	-60.24	43.76	-4.77	-16.42	-29.48	-50.66	*	-13.88	-8.78	-3.42	2.20	7.95	11.86	17.54	24.27	29.06
6.25	-39.33	38.27	1.00	-7.38	-17.68	-37.68	-30.88	*	-7.10	-2.92	1.16	5.52	8.66	12.19	16.43	20.50
5.88	-29.30	28.60	3.36	-2.27	-8.99	-27.53	-25.24	-21.95	*	0.13	3.11	6.73	9.25	11.66	14.78	17.43
5.56	-23.13	21.29	5.34	1.91	-0.85	-17.90	-20.58	-19.21	-19.03	*	6.44	9.70	11.39	13.49	16.08	16.82
5.26	-18.46	14.78	7.62	6.48	7.18	-8.28	-16.27	-16.30	-17.27	-19.09	*	12.96	14.23	16.36	17.25	18.13
5.00	-14.49	11.09	10.13	10.12	16.30	0.21	-12.43	-13.75	-15.22	-17.74	-20.90	*	16.66	18.46	19.81	23.16
4.76	-11.14	8.43	11.56	13.85	23.32	11.34	-7.97	-11.89	-13.99	-16.85	-20.12	-24.05	*	21.16	25.61	25.01
4.55	-8.26	5.81	12.36	17.02	28.46	19.64	-3.18	-8.68	-11.14	-14.03	-18.40	-21.80	-25.95	*	26.48	31.43
4.35	-5.48	0.54	12.94	18.98	32.33	25.69	1.13	-4.65	-7.47	-11.09	-15.61	-19.07	-22.64	-25.51	*	36.23
4.17	-3.35	-5.22	13.03	19.35	35.65	31.19	3.40	-3.33	-6.54	-9.38	-11.22	-13.40	-19.39	-24.10	-25.41	*
	Imaginary part:															

Table 9: Sum-frequency force QTFs (f^+) in surge for the single truncated cylinder.

	Real part:															
T [s]	**11.11**	**10.00**	**9.09**	**8.33**	**7.69**	**7.14**	**6.67**	**6.25**	**5.88**	**5.56**	**5.26**	**5.00**	**4.76**	**4.55**	**4.35**	**4.17**
11.11	*	-3.23	-0.29	-0.99	-6.82	-17.28	-8.87	-3.72	-0.60	2.23	5.49	8.75	12.59	16.07	17.02	19.71
10.00	2.52	*	-1.68	0.83	5.09	3.91	0.25	0.75	2.13	4.16	7.06	12.60	16.91	25.40	28.32	28.21
9.09	-1.89	0.23	*	-2.05	-5.32	-9.15	-4.38	-1.95	-0.35	1.47	4.05	8.09	13.05	19.04	24.34	30.16
8.33	-5.85	1.57	-1.37	*	-6.64	-11.11	-5.50	-2.53	-0.49	1.81	5.01	9.52	15.55	22.30	30.69	39.69
7.69	-10.98	1.88	-2.67	-1.85	*	-15.47	-9.73	-6.76	-4.99	-3.15	-0.50	3.21	8.67	14.77	24.32	31.22
7.14	-0.79	-2.00	4.12	5.44	7.45	*	-16.73	-15.07	-15.72	-17.82	-20.96	-25.01	-28.83	-34.69	-39.81	-45.76
6.67	6.92	3.46	8.14	9.66	12.03	4.87	*	-10.30	-10.49	-12.01	-14.66	-18.38	-22.44	-28.47	-34.69	-41.45
6.25	6.96	9.73	9.39	10.76	13.58	6.06	0.07	*	-7.45	-7.91	-9.12	-11.00	-13.20	-16.51	-20.06	-23.72
5.88	6.89	15.72	11.35	12.85	16.72	8.58	0.50	-0.17	*	-6.52	-6.95	-7.78	-8.89	-10.66	-12.74	-14.03
5.56	7.25	21.80	14.09	16.10	21.86	13.09	1.90	0.32	0.06	*	-6.28	-6.54	-7.01	-7.86	-9.01	-9.55
5.26	7.70	28.26	17.45	20.35	28.97	19.84	4.34	1.64	0.83	0.34	*	-6.25	-6.33	-6.59	-7.04	-7.46
5.00	7.67	32.19	20.60	25.00	37.64	28.54	7.55	3.51	2.26	1.35	0.57	*	-6.22	-6.10	-6.12	-6.18
4.76	7.48	35.70	23.79	30.21	47.66	39.09	11.54	5.87	4.20	3.01	1.78	0.70	*	-6.07	-5.80	-5.60
4.55	5.15	38.03	25.39	34.10	58.36	51.76	16.13	8.46	6.27	4.86	3.42	1.91	0.69	*	-5.85	-5.55
4.35	3.52	33.07	25.05	37.26	69.23	64.57	18.47	9.15	7.35	6.32	5.02	3.49	1.96	0.64	*	-5.68
4.17	2.47	36.22	24.42	39.06	80.48	78.55	25.38	11.59	8.08	7.21	6.35	5.02	3.44	1.85	0.52	*
	Imaginary part:															

Table 10: Difference frequency force QTFs (f⁻)in surge for the single truncated cylinder.

	Real part:															
T [s]	**11.11**	**10.00**	**9.09**	**8.33**	**7.69**	**7.14**	**6.67**	**6.25**	**5.88**	**5.56**	**5.26**	**5.00**	**4.76**	**4.55**	**4.35**	**4.17**
11.11	*	-51.98	-7.73	-0.63	1.99	-3.12	-3.49	-1.99	-1.03	-0.43	-0.07	0.15	0.26	0.30	0.29	0.26
10.00	-44.23	*	18.48	10.85	7.81	-1.01	-2.01	-0.64	0.21	0.72	0.98	1.12	1.12	1.02	0.90	0.73
9.09	-3.02	19.20	*	6.91	5.72	-3.62	-2.89	-0.53	0.79	1.53	1.92	2.06	2.03	1.88	1.63	1.33
8.33	-2.81	4.14	-4.34	*	5.30	-5.49	-1.85	1.76	3.56	4.49	4.89	4.95	4.74	4.31	3.75	3.09
7.69	-5.73	-3.99	-9.03	-12.47	*	-7.10	3.82	9.28	11.78	13.05	13.53	13.42	12.82	11.87	10.58	9.13
7.14	-7.17	-6.65	-8.34	-7.99	-4.20	*	9.65	11.55	13.13	14.55	15.67	16.37	16.54	16.17	15.42	14.39
6.67	-2.44	-1.72	-1.18	0.83	2.95	-8.41	*	-0.26	0.51	1.84	3.26	4.52	5.50	6.11	6.47	6.61
6.25	-0.83	-0.30	0.76	2.65	2.90	-12.20	-13.28	*	-3.41	-2.02	-0.49	0.92	2.05	2.85	3.38	3.73
5.88	-0.24	0.23	1.46	3.29	2.90	-13.40	-13.52	-9.09	*	-3.53	-1.90	-0.35	0.88	1.76	2.34	2.72
5.56	0.05	0.55	1.83	3.71	3.27	-13.43	-13.60	-9.05	-5.47	*	-2.70	-1.06	0.28	1.23	1.84	2.20
5.26	0.21	0.78	2.06	3.97	3.78	-12.85	-13.47	-9.15	-5.69	-2.52	*	-1.50	-0.12	0.87	1.48	1.83
5.00	0.29	0.90	2.16	4.12	4.22	-11.87	-13.10	-9.21	-6.09	-3.18	-0.13	*	-0.35	0.61	1.15	1.46
4.76	0.34	0.98	2.20	4.14	4.61	-10.60	-12.45	-9.09	-6.42	-3.94	-1.27	1.71	*	0.42	0.86	1.05
4.55	0.36	1.01	2.16	4.06	4.94	-9.04	-11.52	-8.77	-6.54	-4.53	-2.36	0.12	2.93	*	0.44	0.48
4.35	0.35	0.99	2.07	3.93	5.16	-7.35	-10.32	-8.13	-6.33	-4.76	-3.11	-1.17	1.09	3.55	*	-0.44
4.17	0.33	0.95	1.94	3.75	5.28	-5.58	-8.92	-7.25	-5.84	-4.62	-3.38	-1.96	-0.27	1.65	3.64	*
	Imaginary part:															

Table 11: Sum-frequency force QTFs (f^+) in heave for the single truncated cylinder.

	Real part:															
T [s]	**11.11**	**10.00**	**9.09**	**8.33**	**7.69**	**7.14**	**6.67**	**6.25**	**5.88**	**5.56**	**5.26**	**5.00**	**4.76**	**4.55**	**4.35**	**4.17**
11.11	*	-20.49	-4.13	-1.55	-0.22	-0.52	-1.63	-1.85	-1.91	-1.91	-1.95	-1.44	-2.05	-1.48	-1.14	-1.44
10.00	-22.35	*	8.44	2.78	1.98	-0.61	-3.33	-3.72	-3.69	-3.54	-3.12	-5.16	0.15	-5.70	0.01	-2.35
9.09	-1.43	-4.49	*	1.94	4.16	0.37	-4.31	-4.82	-4.76	-4.64	-4.46	-5.36	-3.42	-5.28	-2.74	-3.93
8.33	-0.56	-1.42	-0.34	*	10.39	4.15	-5.56	-6.78	-6.73	-6.55	-6.44	-7.10	-6.03	-7.05	-5.18	-6.76
7.69	-0.76	-1.58	-2.83	-4.57	*	24.37	1.42	-3.60	-4.53	-4.59	-4.64	-5.21	-5.36	-5.39	-6.50	-6.93
7.14	-2.30	-4.57	-9.36	-18.38	-32.95	*	37.58	24.95	20.13	18.14	17.22	16.15	15.57	15.58	11.18	11.82
6.67	-1.99	-3.52	-7.12	-14.37	-31.60	-25.14	*	24.06	19.83	17.69	16.64	15.58	15.67	16.16	12.26	15.69
6.25	-1.62	-2.79	-5.46	-10.93	-25.08	-24.44	-4.42	*	14.66	12.76	11.74	10.73	10.98	11.69	8.63	10.89
5.88	-1.43	-2.55	-4.79	-9.51	-21.90	-22.20	-4.79	-0.74	*	10.08	9.03	7.99	8.27	8.69	6.89	6.89
5.56	-1.28	-2.41	-4.45	-8.85	-20.35	-20.61	-4.47	-0.70	0.01	*	7.52	6.50	6.57	6.49	5.57	4.95
5.26	-1.17	-2.77	-4.34	-8.60	-19.74	-19.93	-4.31	-0.65	0.10	0.18	*	5.81	5.22	4.67	4.30	3.78
5.00	-0.95	-0.05	-3.47	-7.62	-18.44	-18.66	-3.58	-0.20	0.31	0.19	0.04	*	4.47	3.52	3.05	3.17
4.76	-1.11	-2.90	-3.52	-7.72	-18.85	-20.40	-5.05	-1.06	0.01	0.43	0.50	0.38	*	3.22	3.12	2.31
4.55	-0.28	-1.25	-2.70	-5.92	-16.04	-17.41	-3.29	0.03	0.84	1.11	1.10	0.22	0.14	*	2.72	2.22
4.35	-0.77	0.90	-1.93	-5.89	-16.05	-19.46	-4.69	-0.07	1.21	1.45	1.10	0.77	0.06	0.12	*	1.51
4.17	-0.38	-3.72	-2.65	-4.18	-11.99	-17.00	-5.55	-2.55	-1.69	-0.63	0.36	0.11	-0.14	0.35	0.38	*
	Imaginary part:															

Table 12: Difference-frequency force QTFs (f^-) in heave for the single truncated cylinder.

	Real part:															
T [s]	**11.11**	**10.00**	**9.09**	**8.33**	**7.69**	**7.14**	**6.67**	**6.25**	**5.88**	**5.56**	**5.26**	**5.00**	**4.76**	**4.55**	**4.35**	**4.17**
11.11	*	14.86	219.40	333.60	308.40	-568.50	-611.40	-435.00	-333.90	-279.00	-242.10	-218.20	-197.50	-176.10	-157.20	-142.40
10.00	-202.20	*	-561.70	-927.40	-1317.00	574.60	1273.00	998.90	765.70	593.00	455.70	342.90	259.60	185.50	114.10	56.15
9.09	-126.90	63.74	*	74.64	245.70	521.50	316.20	192.60	126.20	75.91	31.11	1.55	-19.67	-38.48	-58.78	-78.46
8.33	-294.70	358.70	212.80	*	378.70	434.00	211.40	126.20	77.12	33.08	-5.04	-39.67	-82.15	-114.90	-144.10	-178.30
7.69	-754.10	1438.00	322.60	158.10	*	519.30	286.90	209.10	159.90	112.40	70.06	30.06	19.83	-13.54	-63.03	-110.70
7.14	-853.70	2539.00	58.20	-144.50	-260.30	*	228.70	185.40	187.70	211.20	249.80	287.20	331.90	385.00	433.40	444.60
6.67	-229.90	1154.00	-130.60	-177.20	-234.60	-501.70	*	17.34	43.29	88.57	147.10	211.90	254.30	317.00	390.90	438.80
6.25	-65.43	600.10	-110.80	-112.50	-143.60	-380.20	-354.90	*	17.51	53.71	98.08	150.90	189.60	231.40	278.90	322.80
5.88	-24.05	399.10	-78.10	-60.13	-60.10	-267.80	-281.20	-231.60	*	59.09	90.01	135.20	168.90	198.90	234.10	262.10
5.56	-8.93	314.80	-45.04	-13.79	25.00	-153.00	-217.30	-189.30	-164.80	*	104.20	143.20	166.20	192.30	221.70	224.40
5.26	1.74	264.60	-8.95	38.37	112.90	-34.32	-158.60	-148.70	-136.80	-131.00	*	159.10	173.20	198.00	203.60	206.00
5.00	11.40	253.90	29.49	80.22	216.60	72.69	-107.50	-116.70	-111.70	-111.90	-117.40	*	179.30	195.00	202.50	234.60
4.76	19.49	256.90	55.30	124.20	295.90	212.80	-50.02	-96.22	-102.80	-108.50	-112.40	-124.80	*	203.70	247.00	222.90
4.55	25.53	259.90	74.72	162.60	352.70	317.90	11.90	-59.88	-76.44	-86.52	-105.70	-107.20	-121.50	*	229.70	276.30
4.35	32.92	229.40	92.28	187.10	393.10	396.30	70.62	-11.04	-37.86	-63.05	-89.55	-92.84	-94.71	-93.48	*	310.20
4.17	34.13	189.70	105.10	192.40	427.90	470.30	106.60	7.54	-31.22	-53.40	-50.11	-40.24	-73.70	-91.79	-77.72	*
	Imaginary part:															

Table 13: Sum-frequency force QTFs (f^+) in pitch for the single truncated cylinder.

	Real part:															
T [s]	**11.11**	**10.00**	**9.09**	**8.33**	**7.69**	**7.14**	**6.67**	**6.25**	**5.88**	**5.56**	**5.26**	**5.00**	**4.76**	**4.55**	**4.35**	**4.17**
11.11	*	17.98	-0.89	-41.72	-311.50	-833.50	-494.90	-294.40	-200.00	-140.60	-91.34	-47.63	-2.56	38.59	59.94	93.43
10.00	-104.50	*	299.40	657.80	1592.00	1724.00	463.40	158.50	102.30	109.70	141.40	197.30	247.70	327.90	368.90	385.60
9.09	-170.70	254.00	*	50.54	160.70	291.50	155.70	103.10	92.02	98.81	117.90	150.30	190.50	238.10	280.60	326.50
8.33	-320.80	456.70	74.99	*	55.43	92.99	56.23	46.67	53.16	70.37	98.45	137.90	188.20	242.70	307.00	374.60
7.69	-554.70	373.80	135.40	36.39	*	7.92	-4.71	-6.53	-2.44	9.00	30.77	62.98	107.40	153.90	219.30	262.60
7.14	-114.60	-1393.00	-46.74	-5.00	15.35	*	-89.13	-110.60	-140.30	-176.60	-216.80	-259.50	-298.80	-351.70	-404.20	-468.50
6.67	246.20	-1394.00	-118.20	-13.55	43.37	30.85	*	-94.61	-111.80	-138.00	-171.20	-209.70	-248.70	-298.70	-350.50	-407.40
6.25	236.90	-979.90	-78.17	14.42	78.91	50.77	-1.49	*	-88.36	-100.50	-117.80	-138.60	-159.80	-186.50	-214.20	-242.80
5.88	205.30	-718.40	-34.57	49.18	125.30	81.28	-1.25	-6.16	*	-89.67	-98.48	-109.30	-120.50	-134.30	-149.20	-159.10
5.56	183.50	-538.60	8.50	90.07	185.60	128.50	7.43	-7.12	-4.59	*	-94.56	-100.00	-105.50	-111.90	-119.20	-122.20
5.26	169.20	-396.50	52.58	137.00	260.10	194.60	26.03	-0.64	-3.16	-1.90	*	-99.70	-102.00	-103.90	-105.90	-107.00
5.00	156.20	-291.50	93.67	186.30	345.10	276.40	52.62	11.86	4.34	1.76	0.29	*	-103.10	-102.40	-101.40	-99.79
4.76	144.70	-199.80	134.50	239.30	438.80	370.30	85.54	28.96	16.43	10.55	5.17	1.08	*	-103.60	-101.00	-97.78
4.55	119.20	-121.10	164.90	284.60	537.30	475.70	121.30	47.57	29.89	21.13	13.05	5.19	0.20	*	-102.40	-99.04
4.35	99.19	-97.31	182.40	326.80	638.90	579.10	140.30	53.20	36.92	29.45	20.92	11.48	3.26	-1.49	*	-101.00
4.17	83.84	-15.11	198.40	361.40	746.10	687.20	184.70	67.42	40.52	33.83	27.26	17.82	7.83	-0.03	-3.60	*
	Imaginary part:															

Table 14: Difference-frequency force QTFs (f) in pitch for the single truncated cylinder.

	Surge				**Heave**				**Pitch**			
	Sum-freq.		**Diff-freq.**		**Sum-freq.**		**Diff-freq.**		**Sum-freq.**		**Diff-freq.**	
T [s]	**real**	**imag**	**real**	**imag**	**real**	**imag**	**real**	**imag**	**real**	**imag**	**real**	**imag**
11.11	25.80	10.22	-0.05	0.00	24.78	-4.02	12.02	0.00	217.30	9.92	5.02	0.00
10.00	-20.85	-71.46	-5.15	0.00	17.98	184.80	78.63	3.72	-618.30	-177.70	241.50	0.00
9.09	4.47	-9.62	-1.39	0.00	7.59	-1.61	2.64	0.00	-2.61	159.20	31.32	0.00
8.33	21.07	-10.38	-2.90	0.00	7.48	-7.22	5.62	0.00	203.70	180.10	29.57	0.00
7.69	39.55	-32.08	-10.58	0.00	0.19	-16.69	27.42	0.00	545.60	58.46	26.04	0.00
7.14	4.06	-68.11	-21.59	0.00	2.99	-0.21	61.99	0.00	449.20	-565.60	-67.47	0.00
6.67	-17.60	-39.36	-12.18	0.00	1.55	-13.21	33.59	0.00	35.97	-450.20	-89.95	0.00
6.25	-11.19	-25.24	-7.94	0.00	-3.69	-10.09	19.00	0.00	-2.85	-282.70	-84.09	0.00
5.88	-3.43	-20.44	-6.58	0.00	-4.47	-6.22	12.81	0.00	31.74	-195.20	-84.89	0.00
5.56	3.65	-19.29	-6.22	0.00	-3.92	-2.91	9.53	0.00	79.97	-146.30	-90.16	0.00
5.26	9.52	-20.80	-6.22	0.00	-2.75	-0.05	7.47	0.00	123.50	-127.10	-96.78	0.00
5.00	16.29	-24.60	-6.28	0.00	-1.40	2.26	6.01	0.00	184.40	-137.60	-102.10	0.00
4.76	20.95	-26.32	-6.24	0.00	-0.23	3.95	4.87	0.00	215.70	-127.40	-104.50	0.00
4.55	24.82	-28.60	-6.08	0.00	0.31	4.88	3.93	0.00	228.30	-131.90	-104.20	0.00
4.35	33.04	-29.99	-5.88	0.00	-0.20	5.16	3.14	0.00	289.10	-131.70	-102.80	0.00
4.17	36.85	-29.24	-5.75	0.00	-1.83	4.87	2.46	0.00	292.70	-119.10	-102.10	0.00

Table 15: Sum- and difference- force QTFs at double and zero frequency correspondent to the diagonals of Table 9 to Table 14 for the single truncated cylinder.